DESIGN STUDY OF TORSATRON POWER REACTORS ON THE BASIS OF MAINTENANCE REQUIREMENTS

by

TAKASHI UCHIKAWA

PFC/RR-80-20

DESIGN STUDY OF TORSATRON POWER REACTORS ON THE BASIS OF MAINTENANCE REQUIREMENTS

by

TAKASHI UCHIKAWA

Submitted to the Department of Nuclear Engineering on May 9, 1980 in partial fulfillment of the requirements for the Degree of Master of Science in Nuclear Engineering.

ABSTRACT

Conceptual design study of a Torsatron power reactor (M.I.T.'s T-1 Reactor) is done with special emphasis given to questions of maintenance. It includes investigations and designs of superconducting magnet windings, blanket, vacuum/exhaust systems, vessel structures, and reactor layout, as well as investigations of maintenance procedures.

T-1 Reactor has several inherent advantages such as large aspect ratio which provides an ample space around the reactor, steady-state reactor operation, natural divertor. On the other hand, the helical magnet windings is another feature of this reactor, which gives rise to complications of reactor structures and maintenance procedures. Based on these characteristics of Torsatron reactors, this study has examined and developed the modular reactor concept of T-1 Reactor proposed by the preceding work at M.I.T..

Thesis Supervisor: Dr. Lawrence M. Lidsky

Title: Professor of Nuclear Engineering

Acknowledgements

I would like to express my deep gratitude to Professor Lidsky for his continual encouragement and guidance throughout this study. I also thank Professor Politzer for his help and useful suggestions given to me since I first attended M.I.T.

I will give special thanks to my employer, Mitsubishi Heavy Industries, Ltd., who gave me the opportunity of studying abroad at M.I.T. as a graduate student.

Ms. Cathy Lydon at Professor Lidsky's office and John Aspinal also deserve a great appreciation for their kind care and aid.

Finally, my wife Akemi and my daughter Waka well understood my situation and put up with graduate student life. I would like to express my thanks to them both.

TABLE OF CONTENTS

LIST OF FIGURES

LIST OF TABLES

NOMENCLATURE

A	Cross-sectional area
	Surface area
A_c	Heat conducting area
A_g	Surface area in vacuum space
A_u	Heat transfer area in an unit cell
a	Half height of a rectangular duct in $B_\perp$ direction
B	Magnetic field
$B_{//}$	Magnetic field component parallel to flow
$B_\perp$	Magnetic field component transverse to flow
C	Specific heat
	Conductance
C_p	Specific heat at constant volume
C_r	Coefficient of performance of refrigeration system
D	Diameter
E	Young's modulus
F	Force
f	Friction factor
G	Mass flux
g_o	Acceleration of gravity
Ha	Hartmann number
h	Heat transfer coefficient
h_{cal}	Calculated heat transfer coefficient
h_c	Forced flow heat transfer component
h_b	Boiling flow heat transfer component
Δh	Difference of enthalpy
I	Current
I_p	Current in each conductor plate
I_u	Current in an unit cell
J	Current density
K	Loss of coefficient
K_{con}	Sudden contraction-loss coefficient
K_{elb}	Friction-loss coefficient for an elbow
K_{exp}	Sudden expansion-loss coefficient

k	Thermal conductivity
L	Length
	Thickness
ΔL	Thermal contraction length
M	Mass
	Molecular weight
	Moment
$\dot{M}$	Mass flow rate
$\dot{m}$	Mass flow rate
N	Number of elements
N_c	Number of contact surfaces
Nu	Nusselt number
P	Pressure
p	Pressure
P_c	Contact pressure
Pr	Prandtl number
Δp	Pressure drop
Δp_a	Acceleration pressure drop
Δp_c	Contraction pressure drop
Δp_f	Friction pressure drop
Q	Heat load
	Gas flow
Q_c	Conducting heat load
Q_l	Heat leak
Q_m	Heat generation rate in a module
Q_r	Refrigeration heat load
Q_u	Ohmic heat in an unit cell
q	Heat flux
q''_c	Required heat flux in conductor
q_g	Out-gassing rate
R	Gas constant
Re	Reynolds number
R_u	Electrical resistance of an unit cell
r	Radius

S	Pumping speed
	Stress intensity
S_c	Contact surface area
S_e	Effective pumping speed
S_p	Required pumping speed
S_u	Cross-sectional area of an unit cell
S_o	Maximum allowable stress intensity
T	Temperature
ΔT_f	Film temperature drop
t	Time
	Thickness
t_w	Wall thickness
Δt	Cooling time
V	Velocity
V_f	Velocity of liquid
V_g	Velocity of vapor
v_f	Specific volume of liquid
v_g	Specific volume of vapor
W_p	Pumping power
W_r	Refrigeration power
w	Weight
x	Quality
Z	Section modulus
α	Void fraction
ϵ	Strain
η_c	Ratio of effetive contact area to total surface area
η_f	Friction coefficient
μ	Viscosity
ξ	Pitch angle
ρ	Density
ρ_{cu}	Electrical resistivity of copper
ρ_f	Density of liquid
ρ_g	Density of vapor
σ	Electrical conductivity
	Stress

σ_o	Allowable stress
τ_E	Energy confinement time
ϕ^2	Two-phase friction multiplier

(Subscripts)

ave	Average
f	Liquid
g	Vapor
h	High
l	Low
in	Inlet
out	Outlet
e	Exit
w	Wall
1	Region 1
2	Region 2

1. Introduction

1.1 Purpose of Study

Compared with Tokamaks, Torsatron fusion reactors have substantially different engineering features; that is, helical magnet windings, large aspect ratio, steady-state reactor operation, natural divertors, etc.. The first Torsatron reactor (MIT's T-1 Reactor) study showed that there are remarkable inherent advantages based on some of the above features, as well as obvious complications formed by helically wound magnets.

In developing conceptual design of fusion reactors in general, maintainability or serviceability of the reactors is one of major concerns because the first wall/blanket structures will need periodic replacement which will require either disassembly of the basic reactor structures or complicated remote operation, and because the large capital cost of the reactors will require that down-time for both scheduled and unscheduled maintenance be kept to a minimum in order to increase availability.

This study investigates conceptual reactor designs for a Torsatron power reactor (T-1 Reactor) with special emphasis given to questions of maintenance. Specifically it includes investigation and design of superconducting magnet windings, blanket, vacuum/exhaust system, vessel joints and other reactor structures, and reactor layout, as well as investigation of maintenance procedures.

1.2 Main Features of T-1 Reactor

T-1 Reactor is a Torsatron power reactor producing about 1500 MW_e. As MIT's report [1] describes, the Torsatron is a steady-state toroidal magnetic trap in which both the toroidal and poloidal magnetic field components are generated by a set of helical magnet windings; the internal magnetic topology of a Torsatron is similar to that of a Stellarator; the magnet coil structure, however, is much simpler in a Torsatron since separate toroidal field coils are not needed, and the helical windings are unidirectional.

In T-1 Reactor three circular coils are used to compensate vertical fields generated by the helical conductors bent into a torus. By selecting a suitable winding law the helical conductors can be significantly "force-reduced". The Torsatron configuration provides a natural divertor without any divertor coils. Since an externally driven plasma current is not required, the Torsatron can operate as a steady-state, ignited reactor. No coils, other than the helical and compensating windings are needed. Both plasma physics and reactor engineering considerations lead to the choice of a moderate aspect ratio for the Torsatron. In T-1 Reactor the aspect ratio of the helical windings is about 6; the major radius is about 25 m and the minor radius is 4 m. The reactor structures are composed of 20 modules and the superconducting helical windings are connected from module to module with normally conducting joints.

Thus T-1 Reactor is a steady-state, ignited, modular power reactor. Fundamental parameters of T-1 Reactor are given in Table 1.2.1.

Table 1.2.1 Characteristics of T-1 Reactor

Output		
Power density	p_f	1.18 MW/m^3
Thermal output	P_{th}	4320 MW
Electric output	P_{el}	1500 MW
Plasma		
Plasma radius	a_p	2.3 m
Plasma volume	V_p	3240 m^3
Plasma density	n_o	2×10^{20} m^{-3}
	$\overline{n}$	1.33×10^{20} m^{-3}
Plasm temperature	T_o	11.0 keV
	$\overline{T}$	7.33 keV
Beta value	β_o	7.09 %
	$\overline{\beta}$	3.54 %
Energy confinement time	τ_E	2.24 sec
$\overline{n}\tau_E$		3×10^{20} sec·m^{-3}
Helical windings		
Type of windings		$\ell = 3$
Number of field periods	N	20
Major radius	R_o	24.8 m
Minor radius	a_o	4 m
Current	I_o	36.5 MA
Current density	J	3000 A/cm^2
Magnetic field	B_o	5 T
	B_{max}	8.7 T
Stored energy	U_m	460 GJ
Others		
Number of VF cois		3
Number of reactor modules		20
Plasma heating method		Neutral beam injection

2. Superconducting Magnet Windings

2.1 General

Table 2.1.1 shows main design parameters and specifications of the superconducting magnet windings spiraling along the torus in T-1 Reactor.

Table 2.1.1 Characteristics of superconducting magnet windings

Number of segments	60 (3 segments/1 module)
Operating temperature	4.2 K
Superconductor	Nb-Ti
Stabilizer	Copper (O.F.H.C.)
Coil case	316 SS
Maximum field	8.7 T
Stored energy	460 GJ
Total ampere turns	36.5 M Amp. turns (500 kA x 73 turns)
Current density	3000 A/cm^2
Stabilizer to superconductor ratio	~ 9 : 1
Current density in superconductor	~ 30000 A/cm^2

2.2 Selection of Cooling Methods

There are several cooling methods which are proposed to apply to fusion magnets:

1) Pool boiling of liquid helium
2) Cooling by superfluid helium (He-II)
3) Forced circulation of supercritical helium
4) Forced circulation of subcooled helium
5) Forced circulation of two-phase helium

The pool boiling method has been proved to be successful for small systems; however, it seems to have serious disadvantages in its application to large magnets. Since large magnets have long and narrow cooling channels, it would be difficult to remove bubbles generated in the channels, particularly in the horizontal parts. The remaining bubbles would cause large reduction of nucleate boiling heat flux.

The cooling by superfluid helium provides some remarkable advantages, such as higher heat flux, higher magnetic field, higher current density. However, it also has several disadvantages:

a) Convective resistance in narrow and long cooling channels will be very large and limit the theoretical advantages.
b) The cost of refrigerating systems will increase noticeably due to extremely low temperature (1.8 K) refrigeration.
c) Complicated cryostats will be required
d) Severe requirement for sealing is expected.

Considering a limitation of the cross-sectional size of the magnet windings

and complexity of cryostats, this cooling method does not seem to be most prospective.

According to G. Pasotti and M. Spadoni [2] (CNEN), the forced circulation of helium shows a number of advantages:

1) Effective heat removal from the magnets
2) Mass flow rate can be adjusted to obtain the desired heat flux.
3) Design of the cryostats is greatly sumplified
4) It is easier to achieve a good mechanical stiffness

Comparative evaluation of the various cooling methods [3-7] is summerized in Table 2.2.1. In this study, we select two options of probable methods: forced circulation of supercritical helium and forced circulation of two-phase helium. The former one has advantages of ease of handling, simple cryostats, small inventry of helium coolant, etc.. It also has a few disadvantages, among which low heat flux and low cooling power is most concerned. Some experimental studies are being done, at MIT and other places, to examine cryostability of superconducting magnets cooled by this method.

The latter, forced circulation of two-phase helium has a relatively high heat transfer coefficient and a large cooling power without temperature increase; however, two-phase helium flow has the possibility of flow separation and instability in flow distribution. Recently some operation experience of a large superconducting dipole cooled by forced circulation of two-phase helium has been reported from CERN [8], but still it will need a further experimental reseach and development to examine the feasibility of this method.

Table 2.2.1 Evaluation of cooling methods

	Advantages	Disadvantages	Examples
Pool boiling of liquid He	1) Successful application in small systems	1) Propensity for vapor blockage and subsequent coil burn-out 2) Low cooling power 3) Large cryostats	LCT (GE) LCT (GD)
Cooling by superfluid He	1) High heat flux 2) High critical magnetic field 3) Improvement of heat exchange in cooling channels	1) Increasing cost of refrigeration 2) Complicated cryostats 3) Severe requirement for sealing	NUWMAK PF coil of EPR (ANL)
Forced circulation of supercritical He	1) Easy operation 2) Simple cryostats 3) Small inventry of He coolant	1) Low heat flux and low cooling power 2) Coolant temperature increase 3) Relatively high pressure	ISABELLE (BNL) LCT (WH)
Forced circulation of subcooled He	1) Easy operation 2) Simple cryostats	1) Low heat flux and low cooling power 2) Coolant temperature increase	
Forced circulation of two-phase He	1) Large heat flux and large cooling power 2) Simple cryostats 3) Positive Joule-Kelvin effect (No temperature increase)	1) Potential flow separation and instability 3) Restriction of pressure drop	FINTOR-I (CNEN) T-7 (USSR)

2.3 Cryogenic Design of the Magnet

a. Conductor

The design of conductors is based on the concept of conductor modularization which was proposed in the preceding work on T-1 Reactor. In this study two options of conductor-types are considered. One is a cable-in-conduit type conductor shown in Figure 2.3.1 and the other is an internal-cooling type conductor shown in Figure 2.3.2. The two types of conductors are suitable for a supercritical helium flow and a two-phase helium flow, respectively.

b. Cryostat Design and Required Refrigeration Power

The cryostats should be designed as simply as possible in order to attain structural integrity, to reduce the cross-sectional size, and to improve maintenability of the magnet windings.

Heat loads of the magnet arise from heat conduction, radiation, ohmic heating (particularly in the magnet joints), and nuclear heating. Conduction and radiation are main concerns so far as the bulk cooling of the ohmic magnet is concerned. Figure 2.3.3 a) and Figure 2.3.3 b) show two types of cryostats using intermediate cooling which removes heat at the region of intermediate temperature ($\sim$80 K) between extreme low temperature (4.2 K) and room temperature (300 K). The difference is that the former design allows a bulk heat conduction between the intermediate temprature region and the room temperature region, while the latter one prevents it by adopting another outer super-insulation. Heat loads of each type of cryostats are estimated as follows:

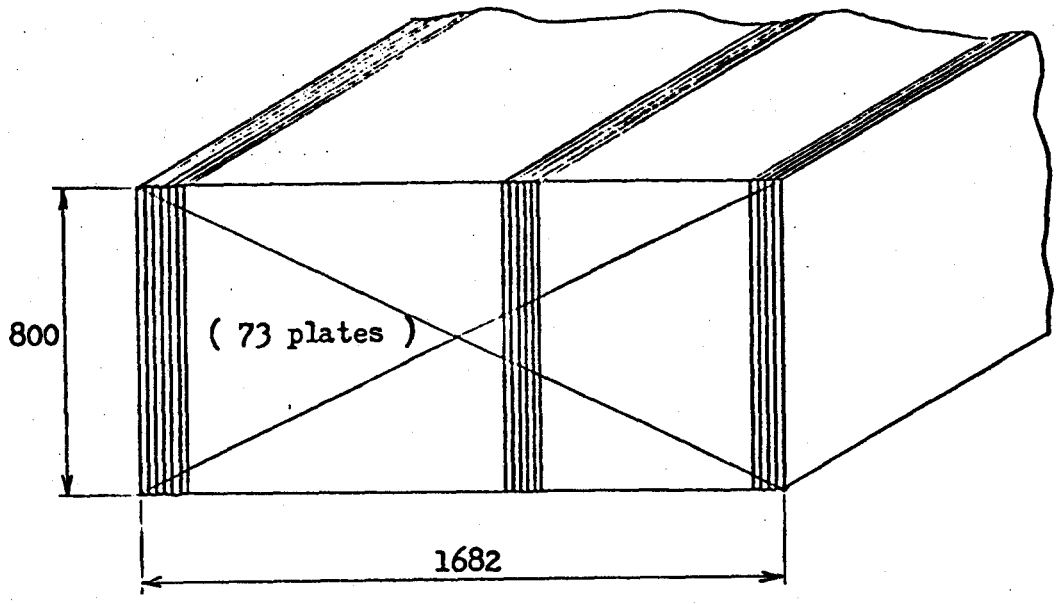

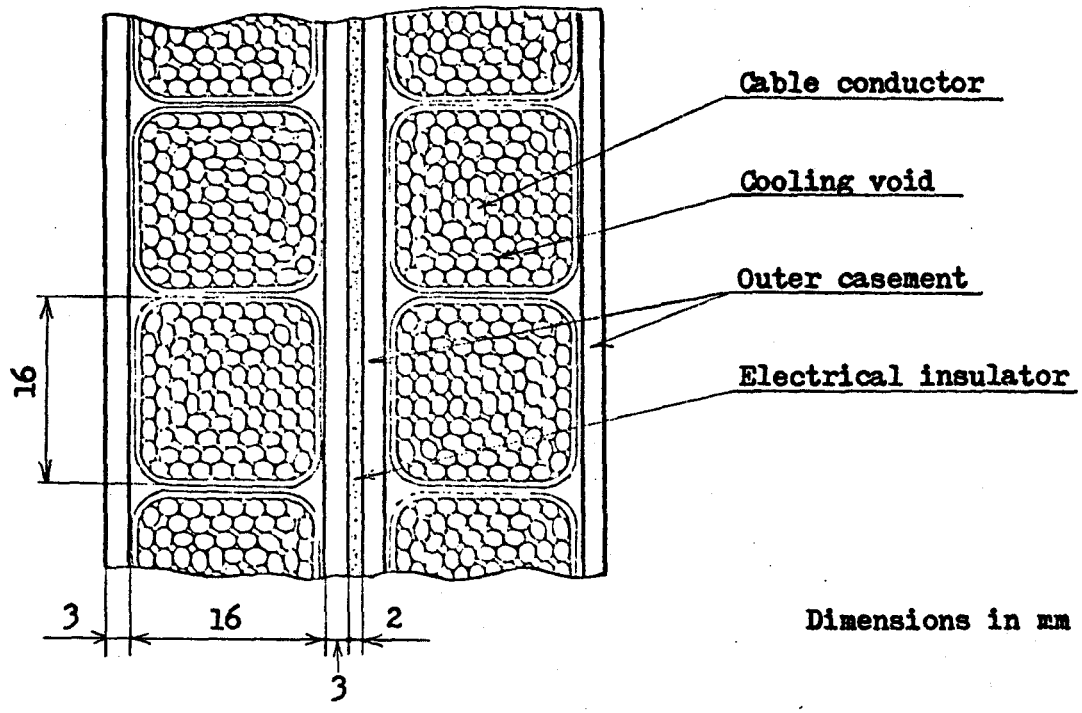

Figure 2.3.1 Cable-in-conduit type conductor

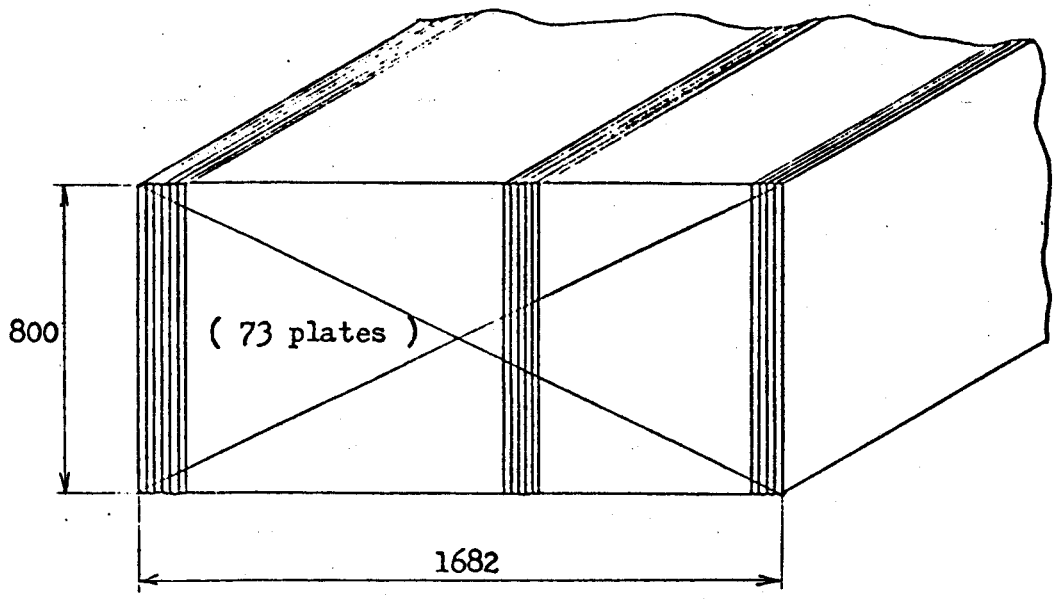

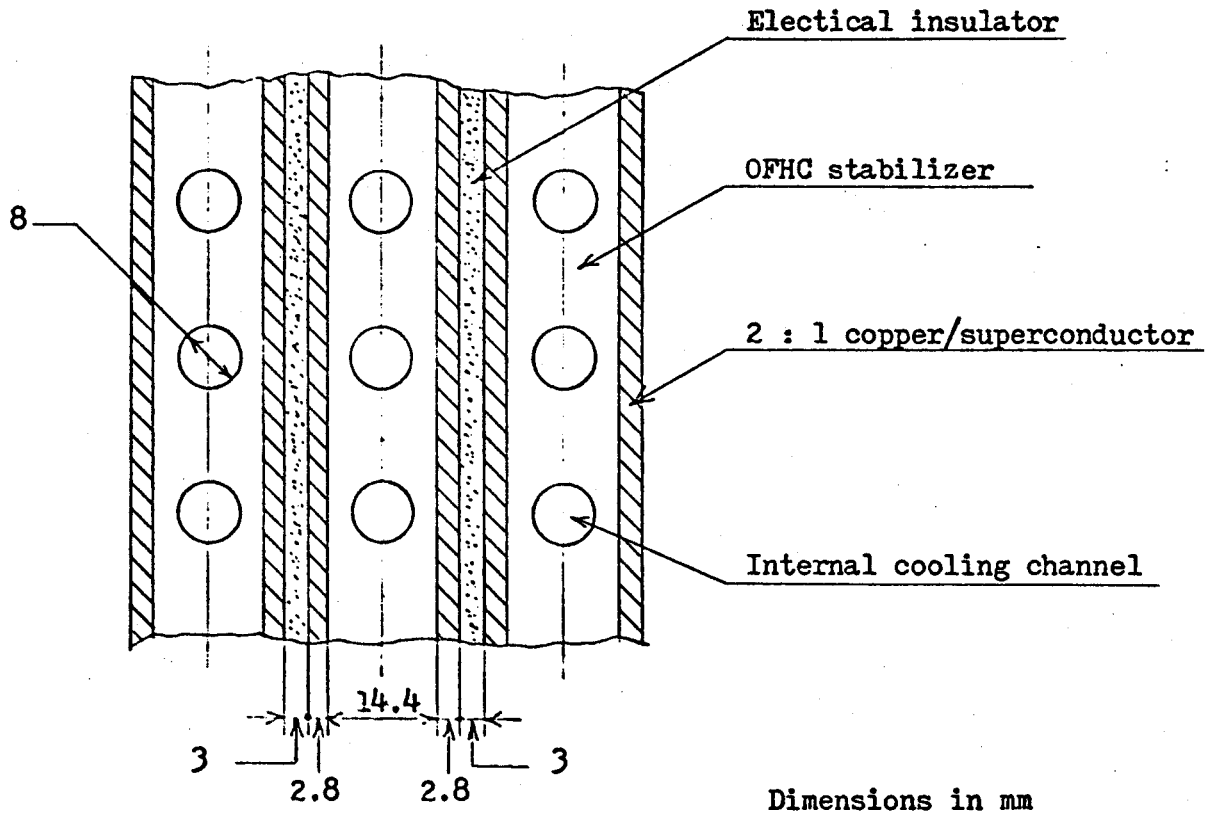

Figure 2.3.2 Internal cooling conductor

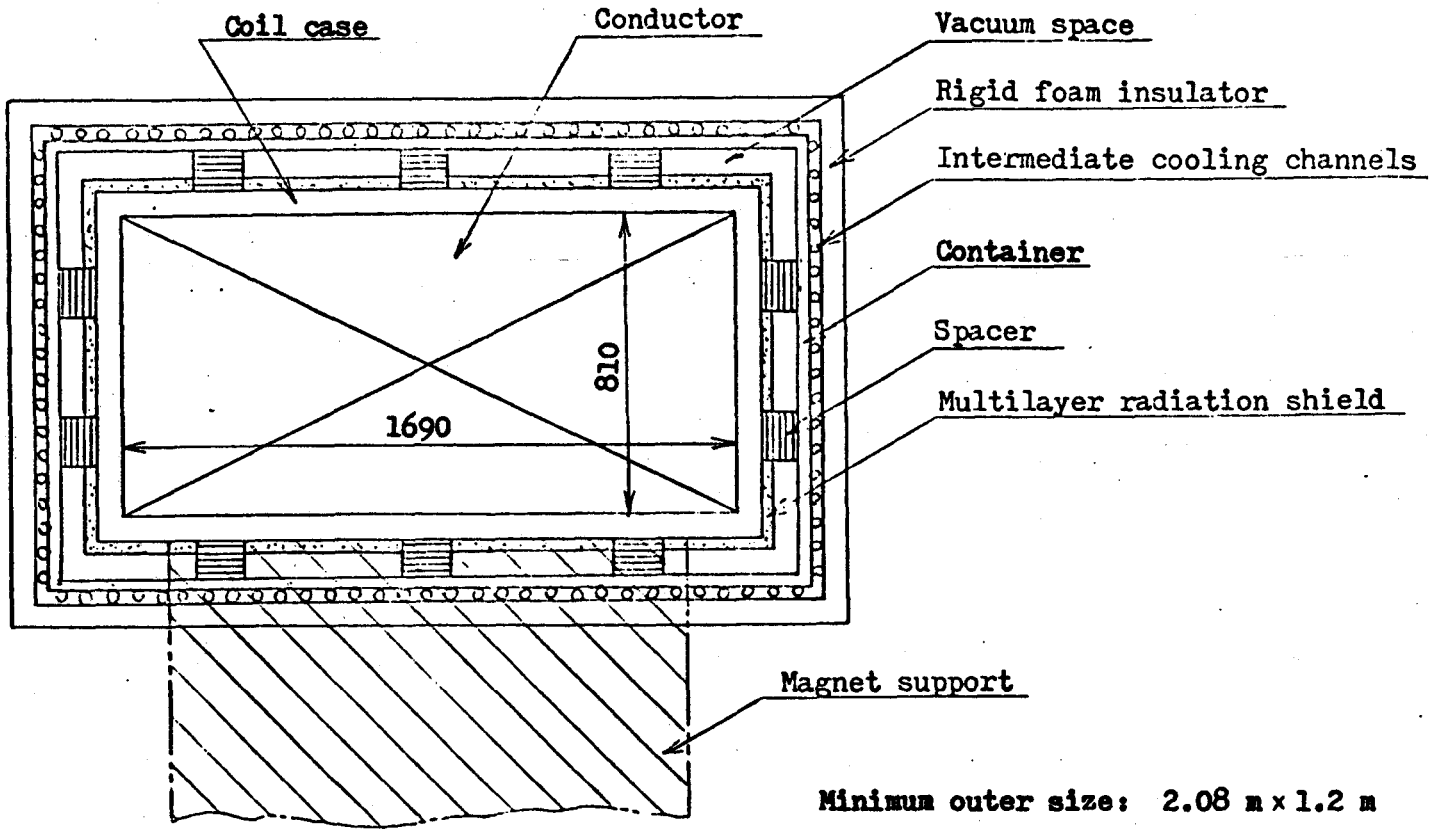

Figure 2.3.3 a) Single-superinsulation cryostat

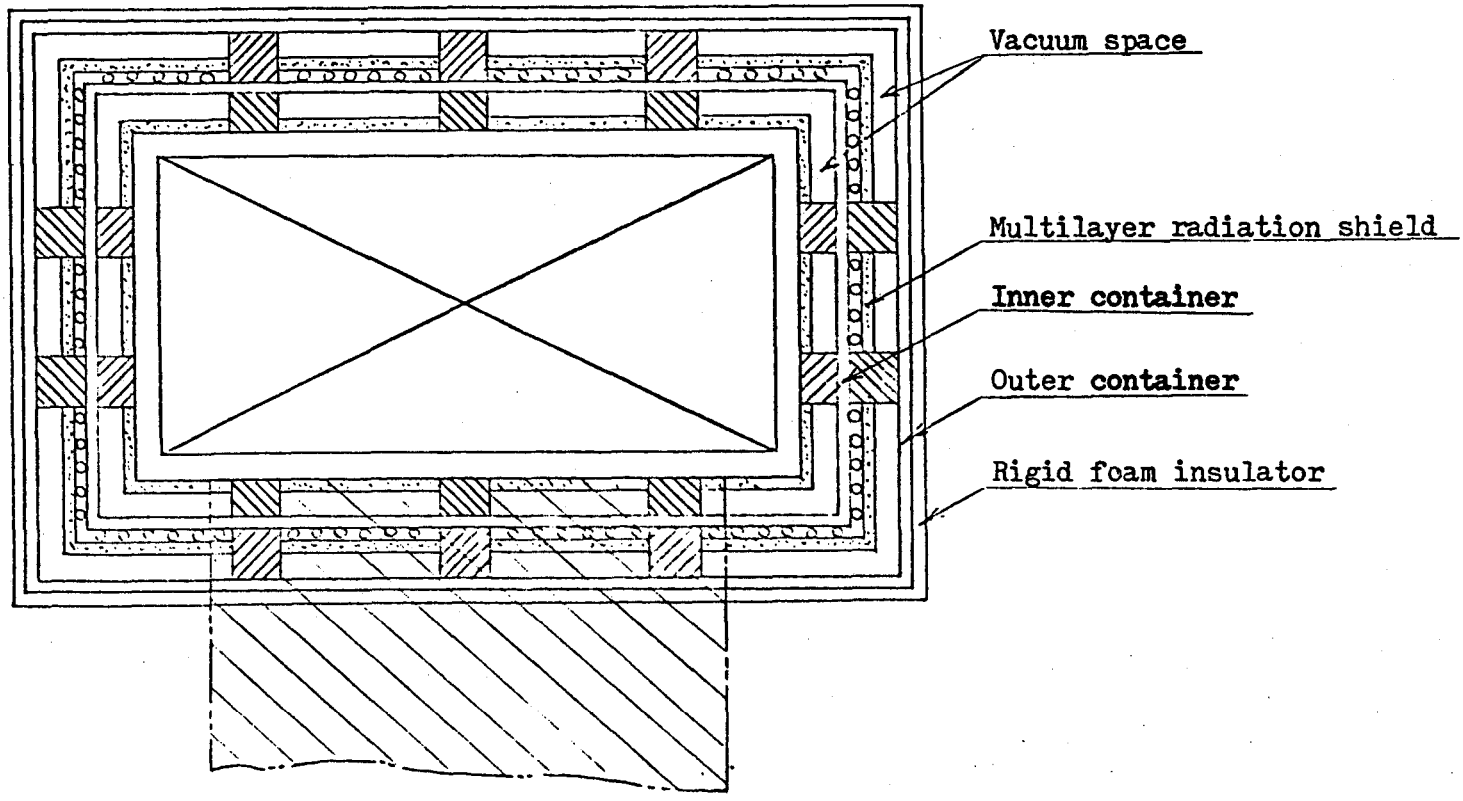

Figure 2.3.3 b) Double-superinsulation cryostat

Heat conduction

Conducting heat loads Q_c between a region of higher temperature T_h and a region of lower temperature T_l is calculated by

$$Q_c = A_c \, k_{ave} \, \frac{T_h - T_l}{L} \qquad (2.3.1)$$

where

A_c = heat conducting area

k_{ave} = average thermal conductivity

L = thickness of a conducting material

and

$$k_{ave} \equiv \frac{\int_0^L k(T) \, \frac{dT}{dx} \, dx}{T_h - T_l} = \frac{\int_{T_l}^{T_h} k(T) \, dT}{T_h - T_l} \qquad (2.3.2)$$

From Equation (2.3.1) and Equation (2.3.2) we obtain

$$Q_c = A_c \, \frac{1}{L} \int_{T_l}^{T_h} k(T) \, dT \qquad (2.3.3)$$

Conducting heat loads through spacers, magnet supports, and other structures are calculated as shown in Table 2.3.1.

Radiation

The contribution of radiation to heat flow can be efficiently reduced by using so-called 'super-insulations' which are a combination of vacuum atmosphere and multiple-layer insulators.

According to experimental studies, the heat transfer rate through multiple-layer insulations in 300 K - 4.2 K is smaller than that in 300 K - 77 K, although the magnitudes of temperature difference are reversed.

Table 2.3.1 Conducting heat loads

	Single-superinsulation cryostat	Double-superinsulation cryostat	
Spacer		(Inner spacer)	(Outer spacer)
Material	Glass epoxy	Glass epoxy	Glass epoxy
A_c	24.5 m^2	24.5 m^2	24.5 m^2
L	0.003 m	0.003 m	0.003 m
T_h	80 K	80 K	300 K
T_l	4.2 K	4.2 K	80 K
$\int k(T)\, dT$	12.2 W/m	12.2 W/m	66.9 W/m
Q_c	10.0 KW	10.0 KW	54.6 KW
Magmet supports			
Material	Glass epoxy	Glass epoxy	
(High temp. region)			
A_c	200 m^2	200 m^2	
L	0.27 m	0.27 m	
T_h	300 K	300 K	
T_l	80 K	80 K	
$\int k(T)\, dT$	115 W/m	115 W/m	
Q_c	85.2 KW	85.2 KW	
(Low temp. region)			
A_c	200 m^2	200 m^2	
L	0.73 m	0.73 m	
T_h	80 K	80 K	
T_l	4.2 K	4.2 K	
$\int k(T)\, dT$	17.4 W/m	17.4 W/m	
Q_c	4.8 KW	4.8 KW	

Table 2.3.1 (continued)

	Single-superinsulation cryostat	Double-superinsulation cryostat
Bulk surface		
Material	Rigid foam insulator	Rigid foam insulator as a thermal buffer
A_c	4200 m^2	
L	0.05 m	
T_h	300 K	
T_l	80 K	
k_{ave}	0.0346 W/m·K (0.02 Btu/hr·ft·°F)	No heat conduction
Q_c	640 KW	

Note

1) A_c :

Spacer: $0.05 \times 0.05\ m^2 \times 160$ (# per segment) $\times$ 60 (# of segments)

$\simeq 24.5\ m^2$

Magnet supports: $1.2 \times 0.9\ m^2 \times 180$ (# of elements) $\simeq 200\ m^2$

Bulk surface: $2(1.0 + 2.0)\ m \times 11.5\ m \times 60$ (# of segments)

$\simeq 4200\ m^2$

2) $\int_{T_l}^{T_h} k(T)\, dT$:

Spacer: due to Figure 2.3.4 (Normal to reinforcement)

Magnet support: due to Figure 2.3.4 (Parallel to reinforcement)

3) k_{ave} of rigid foam insulator: based on the data shown in "Chemical Engineering Handbook" (MaGraw-Hill)[9], Table 11-11

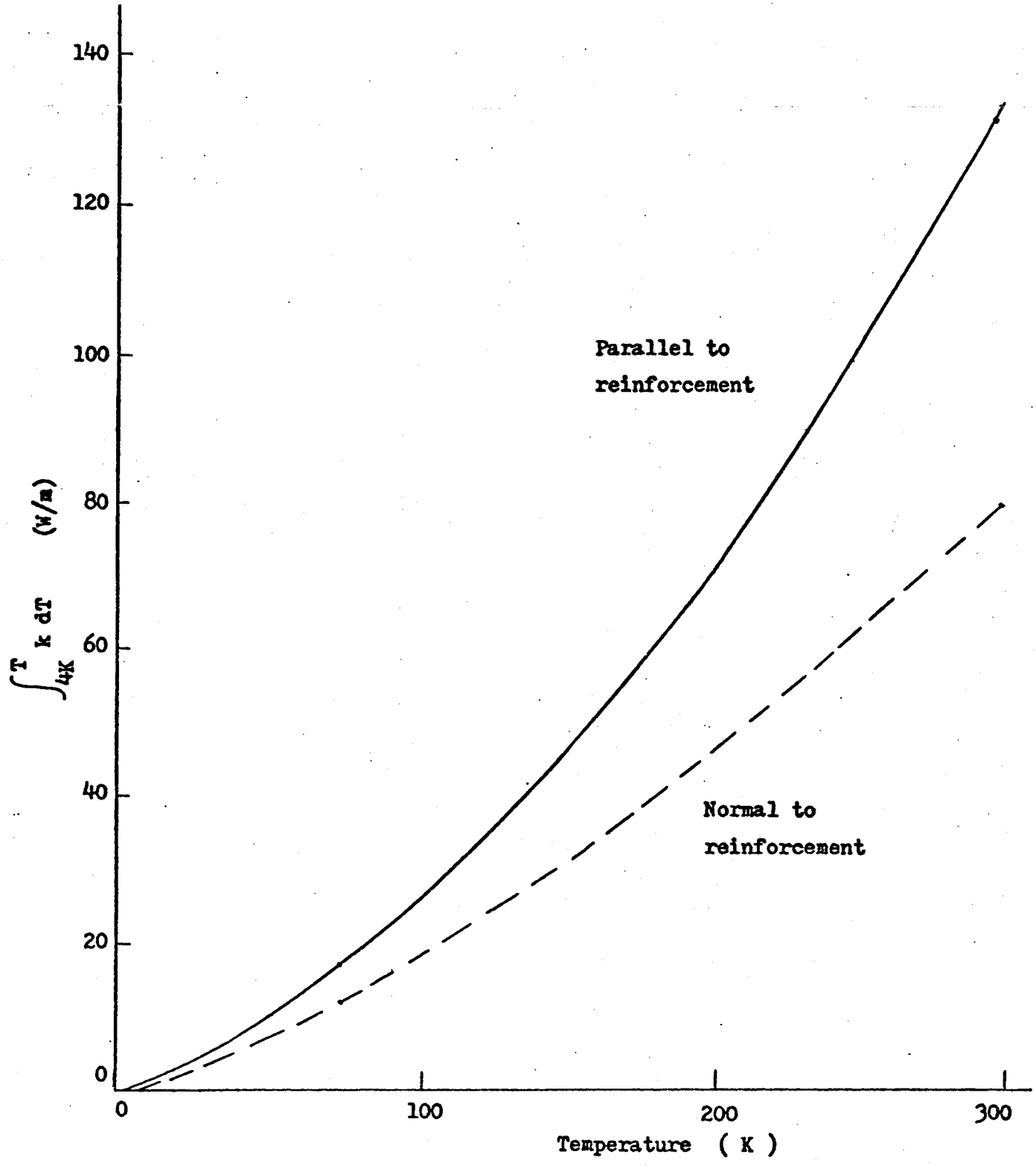

Figure 2.3.4 $\int_{4K}^{T} k\,dT$ of glass epoxy [10]

This experimental result is explained by the fact that the emissivity of the surfaces decreases as the temperature goes down.

The radiation heat loads are estimated as shown in Table 2.3.2. Individual layers of the shield are composed of aluminized Mylar with glass fiber spacer. The layer density (the number of layers per unit thickness) is 16 - 20 cm^{-1}. The heat transfer rates are based on experimental data presented by Inai.[11]

Table 2.3.2 Radiation heat loads

	Single-superinsulation cryostat	Double-superinsulation cryostat	
		(Inner shield)	(Outer shield)
Surface area	3900 m^2	3900 m^2	4600 m^2
Temperature range	80 - 4.2 K	80 - 4.2 K	300 - 80 K
Number of shield layers	50	50	10
Shield thickness	0.03 m	0.03 m	0.006 m
Heat transfer rate	0.7 W/m^2	0.7 W/m^2	1.7 W/m^2
Heat load	2.8 KW	2.8 KW	7.9 KW

Based on the estimated heat loads, the required refrigeration power is calculated as shown in Table 2.3.3. As a matter of course insulating performance of the double-superinsulation type of cryostats is superior to that of the single-superinsulation type; the difference of the requird power is about 4 MW_e. Generally, so-called 'superinsulations' (or other evacuated cryogenic insulations)[12] have a remarkable insulating performance, but, at the same time, they are accompanied with the following defects:

1) Cryostats must have a rigid container to stand for vacuum atmosphere.
2) In order to obtain a high-vacuum condition ($< 10^{-4}$ torr) a large vacuum space and a low outgassing-rate are required for the cryostats.

Especially the above item 2) makes the cryostats much larger than expected. Under the restriction of the magnet cross-sectional size the double-superinsulation type of cryostats will not be applicable to the magnet windings. Even for the single-superinsulation type the allowble space is so tight that careful considerations must be done in vacuum design of the cryostats.

Table 2.3.3 Required refrigeration power

	Single-superinsulation cryostat	Double-superinsulation cryostat
Conduction		
Spacer		
300 - 80 K	———	54.6 KW × 6.5 = 360 KW
80 - 4.2 K	10.0 KW × 300 = 3000 KW	10.0 KW × 300 = 3000 KW
Magnet support		
300 - 80 K	85.2 KW × 6.5 = 560 KW	85.2 KW × 6.5 = 560 KW
80 - 4.2 K	4.8 KW × 300 = 1440 KW	4.8 KW × 300 = 1440 KW
Bulk surface		
300 - 80 K	640 KW × 6.5 = 4160 KW	———
Radiation		
Outer shield		
300 - 80 K	———	7.9 KW × 6.5 = 60 KW
Inner shield		
80 - 4.2 K	2.8 KW × 300 = 840 KW	2.8 KW × 300 = 840 KW
Joule heating in joints		
4.2 K	14.1 KW × 300 = 4230 KW	14.1 KW × 300 = 4230 KW
Total	725 KW × 6.5 + 31.7 KW × 300 } 14.2 MW	148 KW × 6.5 + 31.7 KW × 300 } 10.5 MW

Note

1) The coefficient of performance of refrigeration systems are assumed:[13]

$77/(300 - 77) \times 0.45 \simeq 1/6.5$ for 80 K refrigeration

$20/(300 - 20) \times 0.35 \simeq 1/40$ for 20 K refrigeration

$4.2/(300 - 4.2) \times 0.25 \simeq 1/300$ for 4.2 K refrigeration

2) The joule heating load in joints is due to Section 2.4.

c. Conductor Cooling

Cooling of conductor is closely related to cryostability of superconducting magnets. For a bundled-cable (or cable-in-conduit type) conductor cooled by forced-flow of supercritical helium, some experimental and analytical results have shown the possibility of a cryostable conductor with high current density and further reseach and development are now going on, for example, seeking a significant reduction of pressure drop and pumping power. In this study, thermal-hydraulic analysis is done for an internal-cooling conductor cooled by forced flow of two-phase helium, which is another option of magnet cooling in T-1 Reactor.

1) Heat Flux

As described before the heat loads imposed on the magnet windings are due to heat conduction, radiation, nuclear heating, and ohmic heating in the magnet joints. On the basis of these normal heat loads the average heat flux in the whole cooling channels is very small. However, the required heat flux is determined by a different design condition to obtain cryostability of the magnets. In this study the cooling rate is supposed to be potentially high enough to remove ohmic heat generated in the conductor where the state-transition from a superconducting condition to a normal-conducting condition has taken place locally.

The required heat flux q''_c is approximately given by

$$q''_c > \frac{Q_u}{A_u} = \frac{I_u^2 R_u}{A_u} \qquad (2.3.4)$$

where

Q_u = ohmic heat generated in a certain unit cell around a cooling channel

A_u = heat transfer area in the unit cell

= $\pi \times 0.8$ cm $\times 1$ cm = 2.51 cm^2

I_u = I_p / 40(# of channels per conductor plate) = 12500 A

R_u = $(\rho_{cu} / S_u) \cdot 1$ cm = ρ_{cu} / S_u ohm

ρ_{cu} = electrcal resistivity of copper at 4.2 K

= 1.85×10^{-9} ohm·cm

S_u = conductor's cross-sectional area in the unit cell

= $(1.44 + 0.28 \times 2 \times 2/3)$ cm $\times 2$ cm - $\pi/4 \cdot 0.8^2$ cm^2

= 3.12 cm^2

Thus

$$q''_c > \frac{(12500\ A)^2\ 1.85 \times 10^{-9}/3.12\ ohm}{2.51\ cm^2} = 0.037\ W/cm^2 \qquad (2.3.5)$$

This is the result of a sort of static thermal calculations, which may underestimate the required heat flux. As a design condition the following value which is about five times larger than the above result is used:

$$q'_c = 0.2\ W/cm^2 \qquad (2.3.6)$$

2) Heat Tranfer Coefficient

In forced circulation of two-phase helium the effect of forced convection heat transfer is small and nucleate boiling heat transfer is dominant. V.E. Keilin et al.[14] proposed the following formulation:

$$h_{cal} = \sqrt{h_c^2 + h_b^2} \qquad (2.3.7)$$

$$h_b = 6.74\ p^{0.5}\ q^{0.6} \quad \text{for } 0.11 < p < 0.14 \text{ MPa} \qquad (2.3.8)$$

$$= 2.36\ q^{0.5} \quad \text{for } p = 0.15 \text{ MPa}$$

where

h_{cal} = calculated heat transfer coefficient in W/cm^2 K

h_c = forced flow heat transfer component in W/cm^2 K

h_b = boiling flow heat transfer component W/cm^2 K

p = pressure in MPa

q = heat flux in W/cm^2

Table 2.3.4 shows the coolant conditions which are proposed for two-pahse flow.

Table 2.3.4 Two-phase helium coolant conditions

	Temperature (K)	Pressure (MPa)	Quality	Enthalpy(J/kg)
Inlet	4.4	0.12	0.0	11,200
Outlet	4.2	0.10	0.3	17,300

Uaing Equation (2.3.8) and Table 2.3.4 we obtain

$$h_b = 6.47 \ (0.11)^{0.5} \ q^{0.6} = 2.15 \ q^{0.6} \qquad (2.3.9)$$

For $q = q''_c = 0.2 \ W/cm^2$

$$h_b = 2.15 \ (0.2)^{0.6} = 0.82 \ W/cm^2 \cdot K \qquad (2.3.10)$$

The forced flow heat transfer component h_c depends upon the flow conditions; however, generally h_c is much smaller than h_b as shown later. Thus

$$h_{cal} \simeq h_b = 0.82 \ W/cm^2 \cdot K \qquad (2.3.11)$$

The corresponding film temperature drop ΔT_f is

$$\Delta T_f = q / h_{cal} = 0.2/0.82 = 0.24 \text{ K} \qquad (2.3.12)$$

This is considered to be small enough.

3) Flow Rate and Pressure Drop

The flow rate is restricted by allowable pressure drop. Pressure drop of two-phase flow is due to complicated phenomena and its general calculating methods have not been obtained. In this study, friction pressure drop is calculated by the Martinelli method and other kinds of pressure drop are calculated by using general formulation derived from energy and momentam conservation equations.

The following are some notations and fundamental relationship related to two-phase flow:[15,16]

$$x = \text{quality} = \frac{\text{mass flow rate of vapor}}{\text{total mass flow rate}}$$

$$\alpha = \text{void fraction} = \frac{\text{volume of vapor}}{\text{total volume}}$$

V_f = average velocity of liquid

V_g = average velocity of vapor

and

$$V_f = \frac{\vartheta_f \dot{m} (1 - x)}{A_f} = \frac{\vartheta_f \dot{m} (1 - x)}{A (1 - \alpha)} \qquad (2.3.13)$$

$$V_g = \frac{\vartheta_g \dot{m} x}{A_g} = \frac{\vartheta_g \dot{m} x}{A \alpha} \qquad (2.3.14)$$

where

$\dot{m}$ = mass flow rate

v_f = specific volume of liquid

v_g = specific volume of vapor

A_f = cross-sectional area of liquid

A_g = cross-sectional area of vapor

A = total cross-sectional area

$= (\pi/4)\ 0.008^2\ m^2 = 5.027 \times 10^{-5}\ m^2$

In order to obtain the relationship between x and α experimental data of slip ratio ($= V_g/V_f$) are needed. In this study, however, the following empirical relationship proposed by Von Glahn is used:

$$1/x = 1 - (v_g/v_f)^{0.67}\left[1 - (1/\alpha)^{(v_g/v_f)^{0.1}}\right] \qquad (2.3.15)$$

or

$$\alpha = \left[1 - (1 - 1/x)\cdot(v_g/v_f)^{-0.67}\right]^{-(v_g/v_f)^{-0.1}} \qquad (2.3.16)$$

Friction Prsssure Drop in Cooling Channels

Due to the Martinelli method, the friction pressure drop Δp_f is calculated as follows:

$$\Delta p_f = f\ \frac{L}{D}\ \frac{\rho_f V_f^2}{2 g_c}\ \phi^2 \qquad (2.3.17)$$

where

f = friction factor

L = length of a channel

D = hydrauric diameter of a channel

ρ_f = density of liquid (cf. ρ_g = density of vapor)

g_c = acceleration of gravity = 9.807 $Kg_m \cdot m/kg_f \cdot sec^2$

ϕ^2 = two-phase friction multiplier

ϕ^2 is provided from the chart as a function of X which is given by

$$X^2 = \frac{Re_g^{\,m}}{Re_f^{\,n}} \frac{C_f}{C_g} \left(\frac{1-x}{x}\right)^2 \frac{v_f}{v_g} \qquad (2.3.18)$$

where

$Re_f = \rho_f V_f D/\mu_f$

$Re_g = \rho_g V_g D/\mu_g$

$m = n = 0.2$

$C_f = C_g = 0.046$

for $Re_f \geq 2000$, $Re_g \geq 2000$

μ_f = viscosity of liquid

μ_g = viscosity of vapor

Each cooling channel is divided into series of three sections and the separate contributions to the pressere drop of Equation (2.3.17) are evaluated using an average quality for each section. The calculations are done for various flow rates as shown in Table 2.3.5.

Acceleration Pressure Drop in Cooling Channels

The acceleration pressure drop Δp_a is given by

$$\Delta p_a = 1/g_c \left(\frac{\dot{m}}{A}\right)^2 \left[\frac{(1-x_e)^2}{1-\alpha_e} v_f + \frac{x_e^{\,2}}{\alpha_e} v_g - v_{in} \right] \qquad (2.3.19)$$

where

x_e = quality in exit = 0.3

α_e = void fraction in exit

v_f = 1/125 m^3/kg

v_g = 1/16.5 m^3/kg

Table 2.3.5 Friction pressure drop in cooling channels

		$\dot{m}$	0.002 $\frac{kg}{sec}$	0.003 $\frac{kg}{sec}$	0.004 $\frac{kg}{sec}$	0.006 $\frac{kg}{sec}$
Channel section 1	L = 3.83 m	α	0.204	0.204	0.204	0.204
	T = 4.4 K	V_f	0.389	0.584	0.778	1.17
	x = 0.05	V_g	0.483	0.724	0.966	1.45
	ρ_f = 122	Re_f	1.05×10^5	1.58×10^5	2.11×10^5	3.17×10^5
	ρ_g = 20.2	Re_g	6.50×10^4	9.75×10^4	1.30×10^5	1.95×10^5
	$\mu_f = 3.6 \times 10^{-6}$	f	0.0190	0.0178	0.0171	0.0162
	$\mu_g = 1.2 \times 10^{-6}$	X	7.37	7.37	7.37	7.37
		$\phi 2$	3.94	3.94	3.94	3.94
		Δp_f	33.8	71.3	122	260
Channel section 2	L = 3.83 m	α	0.457	0.457	0.457	0.457
	T = 4.3 K	V_f	0.504	0.756	1.01	1.51
	x = 0.15	V_g	0.712	1.07	1.42	2.13
	ρ_f = 123.5	Re_f	1.38×10^5	2.07×10^5	2.77×10^5	4.14×10^5
	ρ_g = 18.35	Re_g	8.71×10^4	1.31×10^5	1.74×10^5	2.61×10^5
	$\mu_f = 3.6 \times 10^{-6}$	f	0.0181	0.0171	0.0165	0.0158
	$\mu_g = 1.2 \times 10^{-6}$	X	2.08	2.08	2.08	2.08
		ϕ^2	6.75	6.75	6.75	6.75
		Δp_f	93.6	199	343	734
Channel section 3	L = 3.83 m	α	0.627	0.627	0.627	0.627
	T = 4.2 K	V_f	0.640	0.960	1.28	1.92
	x = 0.25	V_g	0.961	1.44	1.92	2.88
	ρ_f = 125	Re_f	1.78×10^5	2.67×10^5	3.56×10^5	5.33×10^5
	ρ_g = 16.5	Re_g	1.06×10^5	1.58×10^5	2.11×10^5	3.17×10^5
	$\mu_f = 3.6 \times 10^{-6}$	f	0.0173	0.0165	0.0160	0.0153
	$\mu_g = 1.2 \times 10^{-6}$	X	1.03	1.03	1.03	1.03
		ϕ^2	19.0	19.0	19.0	19.0
		Δp_f	411	882	1520	3270
	$\sum \Delta p_f$	(kg_f/m^2)	538	1152	1985	4264
		(MPa)	0.0053	0.0113	0.0195	0.0418

Note: ρ (kg_m/m^3), μ ($N \cdot sec/m^2$), V (m/sec)

v_{in} = specific volume of flow in inlet = $1/122\ m^3/kg$

and using Equation (2.3.16)

$$\alpha_e = \left[1 - (1 - 1/0.3)\ (125/16.5)^{-0.67}\right]^{-(125/16.5)^{-0.1}}$$
$$= 0.681$$

Hence

$$\Delta p_a = 4.88 \times 10^5\ \dot{m}^2 \quad (kg_f/m^2)$$

The acceleration pressure drop for each flow rate is shown in Table 2.3.6.

Pressure Drop due to Contraction

For a sudden contraction at the entrance of cooling channels, pressure drop Δp_c is given by

$$\Delta p_c = \left[(K + 1) - (A_2 / A_1)^2\right] \rho V_2^2/(2 g_c) \qquad (2.3.20)$$

where

A_1 = cross-sectional area of a pre-entrance region

A_2 = cross-sectional area of a narrow channel

ρ = density of saturate (or subcooled) helium liquid

V_2 = velocity at an entrance of a cooling channel

K = loss coefficient

$\simeq 0.5 \left[1 - (A_2/A_1)^2\right]$

When A_1 is much larger than A_2 $(A_2/A_1 \simeq 0)$,

$$K \simeq 0.5$$

Then Equation(2.3.20) gives

$$\begin{aligned} \Delta p_c &\simeq 1.5 \rho V_2^2/(2 g_c) \\ &= 1.5 \dot{m}^2/(2 g_c \rho A_2^2) \\ &= 1.5 \, m^2 / \left[2 \times 9.807 \times 122 \times (5.027 \times 10^{-5})^2\right]^{-1} \\ &= 2.48 \times 10^5 \, \dot{m}^2 \quad (kg_f/m^2) \end{aligned}$$

Using this result contraction pressure drop for each flow rate is calculated and shown in Table 2.3.6.

At the exit of cooling channels into a collector header slight pressure rise occurs because of sudden expansion of the two-phase flow. This pressure rise may be neglected as a design margine.

Table 2.3.6 Total pressure drop in cooling channels

$\dot{m}$ (kg_m/s)	0.002	0.003	0.004	0.006
Friction	0.054	0.115	0.199	0.426
Acceleration	0.00020	0.00044	0.00078	0.0018
Contraction	0.000099	0.00022	0.00040	0.00089
Total (kg_f/cm^2)	0.054	0.116	0.200	0.429
(MPa)	0.0053	0.0114	0.0196	0.0421

Since the total pressure drop of two-phase flow should not be greater than 0.02 MPa as shown in Table 2.3.4, the maximum flow rate of each channel is about 0.004 kg_m/sec.

The maximum length L_c of superconductor whose state-transition does not propagate to the rest of the magnet is given by

$$L_c = \frac{\dot{m}\,\Delta h}{\pi\, D\, q''_c} \qquad (2.3.21)$$

where

Δh = maximum difference between inlet enthalpy and outlet enthalpy

= 17300 - 11200 = 6100 J/kg

When $\dot{m}$ = 0.0036 kg/sec is chosen,

$$L_c = \frac{0.0036\ kg/sec \cdot 6100\ J/kg}{0.008\ m \cdot 0.2 \times 10^4\ W/m^2}$$

= 0.437 m

The corresponding heat tranfer coefficient h_{cal} is calculated as follows:

From Equations (2.3.7) - (2.3.10) we obtain

$$h_{cal} = \sqrt{h_c^2 + h_b^2}$$

$$h_b = 0.82 \text{ W/cm}^2 \text{ K}$$

and we can use the following correlation:

$$h_c = \frac{k_f}{D} \; 0.023 \; (Re_f)^{0.8} \; (Pr_f)^{0.4} \qquad (2.3.22)$$

where

k_f = thermal conductivity of liquid helium = 0.028 W/m·K

Pr_f = Prandtl number for liquid helium

$$= C_p \mu_f / k_f$$

$$\simeq \frac{5.88 \times 10^3 \text{ J/kg·K} \cdot 3.6 \times 10^{-6} \text{ N·sec/m}^2}{0.028 \text{ W/m·K}} = 0.756$$

$$Re_f = \rho_f V_f D / \mu_f$$

$$\simeq \frac{122 \text{ kg/m}^3 \cdot 0.701 \text{ m/sec} \cdot 0.008 \text{ m}}{3.6 \times 10^{-6} \text{ N·sec/m}^2} = 1.90 \times 10^5$$

Then

$$h_c \simeq \frac{0.028}{0.008} \; 0.023 \; (1.90 \times 10^5)^{0.8} \; (0.756)^{0.4}$$

$$= 1203 \text{ W/m}^2\text{·K} = 0.12 \text{ W/cm}^2\text{·K}$$

Hence we obtain

$$h_{cal} \simeq \sqrt{0.82^2 + 0.12^2} = 0.83 \text{ W/cm}^2\text{·K}$$

As expected earlier, the contribution of forced convection heat tranfer is small compared with that of nucleate boiling heat transfer.

2.4 Magnet Joints

The superconducting magnet windings are composed of sixty segments and, consequently there are sixty magnet joints which connect the segments in series. Main design requirements which the magnet joints should satisfy are as follows:

1) Electrical resistance should be small enough.
2) Ohmic heat generated in the joints should be removed efficiently.
3) Sliding movement of the magnet windings caused by thermal contraction should be accommodated in the joints.
4) Maintainability should be considered to make it practical to assemble and disassemble the magnet windings.

a. Pressure Contacts

In order to achieve low electrical resistance of the demountable magnet joints, pressure contacts will be applied. Figure 2.4.1 and Figure 2.4.2 show the end part of a magnet segment. Figure 2.4.3 shows a jumper conductor, which consists of about thirty-seven plates and is installed in a gap space between adjacent magnet segments.

Contact surface area of each joint S_c is

$$S_c = 40 \times 80 = 3200 \text{ cm}^2$$

And the total number of the contact surfaces for a whole reactor N_c is

$$N_c = 2 \times 73 \times 60 \simeq 9000$$

Hence required refrigeration power W_r is given by

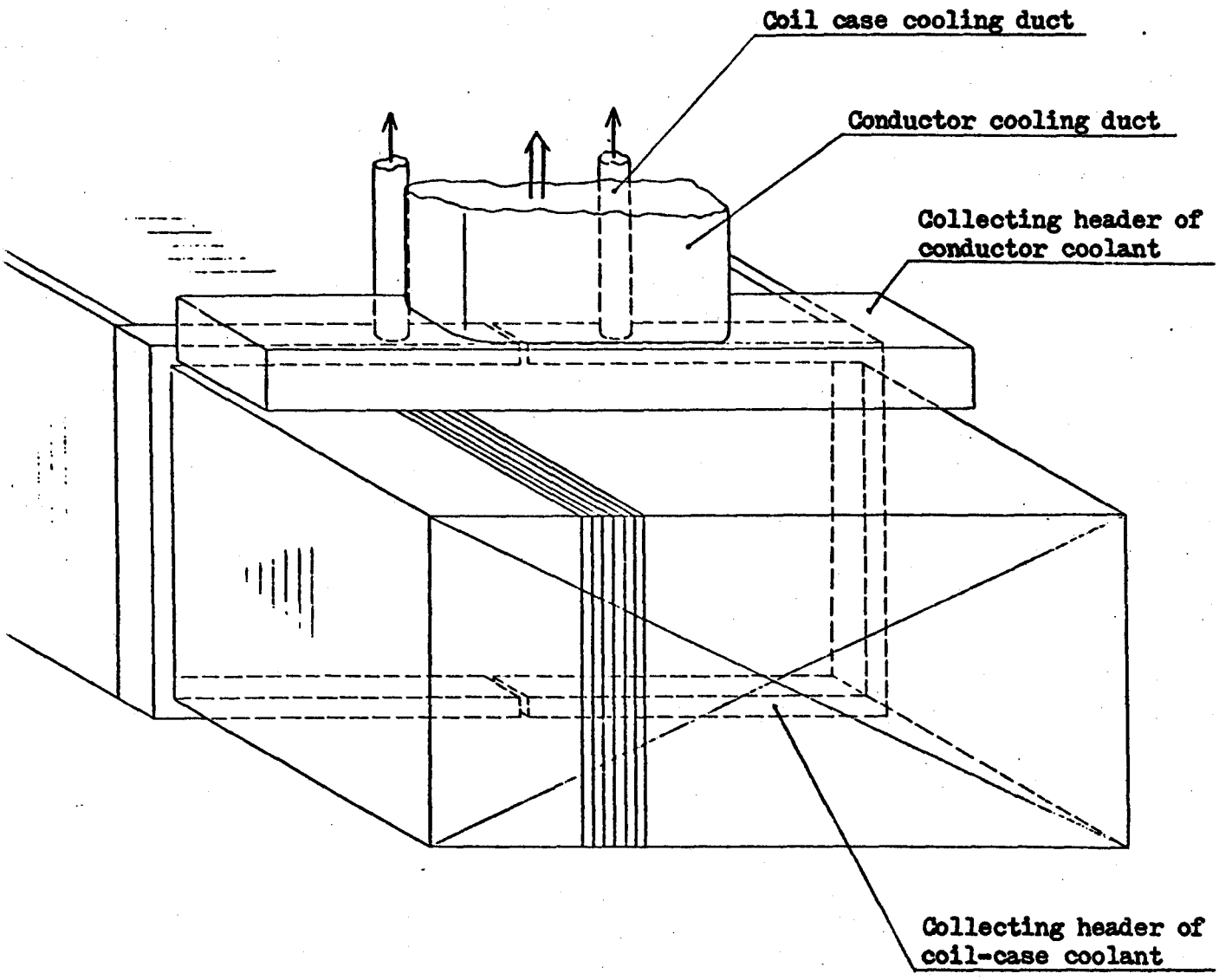

Figure 2.4.1 Structure of the end part of magnet segment

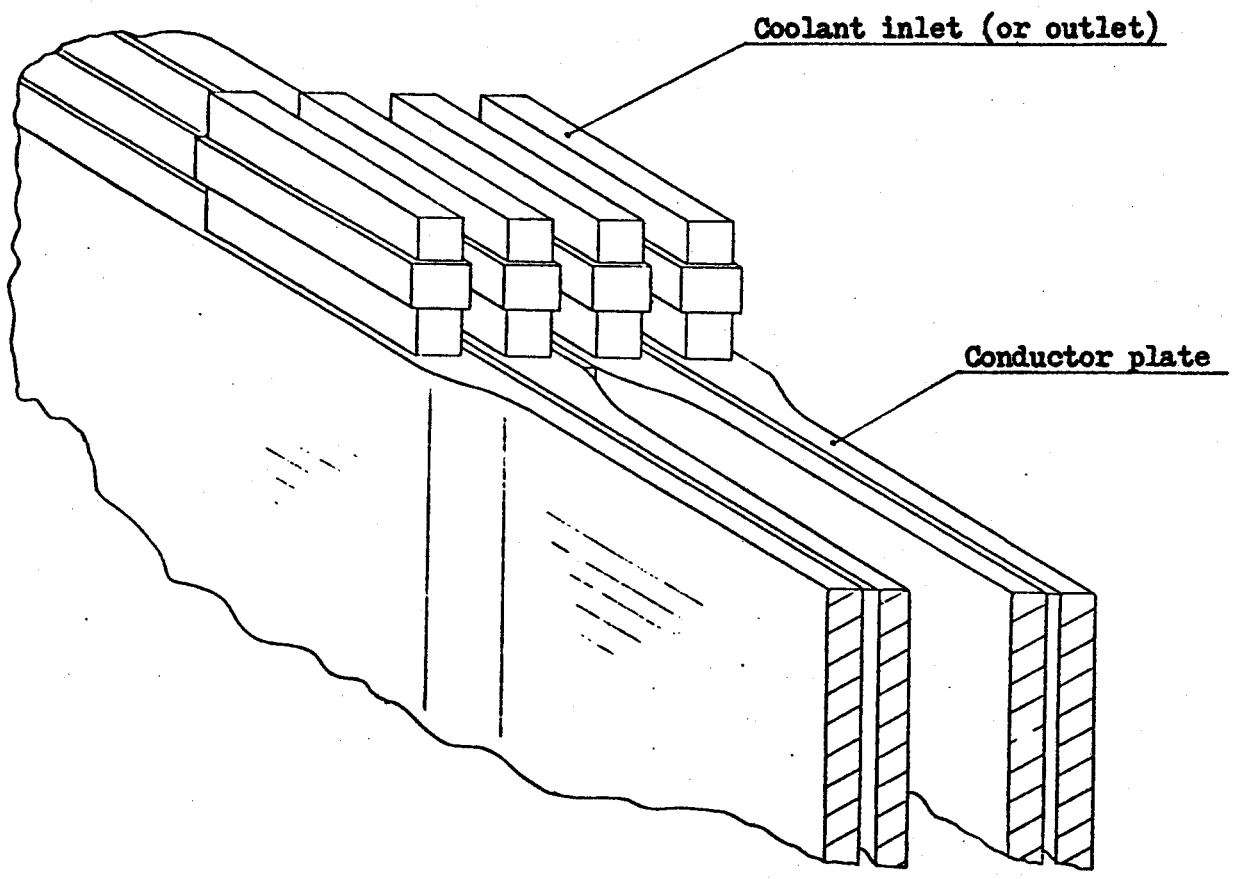

Figure 2.4.2 Structure of the end part of conductor plates

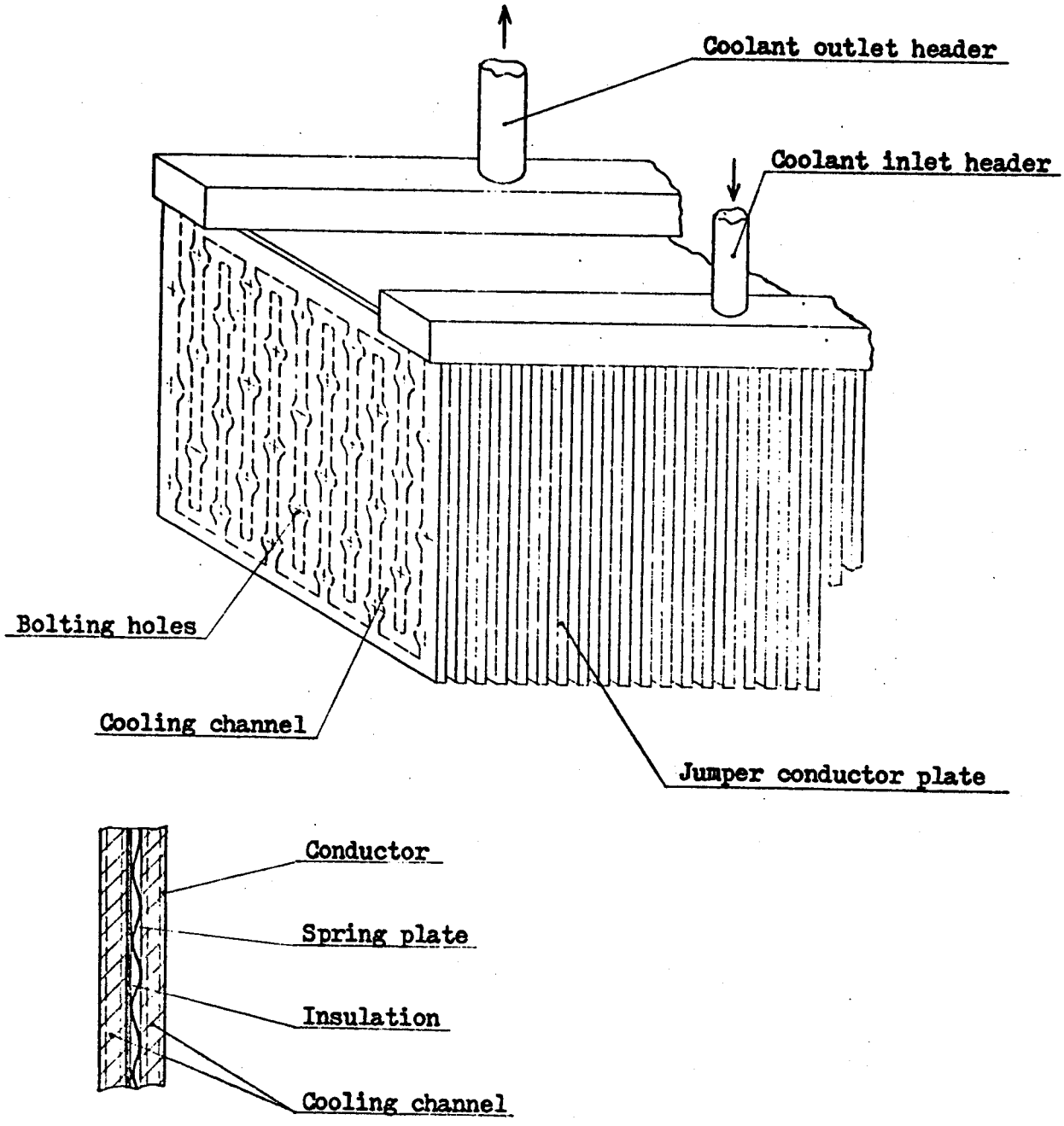

Figure 2.4.3 Jumper conductor

$$W_r = 1/C_r \, I_p^2 \left[\rho_c \cdot N_c/(\eta_c \cdot S_c)\right]$$
$$= 300 \ (5 \times 10^5 \text{ Amp.})^2 \, \rho_c \ (9000/3200 \cdot \eta_c) \qquad (2.4.1)$$
$$= 2.1 \times 10^{14} \, \rho_c / \eta_c$$

where

C_r = coefficient of performance of the refrigeration system

I_p = current in each conductor plate

η_c = ratio of effective contact area to total surface area

Using Equation (2.4.1) the required refrigeration power W_r is plotted as a function of ρ_c and η_c in Figure 2.4.4. When the effective contact area is assumed to be 50 % ($\eta_c = 0.5$) and W_c should be less than 15 MW_e (1 % of plant power output)

$$\rho_c < 3.5 \times 10^{-8} \ \text{ohm} \cdot \text{cm}^2 \qquad (2.4.2)$$

In this study $\rho_c = 1 \times 10^{-8}$ ohm·cm^2 and, as a result, $W_r = 4.23$ MW_e are assumed. Contact resistivity depends upon the magnitude of contact pressure and surface type.

Among several clamping methods, such as hydraulic clamping, various mechanical clamping, thermal clamping using a defference of thermal contraction, bolting will be most applicable under severe restrictions on an available space and maintenance procedures.

Since contact resistivity decreases with increasing contact pressure, bolting is required to be tough enough. Considering limitations of the number and size of the bolts and strength of bolt materials, obtainable contact pressure will be up to 15 MPa (2100 psi). For example, when thirty-three bolts (30 mm in diameter and 500 MPa in allowable stress) are used in [18]

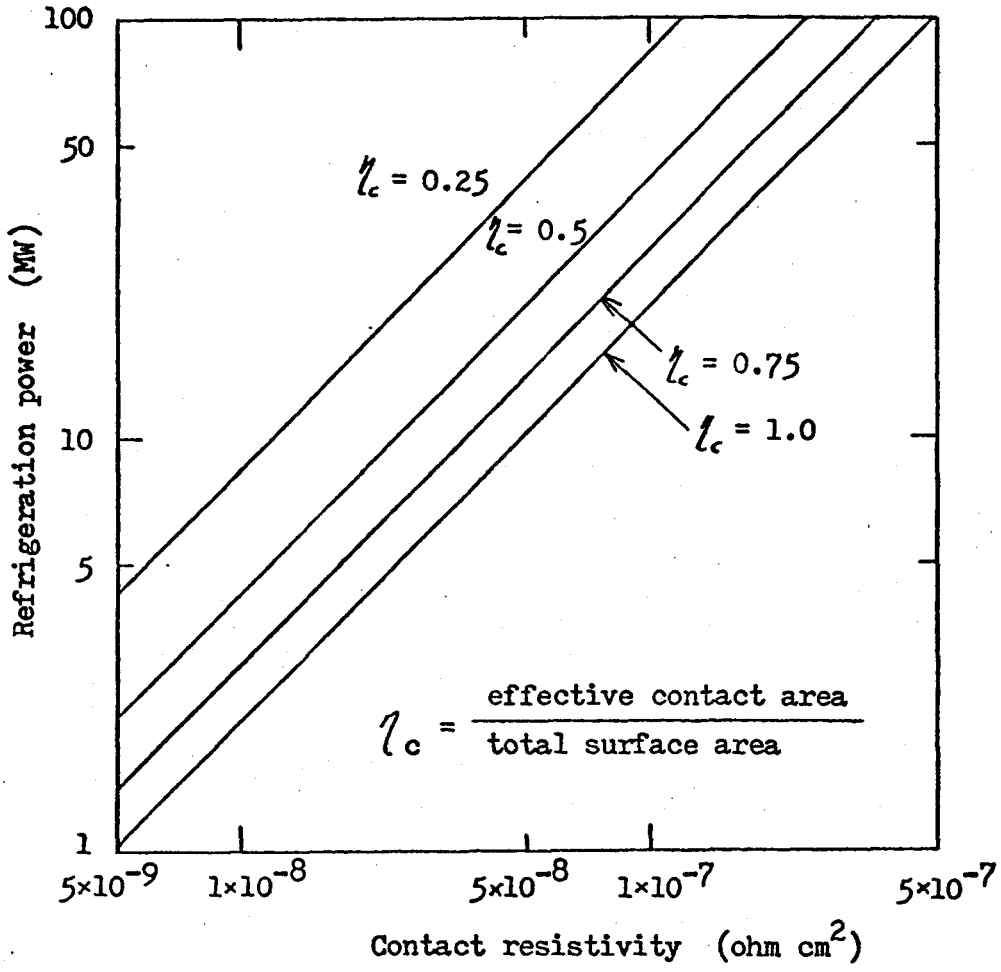

Figure 2.4.4 Refrigeration power required to cool magnet joints

each jumber conductor, maximum contact pressure is about 10 MPa (1500 psi). However, as described later, the clamping pressure is restricted to about 4 MPa (600 psi) by an additional requirement so as to allow sliding movement of conductor plates caused by thermal contraction.

According to a recent report of BNL group [17], measured resistivity of indium-coated copper surfaces is about 5×10^{-7} ohm·cm^2 at 4 MPa contact pressure. Based on this experimental result, it seems to be difficult to attain 1×10^{-8} ohm·cm^2 at 4 MPa contact pressure; however, as BNL people pointed out, substantial reduction of contact resistance is probable by further optimization of joint surfaces.

In addition, as the magnet becomes exited and gives rise to internal magnetic forces, clamping pressure is expected to reach 60 MPa (8700 psi), at which the contact resistivity will be reduced to less than 1×10^{-8} ohm cm^2. Hence no more than 4.23 MW_e refrigeration power will be needed to cool the magnet joints, at least, during reactor operation.

b. Heat Removal

Ohmic heat generated in the magnet joints is removed by helium coolant flowing in the cooling channels shown in Figure 2.4.3. With the reasonable contact resistance of 1×10^{-8} ohm·cm^2, spatially averaged power density in the magnet joints is 0.00022 W/cm^3, which is much smaller than the assumed value as a design condition for cryostability of superconductors. Thus the design requirements for heat removal in the magnet joints are similar to those for a main part of magnet segments described before.

c. Sliding Movement

Thermal contraction length of each magnet segment ΔL is

$$\Delta L = 11.5\ \text{m} \times 0.00325 = 37.4\ \text{mm} \qquad (2.4.3)$$

If this thermal contraction is restrained completely, generated stress in the copper stabilizer σ_{con} is roughly estimated to be

$$\sigma_{con} = (37.4\times 10^{-3}/11.5)\ 1.25\times 10^{4}\ \text{kg/mm}^2 \qquad (2.4.4)$$
$$= 40.7\ \text{kg/mm}^2 = 400\ \text{MPa}$$

This stress is too high compared with copper's yield stress (0.2 % yield stress = 280 MPa). Thus the magnet joints should allow sliding movement of the magnet segments.

According to experimental data[17], friction coefficient of contact surfaces is 0.5 - 0.55 for indium-coated copper and 0.35 - 0.45 for gold-plated copper, depending upon contact pressure slightly. Then the required condition to allow sliding movement is given by

$$A_{cu}\ \sigma_o < \eta_f\ P_c\ S_c \qquad (2.4.5)$$

where

A_{cu} = cross-sectional area of individual copper plates = 80 cm^2

σ_o = allowable stress of copper = 100 MPa

η_f = friction coefficient $\simeq$ 0.5

P_c = contact pressure

S_c = 3200 cm^2

Thus we obtain

$$P_c < 5\ \text{MPa}$$

This may give the reason we choose 4MPa as a design condition of clamping pressure.

2.5 Cooling-down of Superconducting Magnet Windings

Cooling-down characteristics of the superconducting magnet windings is an important factor for maintenance considerations.

For a certain region with uniform temperature we obtain the following relation:

$$Q_r = \left(\sum_i M_i C_i\right)\left(-\frac{dT}{dt}\right) + Q_l \qquad (2.5.1)$$

where

Q_r = refrigeration load

$= C_r W_r$

C_r = refrigeration efficiency or coefficient of performance

W_r = refrigeration power

M_i = mass of material (or region) i

C_i = specific heat of material i

T = temperature

t = time

Q_l = heat leak

Equation (2.5.1) can be tranformed into

$$-\frac{dt}{dT} = \frac{\sum_i M_i C_i}{Q_r - Q_l} \qquad (2.5.2)$$

from which we obtain the required cooling time Δt:

$$\Delta t = t_2 - t_1 = \int_{T_2}^{T_1} \frac{\sum_i M_i C_i}{Q_r - Q_l}\, dT \qquad (2.5.3)$$

For an arbitrary small range of temperature decrease Equation (2.5.3) can be rewritten into

$$\Delta t \simeq \frac{1}{Q_r - Q_{l,ave}} \sum_i \left(M_i \int_{T_2}^{T_1} C_i dT \right) \qquad (2.5.4)$$

where Q_r is assumed to be constant and $Q_{l,ave}$ represents the average value of heat leak. For the magnet cryostats and conductors shown in Figure 2.3.3 a) and Figure 2.3.2 respectively, the mass of each material (or region) M_i is given by

M_{cu} ≡ mass of the conductors

$\simeq (0.02 \times 0.8\ m^2 - \frac{\pi}{4} \times 0.008^2 \times 40\ m^2)\ 73 \times 11.5\ m \times 60 \times 8900\ kg/m^3$

$= 6.3 \times 10^6$ kg

M_{sus} ≡ mass of the coil case (316 SS)

$\simeq (1.79 \times 0.91 - 1.69 \times 0.81 - 0.02 \times 0.015 \times 100)\ m^2 \times 11.5\ m \times 60 \times 7900\ kg/m^3$

$= 1.3 \times 10^6$ kg

M_{ins} ≡ mass of the electrical insulators (Glass epoxy or equivalent)

$\simeq (0.003 \times 0.8 \times 72 + 0.005 \times 5)\ m^2 \times 11.5\ m \times 60 \times 2000\ kg/m^3$

$= 2.7 \times 10^5$ kg

M_{cot} ≡ mass of the container (316 SS)

$\simeq 0.01 \times (1.95 + 1.07)\ m^2 \times 2 \times 11.5\ m \times 60 \times 7900\ kg/m^3$

$= 3.4 \times 10^5$ kg

M_{sp} = mass of the supports and spacers (Glass epoxy or equivalent)

$\simeq 1 \times 200\ m^3 \times 2000\ kg/m^3 = 4.0 \times 10^5$ kg

The specific heat of each material are shown in Table 2.5.1.

Based on the above data the cooling-down rate is calculated and shown in Table 2.5.2. The result is also plotted in Figure 2.5.1.

Table 2.5.1 Specific heat at cryogenic temperature [9,19]

Temperature (K)	Copper 1)		Stainless steel 2)		Glass-epoxy 3)	
	C	$\int C\,dT$	C	$\int C\,dT$	C	$\int C\,dT$
300	0.386	79.6	0.447	81.1	0.88	132.6
200	0.356	42.4	0.384	39.2	0.62	57.6
140	0.313	22.1	0.307	18.16	0.43	26.2
100	0.254	10.6	0.216	7.56	0.31	11.4
80	0.205	6.02	0.154	3.84	0.23	6.02
60	0.137	2.58	0.087	1.43	0.14 4)	2.42
40	0.060	0.61	0.029	0.31	0.055	0.592
30	0.027	0.195	0.0124	0.110	0.024	0.202
20	0.0077	0.034	0.0045	0.0316	0.0090	0.0486
10	0.00086	0.0024	0.00124	0.00537	0.0010	0.0043
4	0.000091	0.00013	0.000382	0.000742	0.00025	0.0002

C in $kJ/kg_m \cdot K$ $\int C\,dT = \int_0^T C\,dT$ in kJ/kg_m

Note

1) A Compendium of the Properties of Materials at Low Temperature (Phase-I), PB177619 (1968)

2) Data for α-iron given in the same literature

3) Mechanical and Thermal Properties of Filamentary-reinforced Structural Composites at Cryogenic Temperature, Cryogenics Vol.15 No. 6 (1975)

4) Estimated values

Table 2.5.2 Calculation of cooling-down time

Temperature range (K)	A / B A: $\int C\,dT$ (kJ/kg$_m$) B: $M\int C\,dT$ (J)					
	Conductor	Coil case	Insulator	Container	Support & Spacer	Total
300 - 200	37.2	41.9	75.0	41.9	75.0	
	2.33 +11	5.45 +10	2.03 +10	1.42 +10	3.00 +10	3.52 +11
200 - 140	20.3	21.0	31.4	21.0	31.4	
	1.28 +11	2.73 +10	8.48 + 9	7.14 + 9	1.26 +10	1.84 +11
140 - 100	11.5	10.6	14.8	10.6	14.8	
	7.25 +10	1.38 +10	4.00 + 9	3.60 + 9	5.92 + 9	9.98 +10
100 - 80	4.58	3.72	5.4	3.72	5.4	
	2.89 +10	4.84 + 9	1.46 + 9	1.26 + 9	2.16 + 9	3.86 +10
80 - 60	3.44	2.41	3.6	2.41	3.6	
	2.17 +10	3.13 + 9	9.72 + 8	0	<1.44+9	2.72 +10
60 - 40	1.97	1.12	1.83	1.12	1.83	
	1.24 +10	1.46 + 9	4.94 + 9	0	<7.32+8	1.51 +10
40 - 30	0.415	0.200	0.39	0.200	0.39	
	2.61 + 9	2.6 + 8	1.05 + 8	0	<1.56+8	3.13 + 9
30 - 20	0.161	0.0784	0.153	0.0784	0.153	
	1.01 + 9	1.02 + 8	4.13 + 7	0	<6.12+7	1.21 + 9
20 - 10	0.0316	0.0262	0.0443	0.0262	0.0443	
	1.99 + 8	3.42 + 7	1.20 + 7	0	<1.77+7	2.63 + 8
10 - 4.2	0.00227	0.00463	0.0041	0.00463	0.0041	
	1.43 + 7	6.02 + 6	1.11 + 6	0	<1.64+6	2.31 + 7

Note 1) a + b stands for $a \times 10^b$

Table 2.5.2 (continued)

Temperature region (K)	Heat input to 80 K region (W)		Heat input to 4.2 K region (W)		Refrigeration power (MW)	
	Bulk[2] surface	Magnet[3] support	Magnet[4] support	Spacer[5]	80 K	4.2 K
300 - 200	1.43 +5	1.78 +4	0	0	15	0
200 - 140	3.77 +5	5.85 +4	0	0	15	0
140 - 100	5.22 +5	7.56 +4	0	0	15	0
100 - 80	6.09 +5	8.30 +4	0	0	15	0
80 - 60	6.38 +5	8.60 +4	790	2370	4.7	15
60 - 40	6.38 +5	8.60 +4	2380	7100	4.7	15
40 - 30	6.38 +5	8.60 +4	3620	10800	4.7	15
30 - 20	6.38 +5	8.60 +4	4030	12000	4.7	15
20 - 10	6.38 +5	8.60 +4	4580	13600	4.7	15
10 - 4.2	6.38 +5	8.60 +44	4930	14700	4.7	15

Note

2) Heat input through the bulk surface = $\frac{A_c}{L} \cdot k_{ave} \cdot \Delta T$

Where $A_c = 4200\ m^2$, $L = 0.05$ m, $k_{ave} = 0.0346$ W/m·K

$\Delta T \simeq 300 - T_{ave}$ (for $T_{ave} \geq 80$ K), $300 - 80$ (for $T_{ave} < 80$ K)

T_{ave} = average temperature in the temperature range

3) Heat input through the magnet supports (high temp. region) = $\frac{A_c}{L}\int_x^{300} k\, dT$

Where $A_c = 200\ m^2$, $L = 0.27$ m; $\int k\, dT$ given by Fig. 2.3.2 (Parallel)

$x = T_{ave}$ (for $T_{ave} \geq 80$ K), 80 (for $T_{ave} < 80$ K)

Table 2.5.2 (continue)

Temperature range (K)	Q_r (W)	Q_l (W)	$t = \frac{\sum M \int C\, dT}{Q_r - Q_l}$ (sec)	Δt (hrs)	$\sum \Delta t$ (hrs)
300 - 200	2.31 + 6	1.61 + 5	$\frac{3.52 +11}{2.31 +6 - 1.61 +5}$	45.5	45.5
200 - 140	2.31 + 6	4.36 + 5	$\frac{1.84 +11}{2.31 +6 - 4.36 +5}$	27.3	72.8
140 - 100	2.31 + 6	5.98 + 5	$\frac{9.98 +10}{2.31 +6 - 5.98 +5}$	14.8	87.6
100 - 80	2.31 + 6	7.24 + 5	$\frac{3.86 +10}{2.31 +6 - 7.24 +5}$	6.8	94.4
80 - 60	3.75 + 5	3160	$\frac{2.72 +10}{3.75 +5 - 3160}$	20.3	114.7
60 - 40	3.75 + 5	9480	$\frac{1.51 +10}{3.75 +5 - 9480}$	11.5	126.2
40 - 30	3.75 + 5	14420	$\frac{3.13 + 9}{3.75 +5 - 14420}$	2.41	128.6
30 - 20	3.75 + 5	16030	$\frac{1.21 + 9}{3.75 +5 - 16030}$	0.94	129.6
20 - 10	5.00 + 4	21000	$\frac{2.63 + 8}{5.00 +4 - 21000}$	2.52	132.1
10 - 4.2	5.00 + 4	22400	$\frac{2.31 + 7}{5.00 +4 - 22400}$	0.23	132.3

Note

4) Heat input through the magnet supports (low temp. region) = $\frac{A_c}{L}\int_x^{80} k\, dT$

Where $A_c = 200\ m^2$, $L = 0.73$ m; $\int k\, dT$ given by Fig. 2.3.2 (Parallel)

$x = 80$ (for $T_{ave} \geq 80$ K), T_{ave} (for $T_{ave} < 80$ K)

5) Heat input through spacers = $\frac{A_c}{L}\int_x^{80} k\, dT$

Where $A_c = 24.5\ m^2$, $L = 0.03$ m; $\int k\, dT$ given by Fig. 2.3.2 (Normal)

$x = 80$ (for $T_{ave} \geq 80$ K), T_{ave} (for $T_{ave} < 80$ K)

6) Refrigeration systems can produce 80 K, 20 K, 4.2 K outputs.

7) Q_l in 20 - 10 K and 10 - 4.2 K ranges includes radiation heat loads.

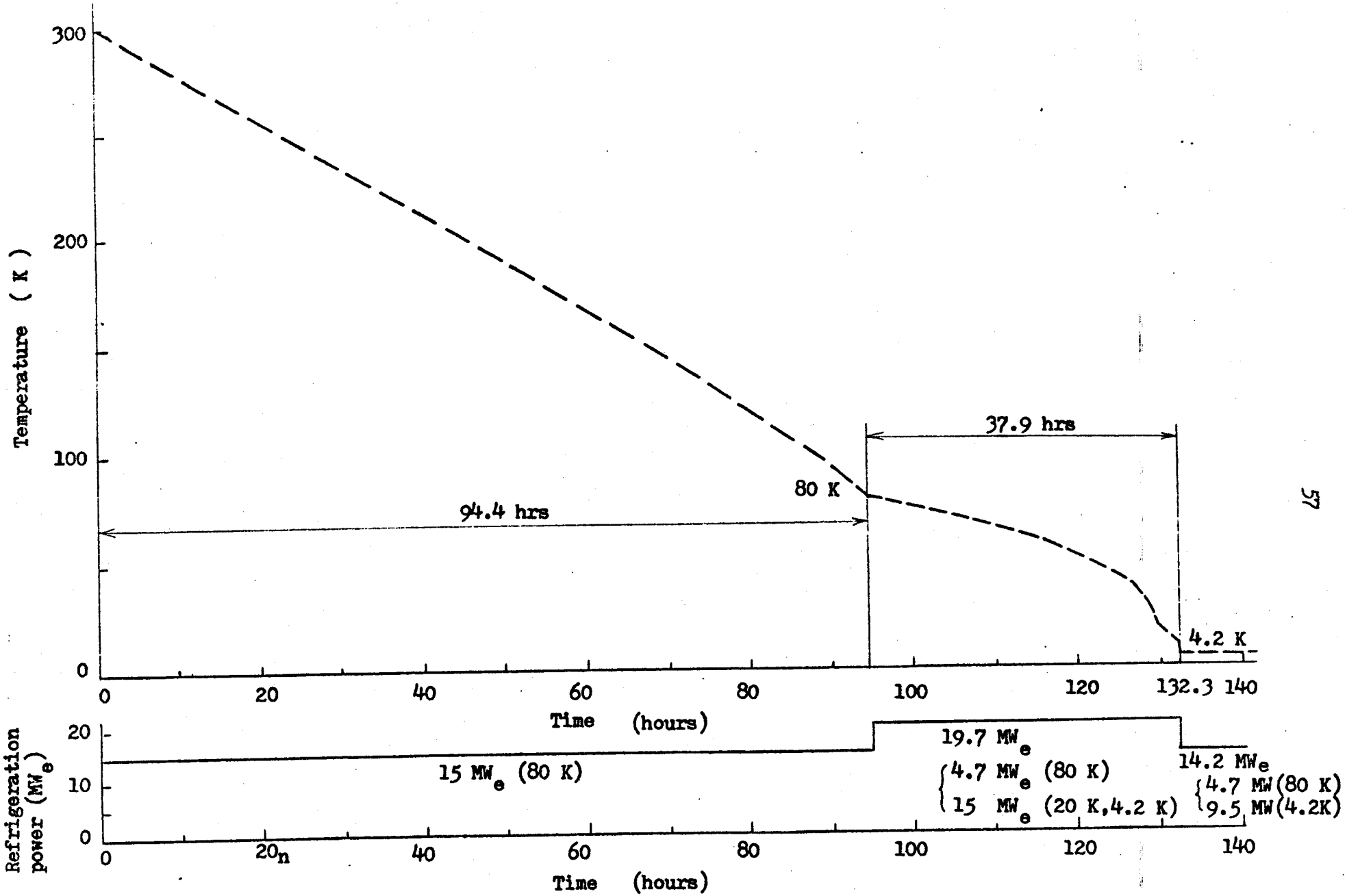

Figure 2.5.1 Cooling-down time of superconducting magnet windings

It takes about 95 hours to cool down the magnet windings from 300 K to 80 K and about 38 hours from 80 K to 4.2 K. This cooling-down rate depends upon the refrigeration power and the refrigeration efficiency. In this case the refrigeration power is 15 MW_e during cooling-down from 300 K to 80 K and 19.7 MW_e from 80 K to 4.2 K. These magnitudes of refrigeration power can not be neglected since all the refrigeration power should be supplied from other power sources before the reactor starts up. Thus the cooling-down time shown here is not expected to decrease significantly.

The refrigeration systems should have 20 K (or other intermediate temperature) coolant output in addition to 80 K and 4.2 K coolant output. Otherwise, the required time for cooling down the magnet windings below 80 K would be 7 - 8 times longer and cause a serious problem in terms of maintenance and plant availability.

So far as the cooling-down of the magnet windings is concerned, the heat transfer will not be a critical factor. This is because the required heat flux is, in general, much smaller than the maximum heat flux necessary for the cryostability of superconductors.

From a maintenance point of view, it is proposed that the most number of segments of the magnet windings be kept cool at about 80 K during a short maintenance operation. This is a necessary procedure to reduce the maintenance time to an allowable level.

3. Thermal-Hydraulic Design of Blanket

3.1 General

The principal constraints which should be considered in blanket cooling thermal-hydraulic design [20] are the following:

1) Reasonable pumping power
2) Reasonable system pressure
3) Structural integrity against high heat flux, high temperature, bombardment of plasma & ion particles and 14.1 MeV neutrons, corrosion, etc.
4) Fabricability and maintainability of blanket modules, i.e.
   - convenient and efficient blanket module shape and coolant flow path geometry for assembly and disassembly
   - reasonable number of joints and welds
   - practical pre-heating, coolant charging and discharging operation
5) Ease of tritium removal from blanket materials and coolant
6) Efficient, high temperature energy conversion
7) Practical vacuum considerations in regard to surface treatment, conductance, etc.

In addition to the above constraints the following factors in nuclear design fields and others should also be taken into account:

a) Breeding ratio
b) Multiplication of neutrons
c) Shielding
d) Tritium permiation and tritium inventry
e) Impurity problem at the first wall

In order to obtain a satisfactory tritium breeding ratio, breeding materials, as well as blanket structures, should be selected suitably. In this design liquid lithium is assumed as a breeding material. Some difficulties are expected in handling liquid lithium, although a high breeding ratio and tritium recovery are theoretically probable.

In the past various blanket cooling design concepts were presented in the world. Particularly in the early Tokamak reactor design study, liquid lithium cooled blankets were proposed; however, for the recent years helium gas cooled blankets have chiefly been investigated. In this study thermal-hydraulic analyses are done for the both cases, helium gas cooling and liquid lithium cooling.

3.2 Helium Gas Cooled Blanket

a. General

Helium gas has several outstanding advantages as well as some disadvantages for its application to fusion reactor blanket cooling.[21]

(Advantages)

1) Negligible nuclear activation
2) Chemical inertness
3) No MHD (magneto-hydro-dynamic) effects
4) Ease of handling such as charging and discharging the coolant
5) Application of HTGR (high temperature gas cooled fission reactor) technology

(Disadvantages)

1) High pressure required to achieve a sufficient heat transfer coefficient
2) Relatively high pumping power
3) Some uncertainty in heat transfer characteristics for complicated flow path geometries given by some specific blanket designs
4) Inefficient space utilization relative to liquid lithium coolant in terms of tritium breeding, heat generation, and shielding
5) Incompatibility of some kinds of structural materials (e.g. Nb, V) with helium gas containing impurity ingredients

Table 3.2.1 provides the comparison of first wall/blanket design parameters of several conceptual fusion reactor designs, including the proposed T-1 Reactor design. Figure 3.2.1 shows the examples of helium gas cooled blanket designs.

Table 3.2.1 Comparison of first wall / blanket design parameters [22-24]

	UWMAK-I	UWMAK-II	UWMAK-III	NWMAK	ORNL	PPPL	TMR	T-1
Thermal output (MW_{th})	5000	5000	5000	2097	1000	5305	2941	4340
Neutron loading (MW/m^2)	1.25	1.16	1.9	4	(0.69)	1.76	2	1.36
Blanket structural material	316 SS	316 SS	TZM	Ti-alloy	Nb-1Zr	PE-16	Inconel 718	316 SS
First wall surface material		C-curtain	C-curtain /ISSEC					
Tritium breeding material	Li	$LiAlO_2$	Li	$Li_{62}Pb_{38}$	Li	Fribe	Li	Li
Blanket coolant	Li	He	Li / He	H_2O	Li	He	He	He
Temperature Inlet/Outlet (°C)	359/489	371/650	630/900 488/870	300	996/1052	360/638	300/530	327/527
Pressure (Kg/cm^2)	29	53	5.6 / 70	88		53	50	40
Reflector	SS	C	C	Graphite				
Shielding material	$Pb/B_4C/SS$	$Pb/B_4C/SS$	$Pb/B_4C/SS$	$B_4C/Pb/W$			Concrete Fe,Pb	$Pb/B_4C/SS$

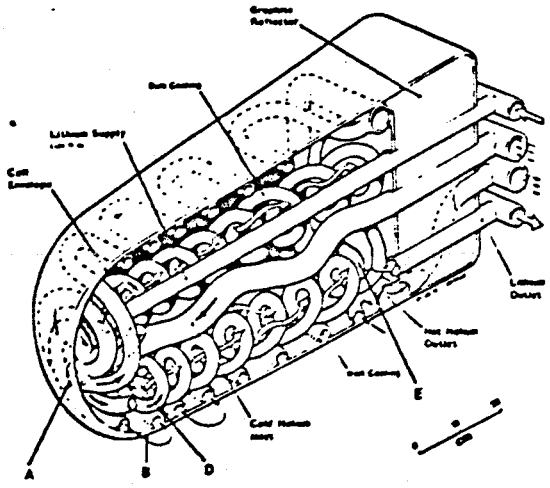

Conceptual design of helium-cooled cell for the Culham fusion reactor

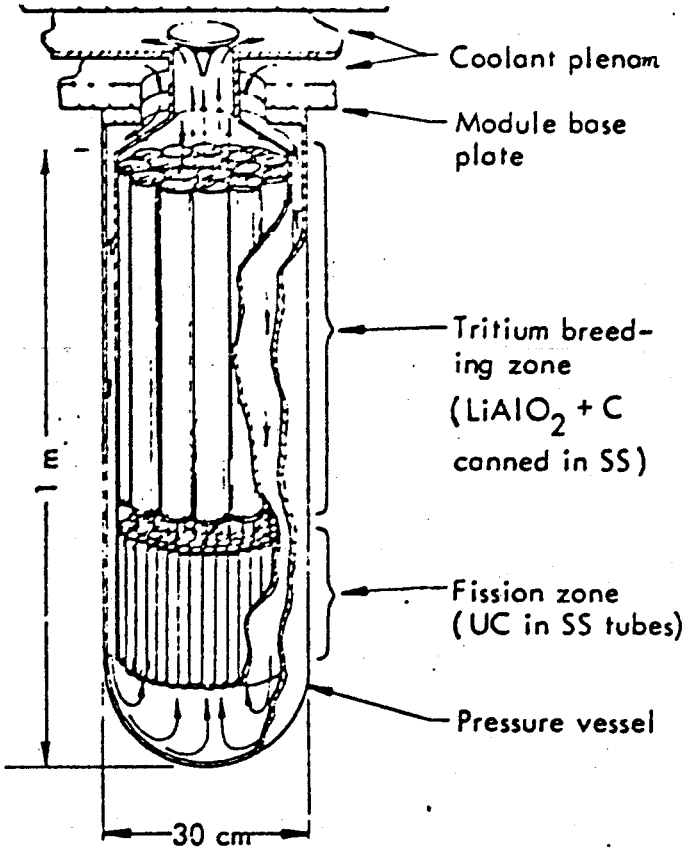

Details of the LLL fusion-fission hybrid mirror reactor conceptual design

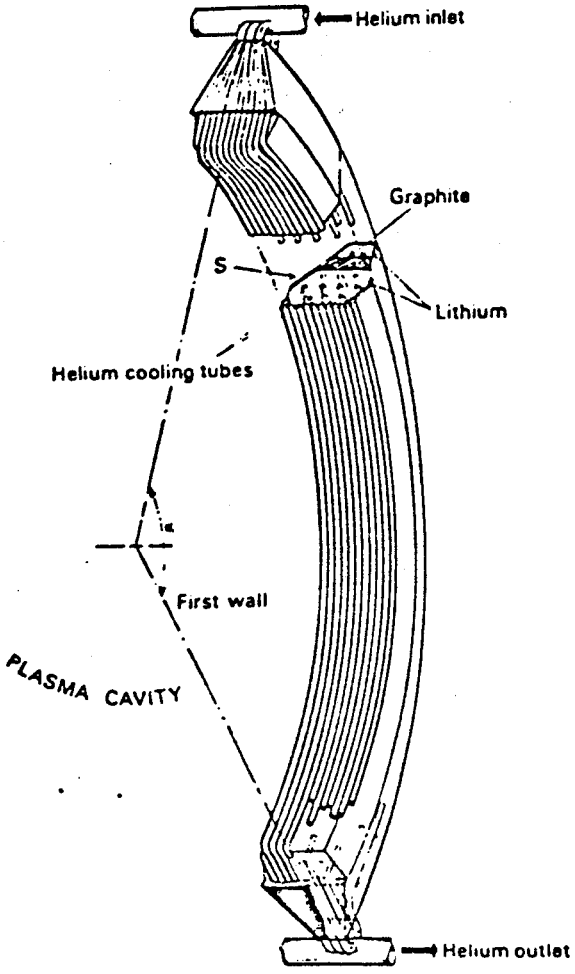

Perspective view of a module for a toroidal blanket with helium cooling (CNEN)

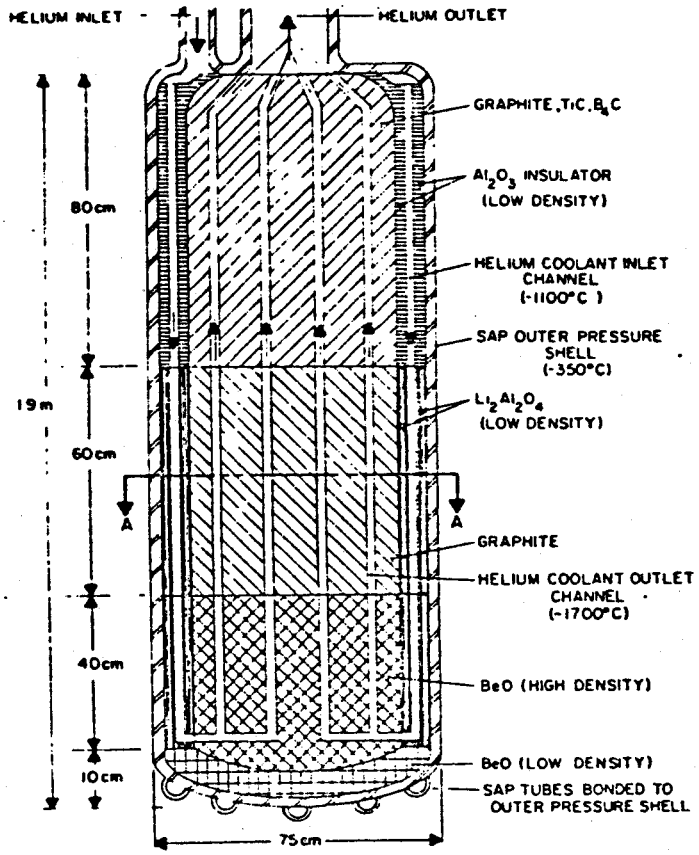

Brookhaven design of a helium-cooled blanket module having an aluminum alloy structure and a solid aluminum-lithium alloy as the fertile material

[20].

Figure 3.2.1 Examples of helium gas cooled blanket designs

b. T-1 Reactor Blanket Design

Thermal-hydraulic design parameters of the proposed T-1 Reactor blankets are given in Table 3.2.2. There are two kinds of blanket modules, Type-A and Type-B. The spatial configurations and schematic views of both types of modules are shown in Figure 3.2.2 and Figure 3.2.3, respectively.

(1) Thermal-Hydraulic Design Calculations for Type-A Blanket Modules

The bulk heat transport in each blanket module is given by

$$Q_m = \dot{M} \cdot C_p \left(T_{out} - T_{in} \right)$$

$$= \pi/4 \, D^2 \cdot \rho \cdot V \cdot N_m \cdot C_p \left(T_{out} - T_{in} \right) \qquad (3.2.1)$$

where

Q_m = heat generation rate in each blanket module

$\dot{M}$ = mass flow rate

C_p = heat capacity of the coolant (average value over the temperature range)

T_{in} = inlet temperature of the coolant

T_{out} = outlet temperature of the coolant

D = inner diameter of cooling channels

ρ = density of the coolant (average value over the temperature & pressure range)

V = velocity of the coolant

N_m = number of cooling channels in each blanket module

We can give another equation for the heat transfer through the cooling channel walls:

Table 3.2.2 Thermal-hydraulic design parameters of proposed T-1 Reactor blanket

	Type-A Blankets	Type-B Blankets / Particle collectors
Number of modules	480 per reactor 24 per sector	480 per reactor 24 per sector
Thermal loading		
Total loading	5.3 MW per module	3.8 MW per module 1.74 MW / 2.04 MW
Neutron loading	1.36 MW/m^2 (max)	0.84 MW/m^2 (max)
Coolant	Helium gas	Helium gas
Coolant temperature		
Inlet	327 °C	327 °C
Outlet	527 °C	527 °C
Coolant pressure	4 MPa (about 40 atm)	4 MPa
Coolant flow rate	5.1 Kg/sec per module	1.67 Kg/sec / 1.97 Kg/sec
Diameter of cooling channels	2.5 cm	1.13 cm / 0.83 cm
Effective heat tranfer length of cooling channels	5 m	1.8 m / 1 m
Number of cooling channels per module	50	75 / 160
Heat transfer coefficient	2960 $W/m^2 \cdot °C$	3660 $W/m^2 \cdot °C$ / 3970 $W/m^2 \cdot °C$
Film temperature drop	94°C	99°C / 123°C
Pressure drop in cooling channels	0.045 MPa	0.045 MPa
Required pumping power	40 MW	35.5 MW 13.2 MW / 22.3 MW

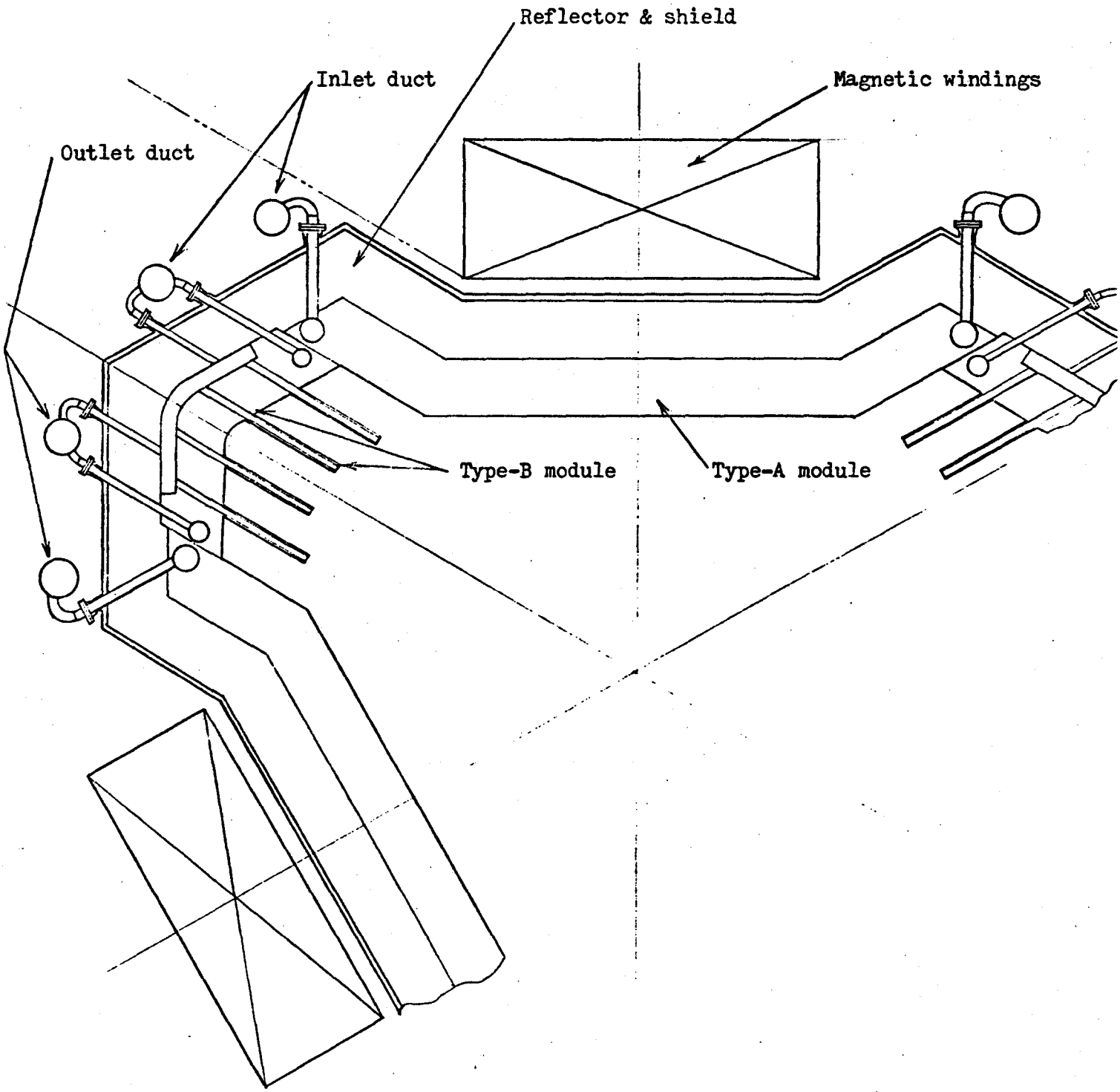

Figure 3.2.2 Cross-sectional configulations of blanket modules

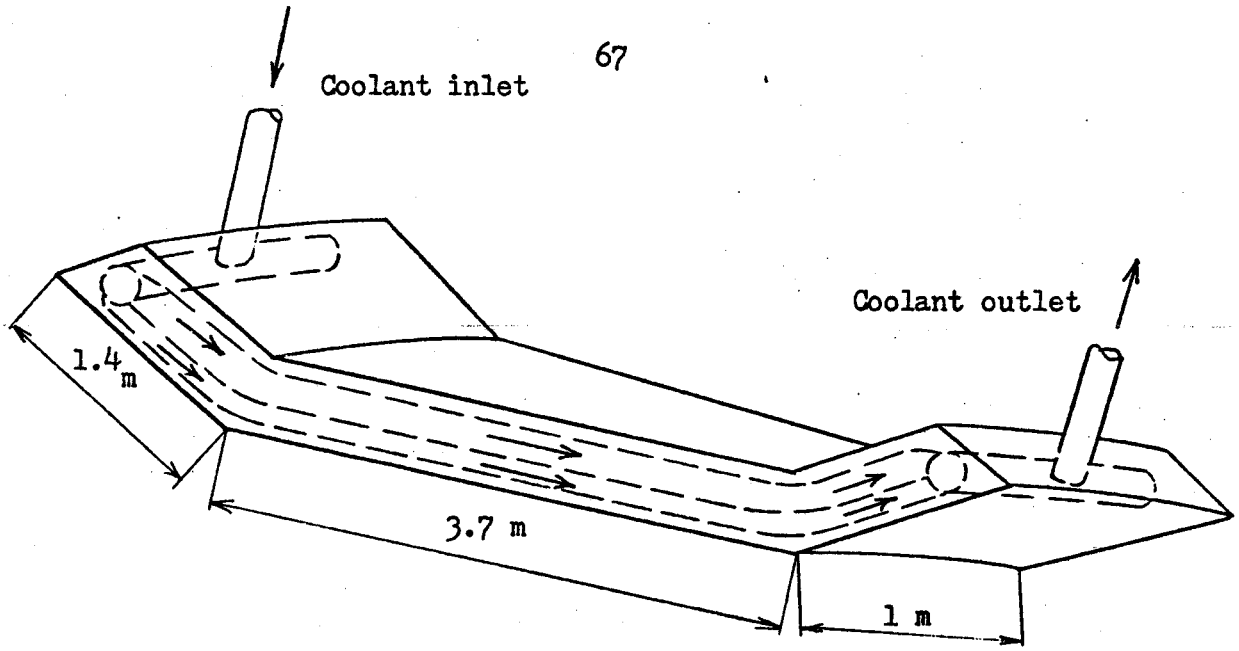

Figure 3.2.3 a) Type-A blanket module

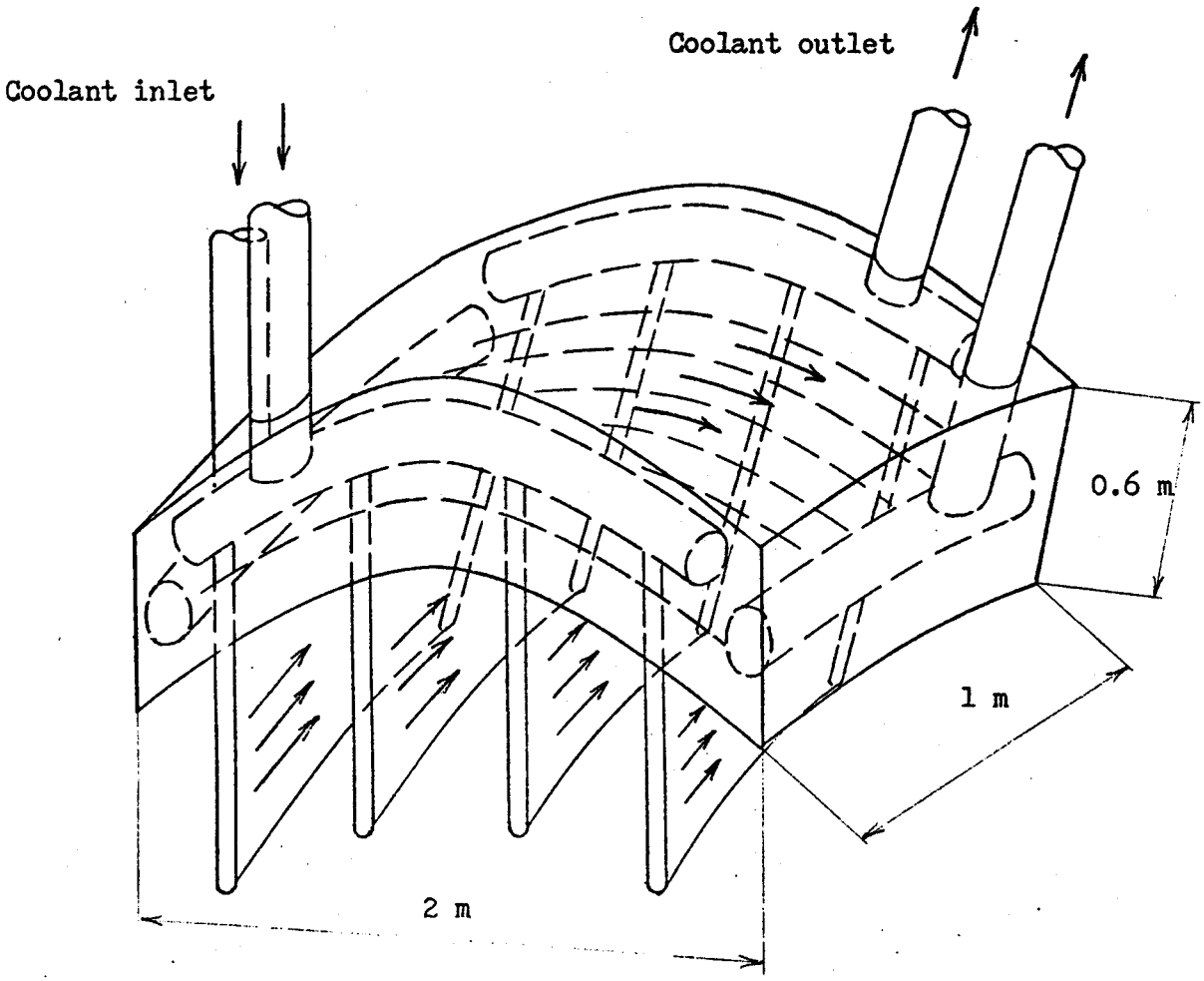

Figure 3.2.3 b) Type-B blanket/particle collector module

$$Q_m = \pi D \cdot L_c \cdot h \cdot \Delta T_f \cdot N_m$$

$$= \pi L_c \cdot Nu \cdot k \cdot \Delta T_f \cdot N_m \qquad (3.2.2)$$

where

L_c = effective length of each cooling channel

h = heat transfer coefficient

$\equiv Nu \cdot k/D$

k = thermal conductivity of the coolant (average value over the temperature range)

Nu = Nusselt number

ΔT_f = film temperature drop at the heat transfer surfaces

In regard to heat transfer characteristics we can use the following correlation:

$$Nu = 0.023\ Re^{0.8}\ pr^{0.4} \qquad (3.2.3)$$

where

Re = Reynolds number

$\equiv \rho \cdot V \cdot D / \mu$

Pr = Prandtl number

$\equiv C_p \cdot \mu / k$

When T_{in} and T_{out} are set at 327 °C and 527 °C respectively, and the system pressure p is set at 4 MPa (about 40 atmosphere), we get [25]

C_p = 5.19×10^3 J/Kg·K

k = 0.279 W/m·K

$$\mu = 3.51 \times 10^{-5} \quad N \cdot sec/m^2$$

$$\rho = 2.73 \quad kg/m^3$$

As seen in Figure 3.2.2 and Figure 3.2.3 a)

$$L_c = 5 \text{ m}$$

Then, using Equation (3.2.1)

$$\dot{M} = 5.3 \times 10^6 \text{ W} / [5.19 \times 10^3 \text{ J/Kg} \cdot \text{K} \times (527 - 327) \text{ K}]$$

$$= 5.1 \text{ kg/sec} \qquad (3.2.4a)$$

or

$$V = \dot{M} / [(\pi/4) D^2 \cdot \rho \cdot N_m]$$

$$= 2.38 / (D^2 \cdot N_m) \qquad (3.2.4b)$$

Equation (3.2.3) and Equation (3.2.2) give

$$Nu = 0.023 \, (2.73 \, V \cdot D / 3.51 \times 10^{-5})^{0.8} \, (5.19 \times 10^3 \cdot 3.51 \times 10^{-5} / 0.279)^{0.4}$$

$$= 158.6 \, V^{0.8} \cdot D^{0.8}$$

$$V^{0.8} \, D^{0.8} \, \Delta T_f \cdot N_m = 5.3 \times 10^6 / (\pi \times 5 \times 158.6 \times 0.279) = 7620 \qquad (3.2.5)$$

Substituting Equation (3.2.4b) into Equation (3.2.5) to eliminate V, we get

$$D^{-0.8} \cdot \Delta T_f \cdot N_m^{0.2} = 3810$$

or

$$\Delta T_f = 3810 \, D^{0.8} \cdot N_m^{-0.2} \qquad (3.2.6)$$

The values of ΔT_f are plotted against D and N_m in Figure 3.2.4.

Now we look into the pressure drop Δp_c in cooling channels which includes the entrance contraction-loss and exit-expansion loss.[9] Δp_c is given by

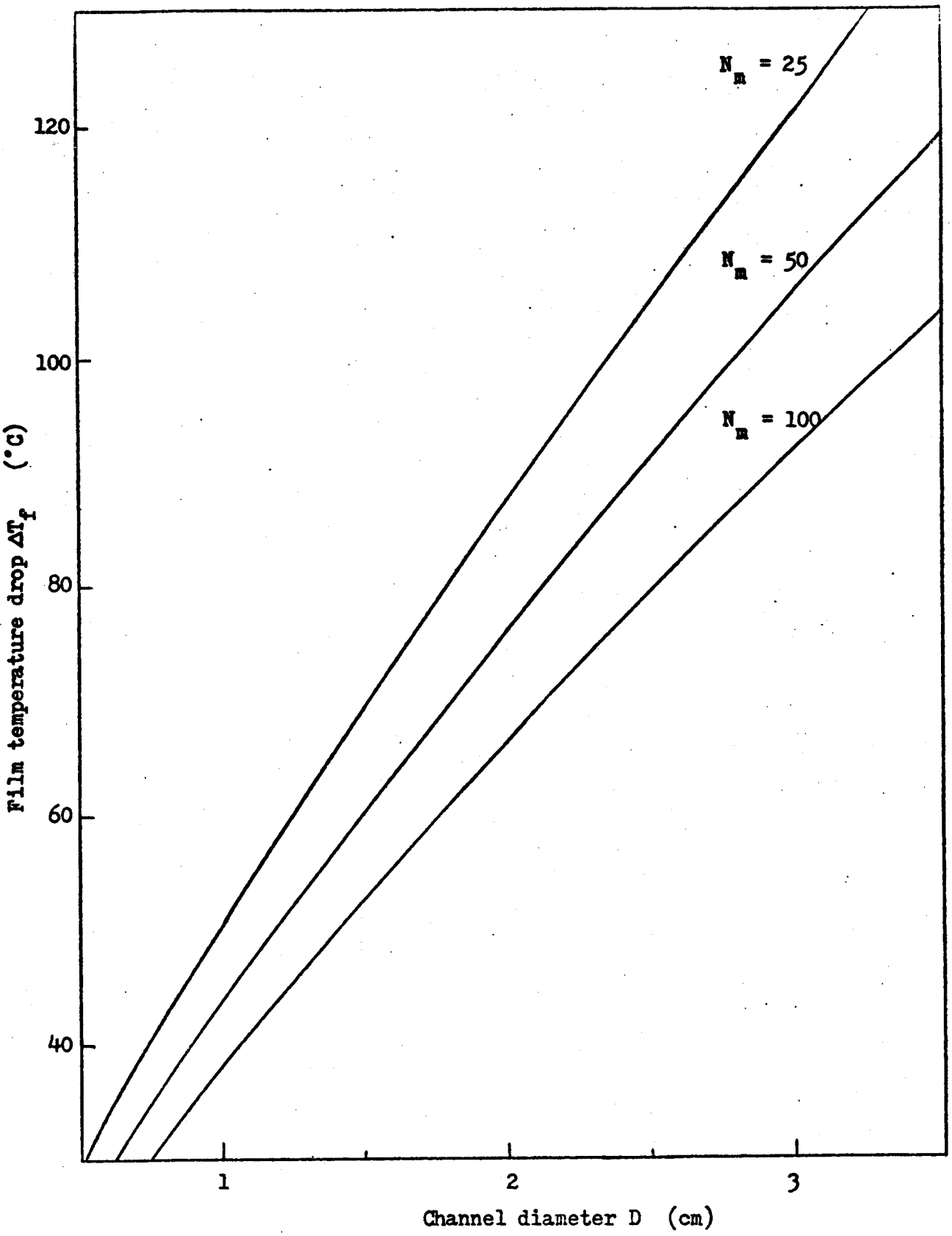

Figure 3.2.4 Film temperature drop in Type-A blanket module

$$\Delta p_c = \Delta p_f + \Delta p_a$$

$$= \left(f \cdot L/D + 4 K_{elb} + K_{con} + K_{exp} \right) \rho V^2/2 + (1/2)\dot{M}^2 \left[(\pi/4) D^2 \cdot N_m \right]^{-2} \left(1/\rho_{out} - 1/\rho_{in} \right) \qquad (3.2.7)$$

where

Δp_f = friction pressure drop

Δp_a = acceleration pressure drop

f = friction factor (given by Moody's chart depending upon the Reynolds number and a relative surface roughness)

L = length of each channel

$\simeq$ 6 m

K_{elb} = friction-loss coefficient for a 45-degree long radius elbow

K_{con} = sudden contraction-loss coefficient

$\simeq$ 0.5

K_{exp} = sudden expansion-loss coefficient

$\simeq$ 0

ρ_{in} = density of the coolant at the inlet

ρ_{out} = density of the coolant at the outlet

Substituting Equation (3.2.4b) into Equation (3.2.7), we have

$$\Delta p_c = 46.4 \, (f/D + 0.22) \, D^{-4} \, N_m^{-4} + 2.18 \, D^{-4} \, N_m^{-4}$$

$$= 46.4 \, (f/D + 0.27) \, D^{-4} \, N_m^{-4} \qquad (N/m^2) \qquad (3.2.8)$$

The corresponding pumping power $W_{p,A}$ (for the whole number of Type-A blankets only) is calculated by

$$W_{p,A} = \Delta p_c \left[(\pi/4)\, D^2 \cdot N_m \cdot 480 \right] V$$
$$= \Delta p_c \left(378\, D^2\, N_m \right) \left[2.38 / \left(D^2\, N_m \right) \right] \qquad (3.2.9)$$
$$= 897\, \Delta p_c \quad (W)$$

The values of Δp_c and $W_{p,A}$ given by Equation (3.2.8) and Equation (3.2.9) are plotted against the variable parameters, D and N_m, in Figure 3.2.5. Considering that the blanket space requires a small number of small-diameter channels and that $W_{p,A}$ is expected to be less than several percent of the total electric output of the plant, the following set of design parameters may be chosen:

$$D = 0.025 \text{ m} = 2.5 \text{ cm}$$
$$N_m = 50$$

and then we get

$$\Delta p_c = 0.045 \text{ MPa}$$
$$W_{p,A} = 40 \text{ MW}$$
$$h = 2960 \text{ W/m}^2 \text{ K}$$
$$\Delta T_f = 94 \text{ °C}$$
$$V = 76.2 \text{ m/sec}$$

The cross-sectional view of the channel arrangement in a Type-A blanket module is shown in Figure 3.2.6. The channel arrangement is based on the spatial distribution of the heat generation rate given by Figure 3.2.7. In Figure 3.2.7 a simple exponential decrease of the spatial heat generation rate is assumed with a decay constant, $\lambda \simeq 0.138 \text{ cm}^{-1}$.

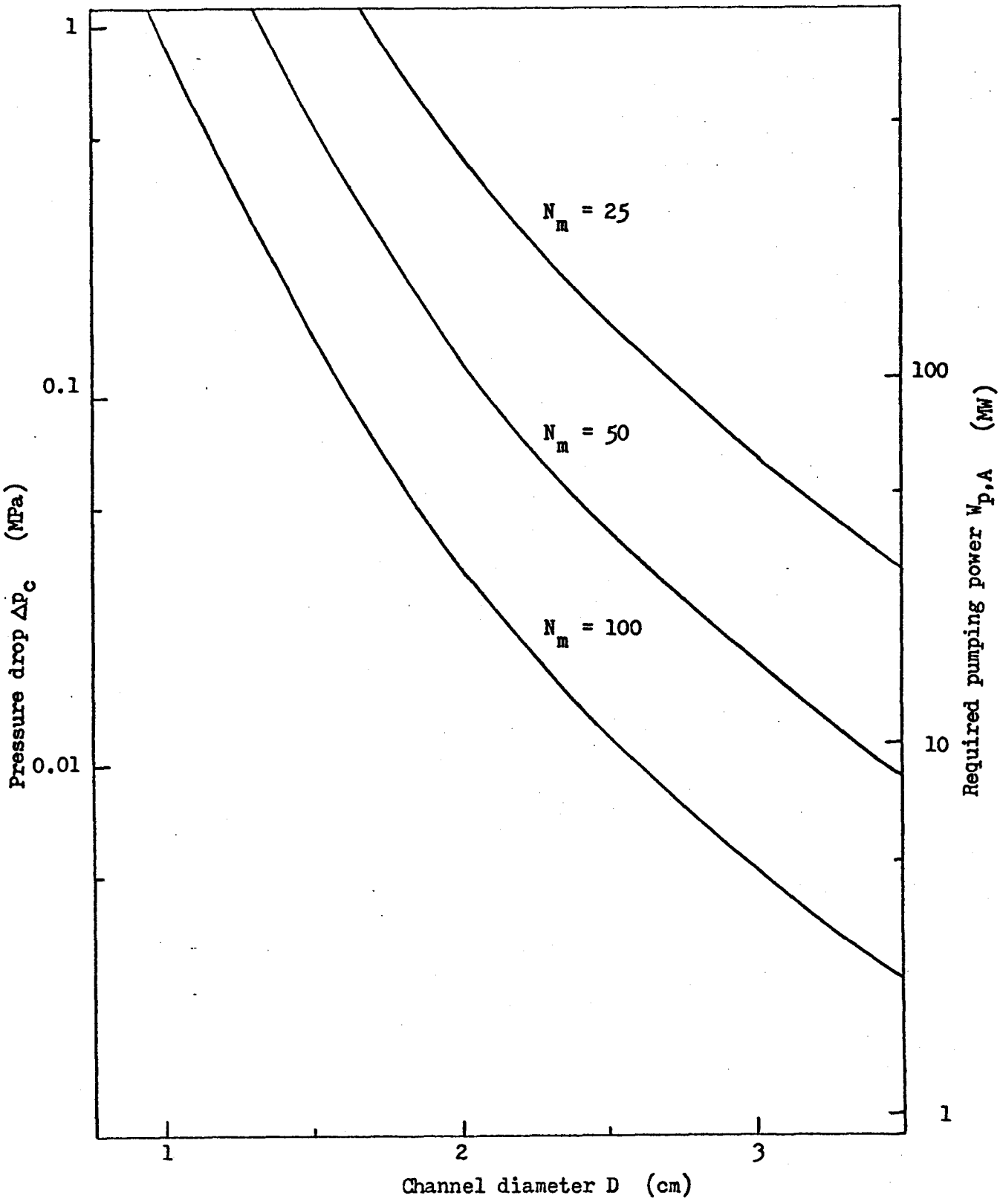

Figure 3.2.5 Pressure drop and required pumping power in Type-A blankets

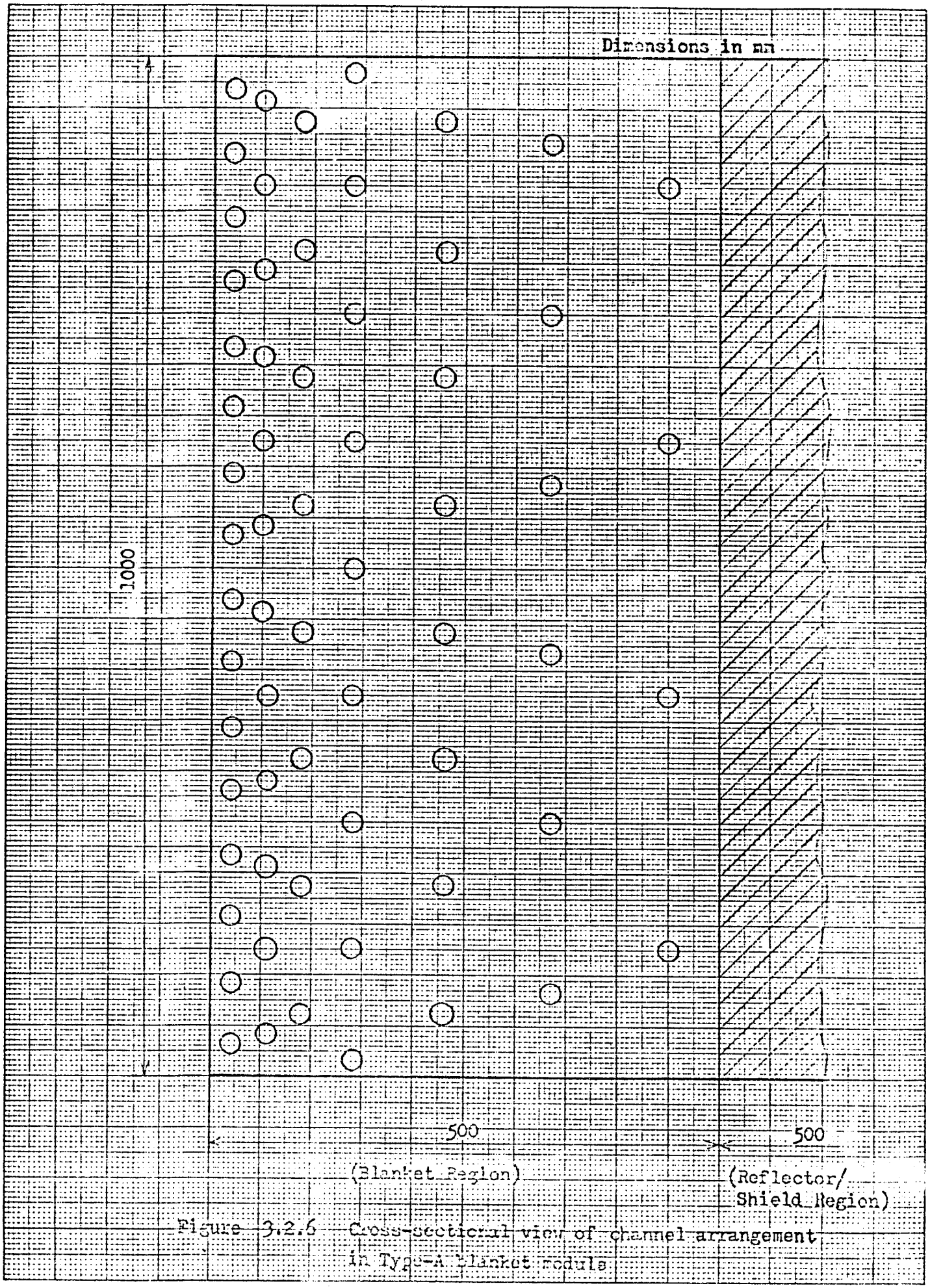

Figure 3.2.6 Cross-sectional view of channel arrangement in Type-A blanket module

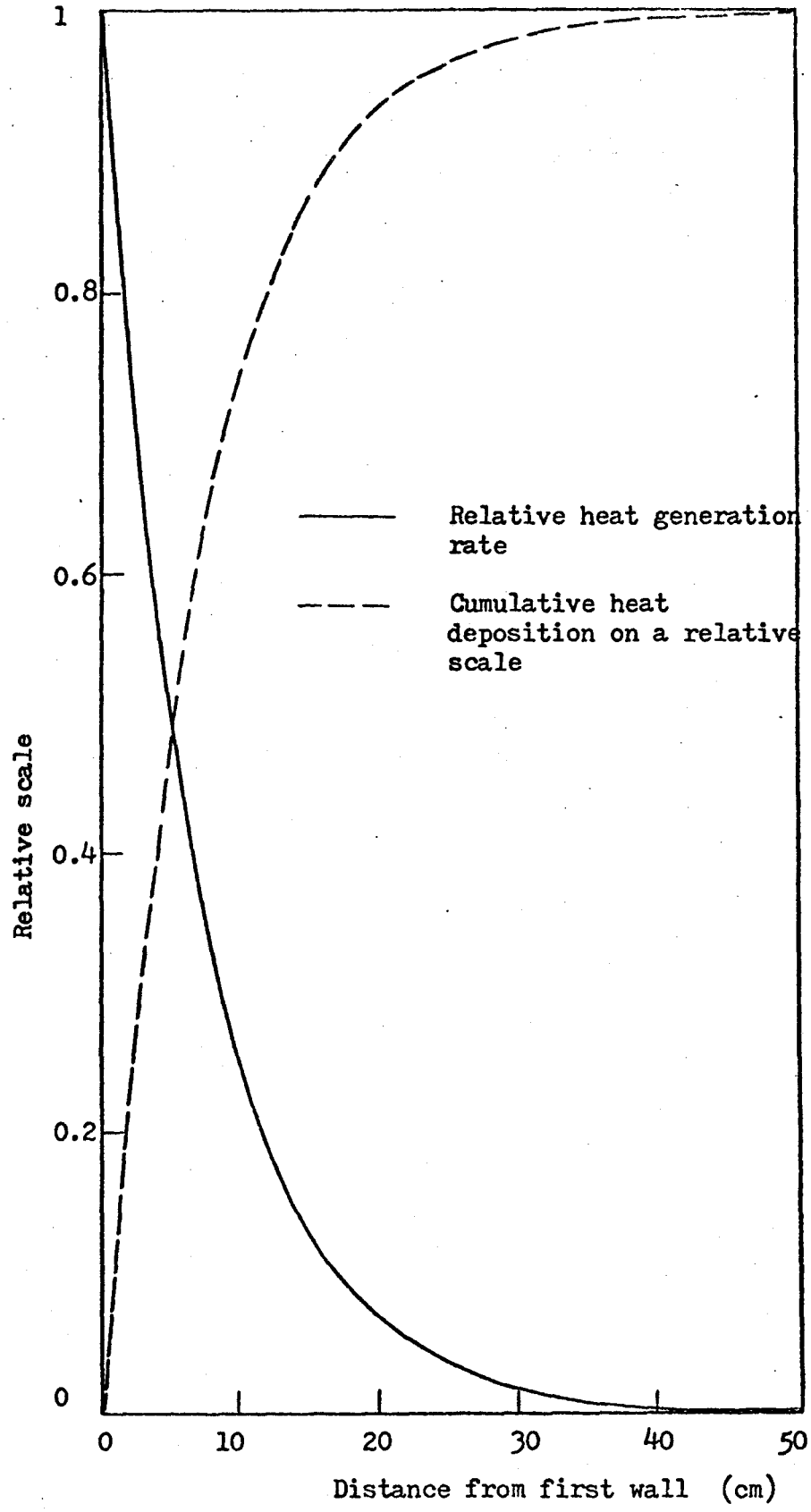

Figure 3.2.7 Spatial distribution of heat generation rate in Type-A blanket module

(2) Thermal-Hydraulic Calculations for Type-B Blanket/Particle Collector Modules

Calculations similar to those for Type-A blanket modules can be done.

a) For the blanket part we get

$$Q_m = 1.74 \text{ MW}$$
$$L_c = L = 1.8 \text{ m}$$

Equation (3.2.1) gives

$$\dot{M} = 1.74 \times 10^6 / \left[5.19 \times 10^3 \, (527 - 327)\right] = 1.67 \text{ kg/sec} \qquad (3.2.10a)$$

and

$$V = 0.779 \, D^{-2} \, N_m^{-1} \text{ m/sec} \qquad (3.2.10b)$$

From Equation (3.2.2) and Equation (3.2.3)

$$Nu = 158.6 \, V^{0.8} \, D^{0.8}$$

and

$$V^{0.8} \, D^{0.8} \, \Delta T_f \, N_m = 1.76 \times 10^6 / (\pi \times 1.8 \times 158.6 \times 0.279)$$
$$= 6950 \qquad (3.2.11)$$

Substituting Equation (3.2.10 b) into Equation (3.2.11), we get

$$\Delta T_f = 8500 \, D^{0.8} \, N_m^{-0.2} \qquad (3.2.12)$$

The values of ΔT_f are plotted in Figure 3.2.8. The pressure drop in cooling channels Δp_c can be calculated by using Equation (3.2.7).

$$\Delta p_c = 1.49 \, (f/D + 0.72) \, D^{-4} \, N_m^{-4} + 0.234 \, D^{-4} \, N_m^{-4}$$
$$= 1.49 \, (f/D + 0.88) \, D^{-4} \, N_m^{-4} \quad (N \cdot m^{-2}) \qquad (3.2.13)$$

The corresponding pumping power $W_{p,Bl}$ is given by

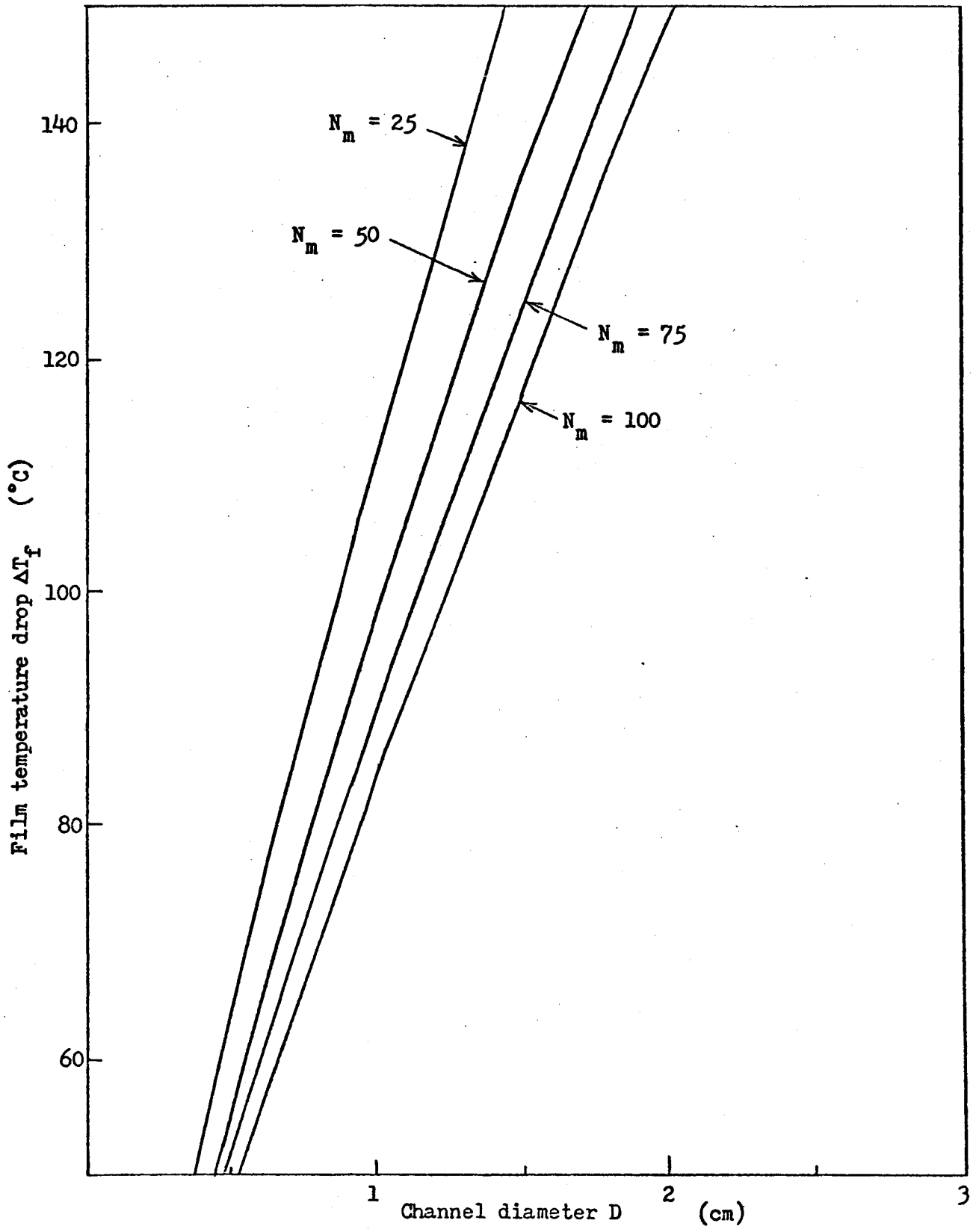

Figure 3.2.8 Film temperature drop in the blanket parts of Type-B modules

$$W_{p,Bl} = \Delta p_c \left[(\pi/4)\, D^2\, N_m\, 480\right] V$$
$$= \Delta p_c\, (120\pi D^2 N_m)\, (0.779\, D^{-2} N_m^{-1})$$
$$= 294\, \Delta p_c \quad (W) \qquad (3.2.14)$$

The values of Δp_c and $W_{p,Bl}$ are plotted with variable parameters D and N_m in Figure 3.2.9. Based on these results the following design parameters are chosen:

$D = 0.0113$ m $= 1.13$ cm

$N_m = 75$

and then we get

$\Delta p_c = 0.045$ MPa

$W_{p,Bl} = 13.2$ MW

$h = 3660$ W/m^{2}K

$\Delta T_f = 99$ °C

$V = 81.3$ m/sec

b) For the particle collector part we get

$Q_m = 2.04$ MW

$L_c = L = 1$ m

Equation (3.2.1) gives

$$\dot{M} = 2.04 \times 10^6 \,/\, 5.19 \times 10^3\, (527 - 327) = 1.97 \text{ kg/sec} \qquad (3.2.15a)$$

and

$$V = 0.919\, D^{-2}\, N_m^{-1} \text{ m/sec} \qquad (3.2.15b)$$

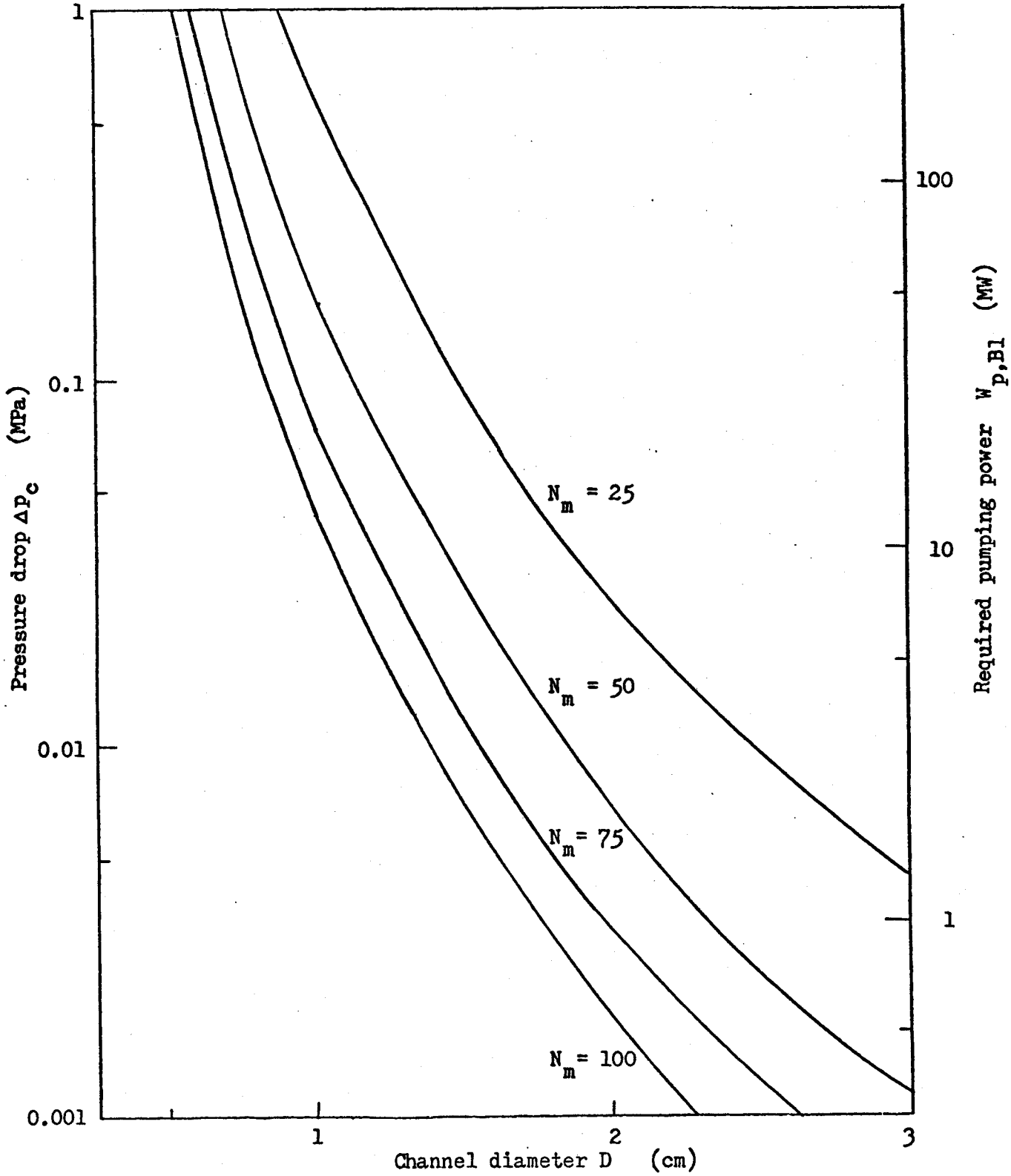

Figure 3.2.9 Pressure drop and required pumping power in the blanket parts of Type-B modules

Using Equation (3.2.2) and Equation (3.2.3)

$$Nu = 158.6\, V^{0.8}\, D^{0.8}$$

and

$$V^{0.8}\, D^{0.8}\, \Delta T_f\, N_m = 2.04\times 10^6/(\pi\times 1\times 158.6\times 0.279)$$
$$= 14700 \qquad (3.2.16)$$

Then we get

$$\Delta T_f = 15700\, D^{0.8}\, N_m^{-0.2} \qquad (3.2.17)$$

Also

$$\Delta p_c = (f\cdot L/D + K_{con} + K_{exp})\ V^2/2 + (1/2)\dot{M}^2 \left[(\pi/4)D^2 N_m\right]^{-2} (\rho_{out} - \rho_{in})$$
$$= 1.15\,(f/D + 0.5)\, D^{-4}\, N_m^{-2} + 0.325\, D^{-4}\, N_m^{-2}$$
$$= 1.15\,(f/D + 0.78)\, D^{-4}\, N_m^{-2} \quad (N/m^2) \qquad (3.2.18)$$

The corresponding pumping power $W_{p,B2}$ is given by

$$W_{p,B2} = \Delta p_c \left[(\pi/4)\, D^2\, N_m\, 480\right] V$$
$$= \Delta p_c\, (120\ D^2\, N_m)\, (1.97\, \bar{D}^2\, \bar{N}_m^{-1})$$
$$= 743\, \Delta p_c \quad (W) \qquad (3.2.19)$$

The values of ΔT_f, Δp_c and $W_{p,B2}$ are plotted against the variable parameters D and N_m in Figure 3.2.10 and Figure 3.2.11. Based on these results the following design parameters are selected:

$$D = 0.0083\ m = 0.83\ cm$$

$$N_m = 160$$

and then we get

$$\Delta p_c = 0.03\ MPa \quad < 0.045\ MPa$$

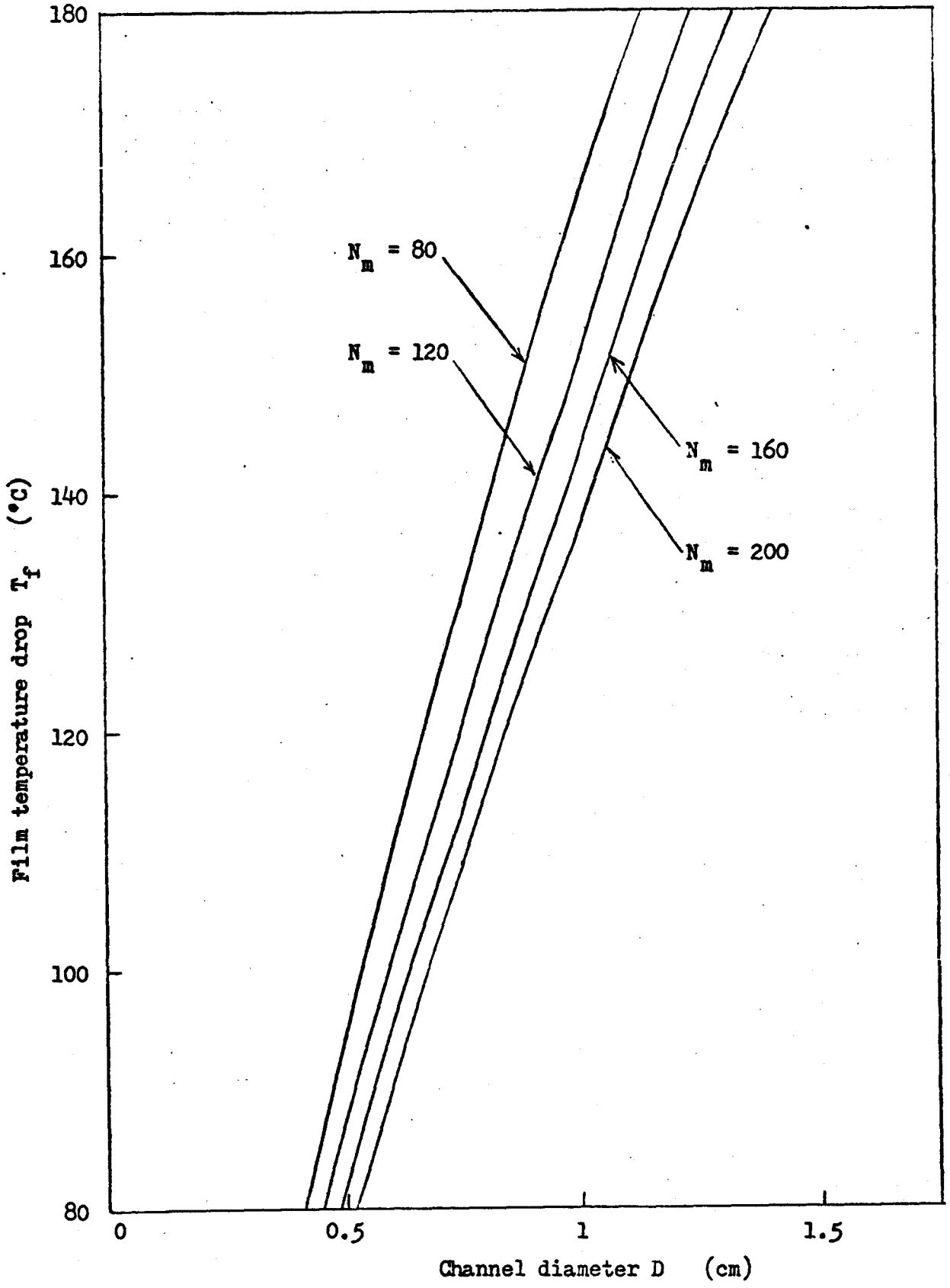

Figure 3.2.10 Film temperature drop in the particle collector parts of Type-B modules

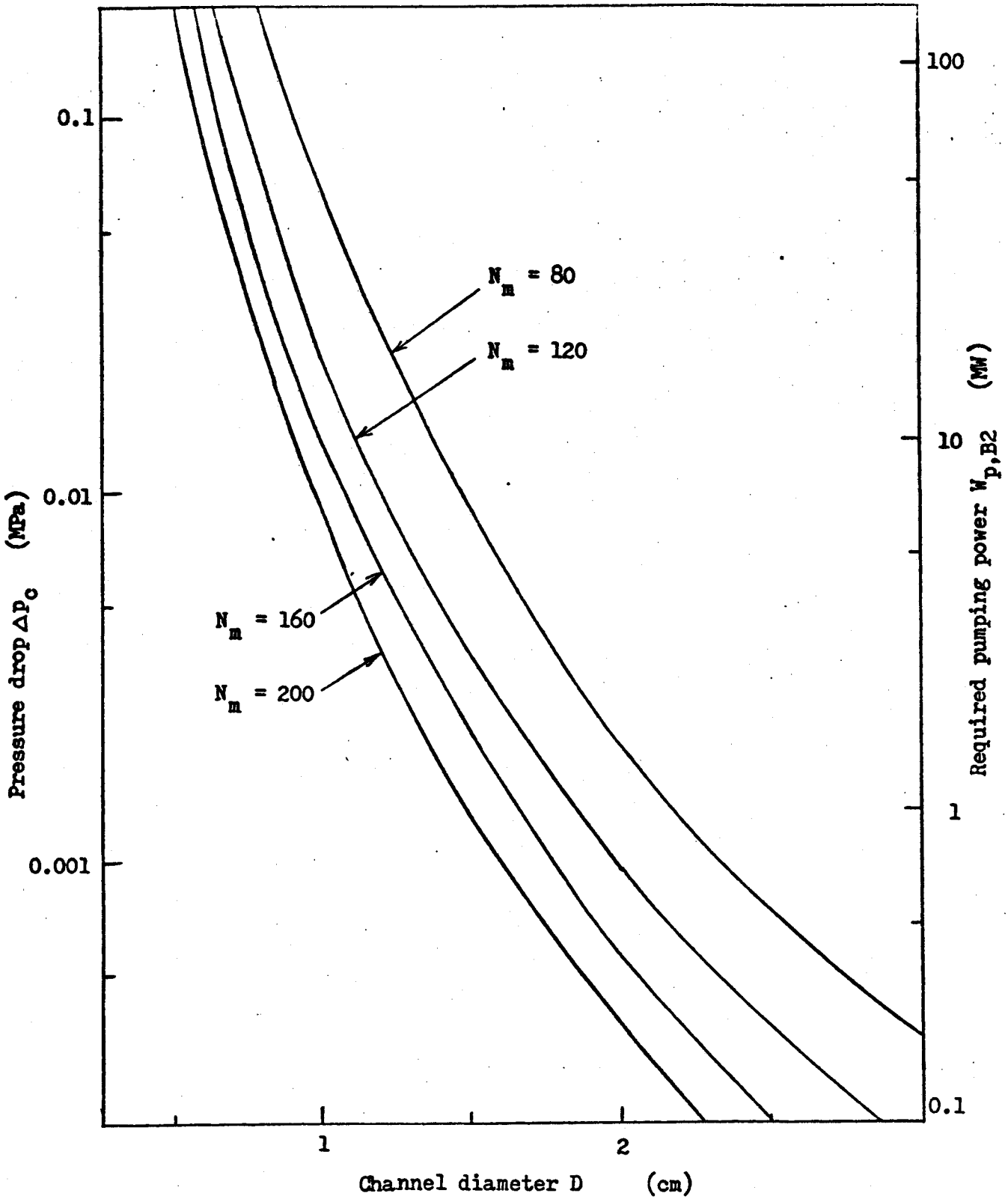

Figure 3.2.11 Pressure drop and required pumping power in the particle collector parts of Type-B modules

$W_{p,B2}$ = 22.3 MW

h = 3970 W/m^2 K

ΔT_f = 123 °C

V = 83.4 m/sec

c. Comparison of He-Gas-Cooling Design Parameters for HTGR and T-1 Reactor

Up to present high-temperature-helium-gas cooling technology has been developed for HTGRs (High Temperature Gas Cooled Reactors) [26-29] and is expected to apply to fusion reactors which have similar design conditions. Table 3.2.3 provides the comparison of helium-gas-cooling design parameters for a representative HTGR and T-1 Reactor. As this comparison implies, the proposed T-1 Reactor blanket design has the following characteristics:

1) The outlet coolant temperature is much lower than that of the HTGR. This is mainly because T-1 Reactor blanket-structures should be designed to avoid severe thermal stresses caused by its rather complicated and asymtetrical geometries.

2) Average heat flux of T-1 Reactor blankets is higher than that of the HTGR. As the result, the mass flux of T-1 Reactor is also higher than that of the HTGR.

3) The number of cooling channels of T-1 Reactor is much greater than that of the HTGR.

It seems that the blanket-structures of T-1 Reactor encounters more difficult and complicated design subjects than the HTGRs; however, this is the case in general for fusion reactors which are accompanied with severe design conditions and restrictions.

Table 3.2.3 Comparison of He-gas-cooling design parameters for HTGR and T-1 Reactor[26,27]

	HTGR (core)	T-1 Reactor (blanket) Type-A / Type-B b./ Type-B p.c.
Thermal output	3000 MW_t	4343 MW_t
Plant efficiency	39 %	(35 %)
Coolant temperature		
Inlet	336 °C	327 °C
Outlet	741 °C	527 °C
Coolant pressure	4.8 MPa (700 psi)	4 MPa (580 psi)
Coolant flow rate	1300 Kg/sec	4200 Kg/sec
Mass flux	114 $Kg/m^2.sec$	208 / 222 / 228 $Kg/m^2.sec$
Number of coolant channels	33400	24000/ 36000/76800
Diameter of coolant channels	2.096 cm	2.5 / 1.13 / 0.83 cm
Effective channel length	6.3 m	5.0/ 1.8 / 1.0 m
Average heat flux	20.4 W/cm^2	27/ 36.3/ 48.9 W/cm^2
Maximum heat flux	58.4 W/cm^2	

3.3 Liquid Lithium Cooled Blanket

a. General

Since D-T fusion reactors have the necessity of generating tritium in the blankets, liquid lithium coolant is very attractive in terms of efficient tritium breeding. In addition, lithium is a rather good moderator of 14.1 MeV neutrons and also has excellent heat transport characteristics (large thermal conductivity, etc.). However, this electrically conducting coolant encounters magneto-hydrodynamic (MHD) effects which give rise to significantly large pressure drops of the coolant and a reduced heat transfer coefficient in some cases. From a maintenance standpoint liquid lithium is considerably difficult to handle in the following respects:

1) Lithium is chemically very active: it reacts with oxygen, nitrogen, etc.. Thus, liquid lithium cooling system should be completely shut off from the air both under reactor operation and under plant shut-down for repair, maintenance, etc..

2) The melting point of lithium is 179 °C, which is much higher than that of sodium (98 °C) used as a coolant for LMFBR. Heavily equipped pre-heating system will be needed to warm up the cooling system before charging lithium coolant and also to keep the system warm enough during a reactor shut-down.

3) Lithium coolant is not compatible with a nickel ingredient in materials, so that neither stainless steels nor nickel alloys can be used for cooling tubes and other structures which contain lithium coolant.

4) Related to the above 1), lithium coolant is generally very corrosive; the corrosion gives serious effects on structural integrity and also on heat transfer characteristics (it will cause a significant reduction of heat transfer coefficient). Careful considerations are needed to keep coolant impurity

within allowable levels.

5) Generally blanket modules of a fusion reactor have rather complicated shapes and are located in various spatial positions surrounding a core regions. Thus it is very difficult (almost impossible) to charge liquid lithium through filling nozzles without leaving any gas space and also to drain liquid lithium through draining nozzles without leaving any residual lithium settling in bottom places.

b. Thermal-Hydraulic Design Considerations for T-1 Reactor

Steady state magnetic fields produce the following MHD effects [20] on a flowing electrically conducting fluid:

1) A magnetic field component transverse to the flow direction $B_\perp$ causes eddy currents to flow from the fluid through the electrically conducting walls. These so-called "Hartmann eddy currents" interact with the magnetic field to create a $\bar{j} \times \bar{B}$ body force which hampers the flow.

2) Where $B_\perp$ changes in the flow direction —— for example, it happens when the flow enters or exits the magnetic field region ——— , so-called "end-loop eddy currents" are generated. They cause an additional retarding $\bar{j} \times \bar{B}$ body force on the fluid.

3) If $B_{//}$, a magnetic field component parallel to the flow, varies along the flow direction, it also creates a $\bar{j} \times \bar{B}$ body force hampering the flow.

4) Both $B_\perp$ and $B_{//}$ tend to suppress the fluid turbulence by inducing eddy currents in turbulent flows. They cause a significant reduction of heat transfer coefficient.

Magnetic pressure drops

Magnetic pressure drop gradient of a straight flow under uniform

magnetic fields - $\left(\frac{dp}{dx}\right)$ is given by

$$-\left(\frac{dp}{dx}\right) = K_G \left[-\left(\frac{dp}{dx}\right)_{B=0} + \frac{\mu V}{a^2}\left(\frac{H_{a\perp}^2 \tanh H_{a\perp}}{H_{a\perp} - \tanh H_{a\perp}} - 3\right) + \frac{\mu V}{a^2} \cdot \frac{C}{1+C} \cdot H_{a\perp}^2 \right] \qquad (3.3.1)$$

where

$-\left(\frac{dp}{dx}\right)_{B=0}$ = friction pressure drop gradient under no magnetic field

$H_{a\perp}$ = transverse Hartmann number

$$\equiv a B_\perp \sqrt{\frac{\sigma}{\mu}} \qquad (3.3.2)$$

a = pipe radius (or the half height of a rectangular duct in the $B_\perp$ direction)

μ = fluid viscosity (average value over the temperature range)

V = fluid velocity

K_G = coefficient near unity depending upon duct cross-sectional geometry, C and $H_{a\perp}$

$\simeq$ 1.3 for a circular pipe

$$C \equiv \frac{\sigma_w t_w}{\sigma a} \qquad (3.3.3)$$

where

σ = fluid electrical conductivity

σ_w = wall electrical conductivity

t_w = effective wall thickness

In Equation (3.3.1) the first term of the right hand side presents an ordinary frictional pressure gradient, the second term accounts for

a pressure gradient due to the steepening of the velocity profile at the wall under magnetic fields, and the last term shows a pressure gradient caused by the magnetic body forces. For a high transverse Hartmann number, which is usually encountered in liquid lithium cooled fusion reactors, the last term is predominant: it is several orders of magnitude higher than the ordinary friction pressure drops. Thus the pressure drop of liquid lithium coolant in cooling channels Δp_c is approximately given by

$$\Delta p_c = L \left(-\frac{dp}{dx}\right)$$

$$= K_G \frac{L \mu V}{a^2} \frac{C}{1 + C} Ha_\perp^2 \qquad (3.3.4)$$

where

L = length of each cooling channel

Heat tranfer

According to Hoffman and Carlson, a magnetic field may completely suppress the fluid turbulence if the field strength is over a critical value:

$$Ha_\perp \geq \frac{Re}{K_1} \qquad (3.3.5a)$$

or

$$Ha_{//} \geq \frac{Re}{K_2} \qquad (3.3.5b)$$

where

Re = Reynolds number of the flow

$Ha_\perp$ = transverse Hartmann number as described in Equation (3.3.2)

$Ha_{//}$ = parallel Hartmann number

$\equiv a B_{//} \sqrt{\frac{\sigma}{\mu}}$

$K_1 \simeq 500$

$K_2 \simeq 60$

As a typical instance we may pick up the following case:

$B_\perp = 5$ T

$B_{//} = 5$ T

$a = 0.03/2 = 0.015$ m

$\sigma = 2 \times 10^6$ ohm^{-1} m^{-1}

$\mu = 2.5 \times 10^{-4}$ N·sec/m^2

In this case

$$Ha_\perp = Ha_{//} = 0.015 \times 5 \times (2 \times 10^6 / 2.5 \times 10^{-4})^{1/2}$$
$$= 6700$$

Thus the critical values of the Reynolds number Re_{cr} are given by

$Re_{cr} = 3.4 \times 10^6$ for transverse magnetic fields

$Re_{cr} = 4.0 \times 10^5$ for parallel magnetic fields

These values are much greater than the actual Reynolds number which is typically represented by

$$Re = \frac{\rho V (2a)}{\mu}$$
$$\simeq 480 \text{ Kg/m}^3 \times 1 \text{ m/sec} \times 0.03 \text{ m} / 2.5 \times 10^{-4} \text{ N·sec m}^{-2}$$
$$= 5.8 \times 10^3$$

Therefore, the flow turbulence of liquid lithium coolant will be completely suppressed and the expected heat transfer capability will be reduced to that for laminar flow of liquid lithium. According to Lyon-Martinelli's correlation [16] for low Prandtl number coolants ($Pr \ll 1$) such as liquid lithium,

$$Nu = 7 + 0.025\ Pe^{0.8} \qquad \text{(for constant heat rate)} \qquad (3.3.6)$$

where

Pe = Péclet number

$\equiv Re \cdot Pr$

Then, for the laminar flow ($Re < 2000$), Equation (3.3.6) gives the Nusselt number

$$Nu \simeq 7 - 7.6 \qquad (3.3.7)$$

This Nusselt number is a little higher than that for laminar flow of water and other ordinary fluids ($Nu = 4.364$ for the case of constant heat rate); however, the Nusselt number can be expected only in the condition of no oxygen-contamination on heat transfer surfaces. In an actual system we should expect a lower value, say

$$Nu \simeq 5 \qquad (3.3.8)$$

Thermal-hydraulic calculations

Based on the above results, i.e. Equation (3.3.4) and Equation (3.3.8), thermal-hydraulic calculations can be done as follows:

The equation on the bulk heat transport in each blanket module is given by

$$Q_m = \dot{M} C_p (T_{out} - T_{in})$$
$$= \pi/4 D^2 \rho V N_m C_p (T_{out} - T_{in}) \qquad (3.3.9)$$

which is equivalent to Equation (3.2.1) described earlier. Another equation on the heat transfer through the cooling channel walls is

$$Q_m = \pi L_c Nu k \Delta T_f N_m \qquad (3.3.10)$$

which accords with Equation (3.2.2).

When we examine thermal-hydraulic design parameters, for example, for Type-A blanket modules, the following can be reasonably assumed for T-1 Reactor:[30]

Q_m = 5.3 MW
T_{in} = 500 °C (773 K)
T_{out} = 300 °C (573 K)
ρ = 480 Kg/m^3
C_p = 4200 J/Kg·K
μ = 2.5×10^{-4} N sec/m^2
L_c = 5 m
L = 6 m
k = 37.7 W/m·K
σ = 2×10^6 ohm^{-1} m^{-1}
σ_w = 1.5×10^6 ohm^{-1} m^{-1}

Equation (3.3.9) gives

$$\dot{M} = 5.3 \times 10^6 \text{ W} / \left[4200 \text{ J/Kg·K} \quad (773 - 573) \text{ K} \right]$$
$$= 6.3 \text{ Kg/sec} \qquad (3.3.11a)$$

or

$$V = \dot{M} / \left[(\pi/4)\, D^2 \rho\, N_m \right]$$
$$= 0.0167 / (D^2 \cdot N_m) \qquad (3.3.11b)$$

From Equation (3.3.8) and Equation (3.3.10) we get

$$\Delta T_f = 1790 / N_m \qquad (3.3.12)$$

In addition, from Equation (3.3.4)

$$\Delta P_c = 1.3 \left[6 \times 2.5 \times 10^{-4}\ V / (D^2/4) \right] \frac{C}{1 + C} \left[(D^2/4)\, B_\perp^2\, \frac{2 \times 10^6}{2.5 \times 10^{-4}} \right]$$

where

$$C = (1.5 \times 10^6 \cdot t_w) / (2 \times 10^6 \cdot D/2) = 1.5\, t_w / D$$

Then

$$\Delta P_c = 1.56 \times 10^7\, B_\perp^2\, \frac{1.5\, t_w}{D + 1.5\, t_w}\, V$$
$$= 2.61 \times 10^5\, B_\perp^2\, \frac{1.5\, t_w}{D + 1.5\, t_w}\, D^{-2}\, N_m^{-1} \quad (N/m^2) \qquad (3.3.13)$$

And then we get the following required pumping power $W_{p,A}$:

$$W_{p,A} = \Delta P_c \left[(\pi/4)\, D^2\, N_m\, 480 \right] V$$
$$= \Delta P_c \left[(\pi/4)\, 480 \right] 0.0167$$
$$= 6.3\, \Delta p_c \quad (W) \qquad (3.3.14)$$

Thus Equations (3.3.11b), (3.3.12), (3.3.13), and (3.3.14) determine the thermal-hydraulic design parameters with controllable variables D, t_w, and N_m under a given transverse magnetic field $B_\perp$.

Figure 3.3.1 and Figure 3.3.2 are the results of parameter surveys based on the above equations, respectively for $N_m = 80$ and for $N_m = 100$. $\Delta p_c = 3$ MPa (about 30 atmosphere) may be far over an allowable limit, because the structures consisting of pressure boundaries against high system pressure may not cope with severe thermal stress (or thermal transient) caused by liquid lithium. In addition, the total pressure drop including the pressure losses in entrance and exit regions will be much greater than Δp_c, for example, about $1.5\,\Delta p_c$ or so. The magnitude of $B_\perp$ depends upon the flow direction relative to the direction of magnetic field vector $\overline{B}$. It is approximately estimated that

$$B_\perp \lesssim B_{max} \cos\xi$$

where

B_{max} = maximum magnetic field

ξ = pitch angle of the magnetic windings

Since $B_{max} = 8.7$ T and $\xi \simeq 42^\circ$, we get

$$B_\perp \lesssim 6.5 \text{ T}$$

Thus it is reasonably assumed that

$$B_\perp \simeq 5 \text{ T}$$

Under the conditions of $\Delta p_c \leq 3$ MPa and $B_\perp \simeq 5$, Figure 3.3.1 and Figure 3.3.2 indicate the following design limitations:

for $N_m = 80$

$D \geq 4.3$ cm at $t_w = 2$ mm (O.D. ≥ 4.7 cm)

$D \geq 4.9$ cm at $t_w = 3$ mm (O.D. ≥ 5.5 cm)

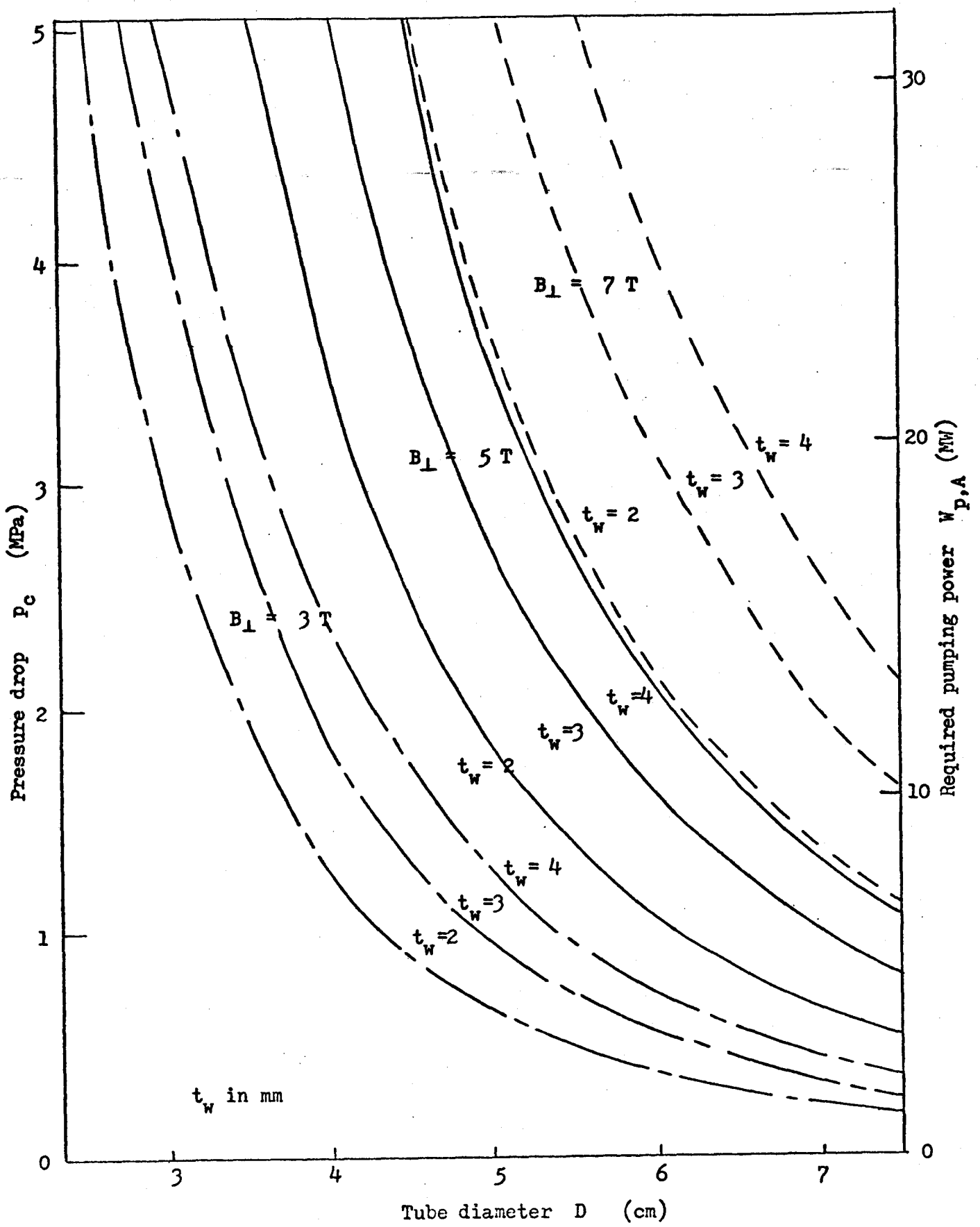

Figure 3.3.1 Pressure drop and required pumping power in Type-A liquid Li cooled blanket with N_m = 80

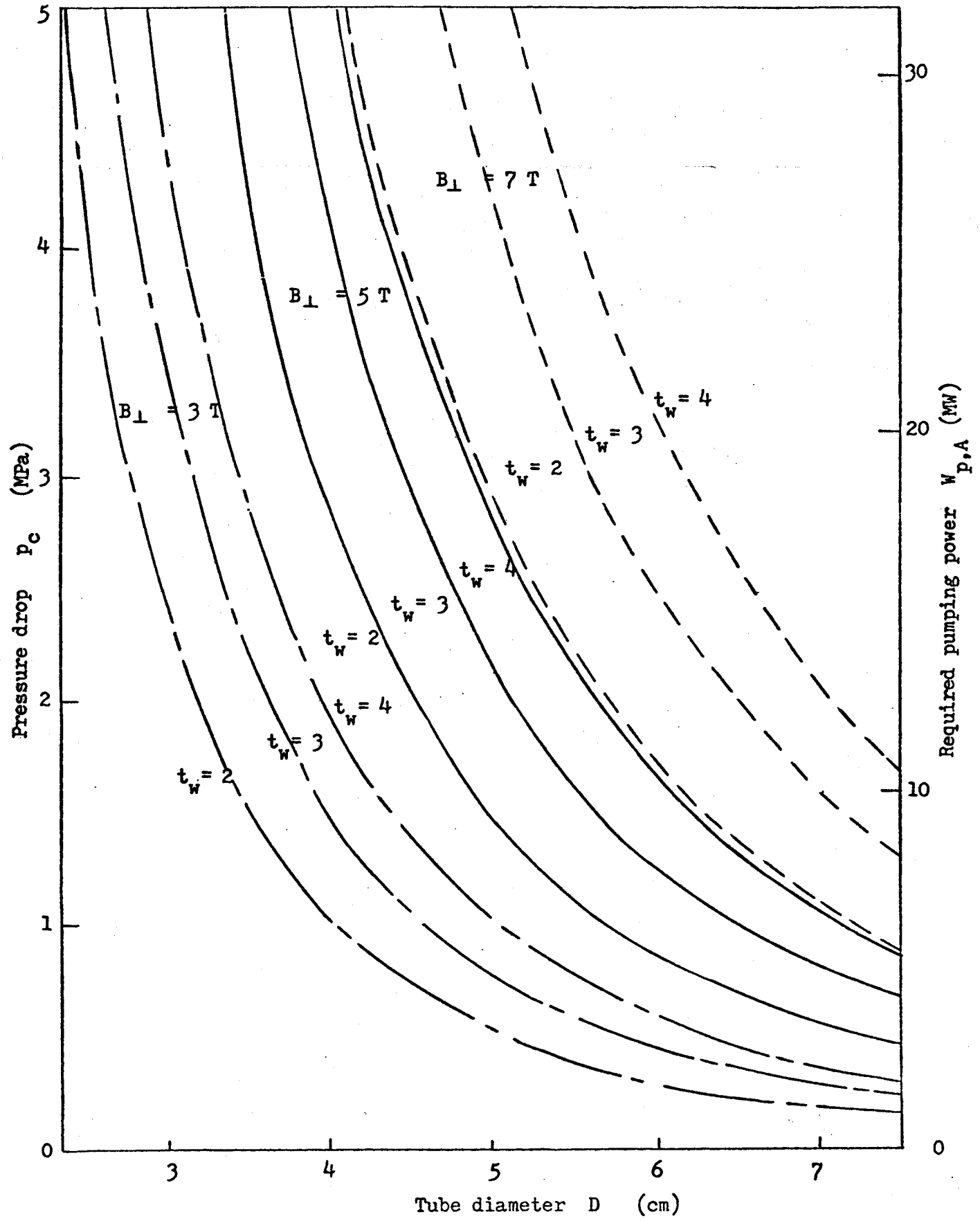

Figure 3.3.2 Pressure drop and required pumping power in Type-A liquid Li cooled blanket with N_m = 100

for $N_m = 100$

$D \geq 3.9$ cm at $t_w = 2$ mm (O.D. ≥ 4.3 cm)

$D \geq 4.4$ cm at $t_w = 3$ mm (O.D. ≥ 5.0 cm)

On the other hand, Figure 3.3.3 shows the cross-sectional view of tube arrangement in a Type-A blanket module which has about 100 tubes ($N_m \simeq 100$) with an outer diameter (O.D.) of 3.5 cm. This tube arrangement is based on the spatial distribution of heat generation rate in the lithium-filled blanket shown in Figure 3.3.4.

As Figure 3.3.3 implies, the required tube diameters are too large to accept. Additionally, since the tube number $N_m = 100$ is almost an upper limit (or already beyond allowance), we can not expect to reduce the tube diameter by increasing the number of tubes. This unacceptable design limitation is obviously due to a large magnetic pressure drop, which mainly depends upon $B_\perp$. In T-1 Reactor it is impractical to find the special configuration and geometry for blanket modules and cooling channels which will provide significantly smaller $B_\perp$ because of its complicated vessel shape and other restrictions such as assembly & disassembly requirements, spatial limitation for entrance & exit ducting.

As a result of this study we have to conclude that liquid lithium cooled blankets may not be introduced to T-1 Reactor, at least, on the basis of present technology. If, in the future, some way is found to produce electrically insulating walls or coatings (on the inside surfaces of tubes) which are compatible with liquid lithium and other severe operating conditions, this blanket cooling concept will be reconsidered as an attractive one with all some other difficulties described earlier.

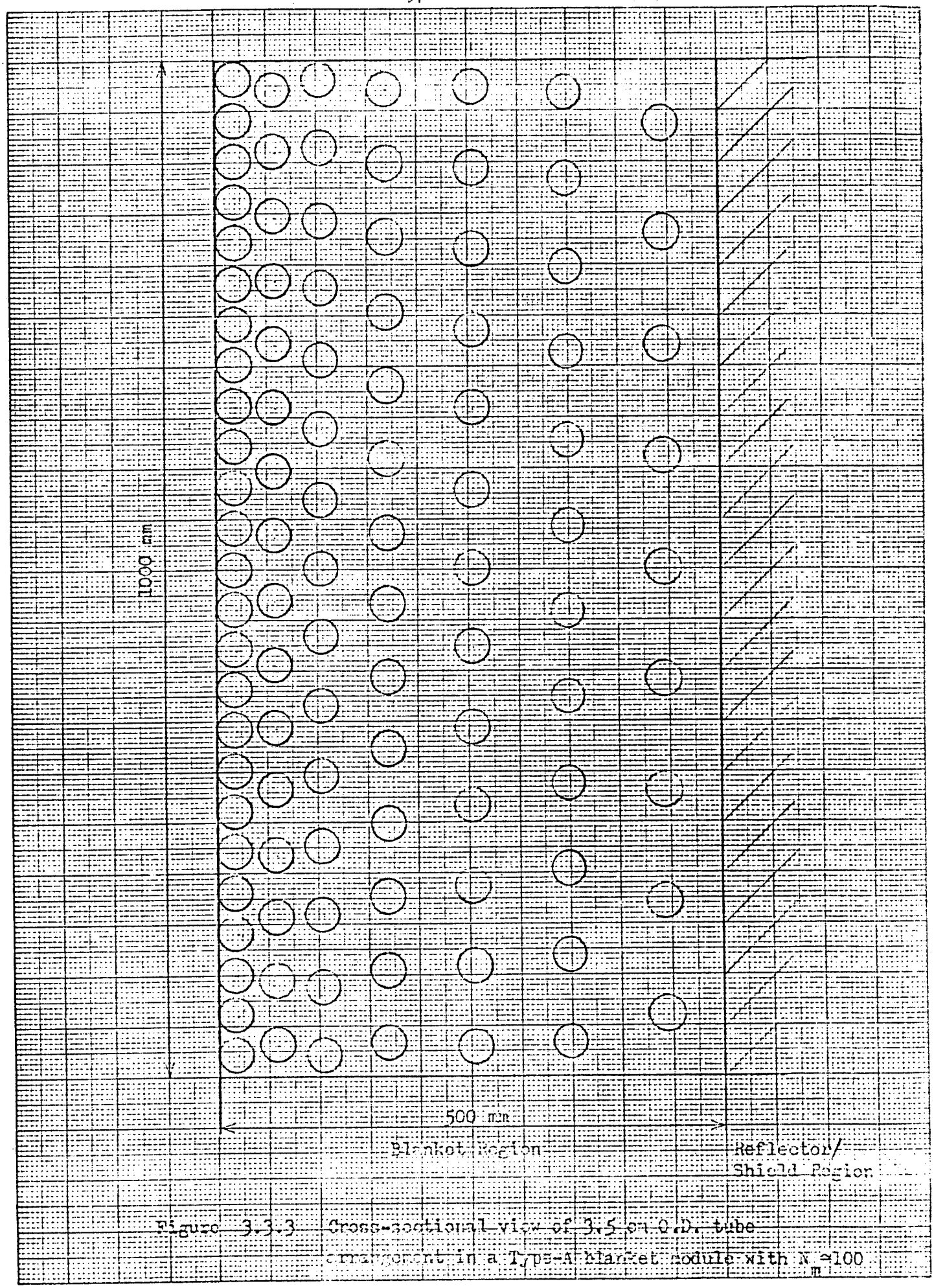

Figure 3.3.3 Cross-sectional view of 3.5 cm O.D. tube arrangement in a Type-A blanket module with $N_m \simeq 100$

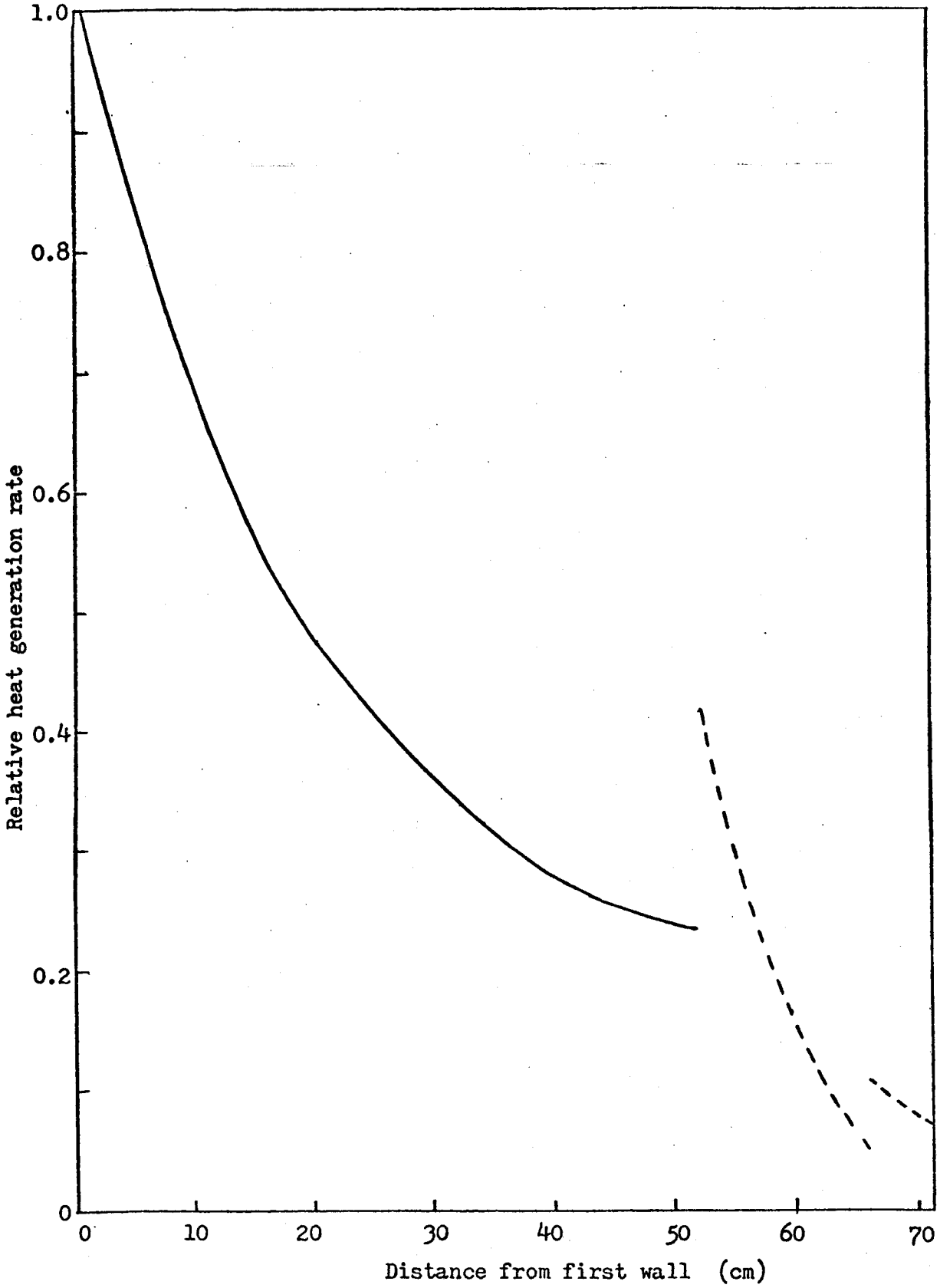

Figure 3.3.4 Spatial distribution of heat generation rate in the blanket (from reference 31)

4. Design of Vacuum / Exhaust System

4.1 Vessel Evacuation

a. General Considerations

Fusion reactors require high vacuum atmosphere. The density of impurity particles, in general, should be two or three orders of magnitude less than plasma density; the plasma density under stable reactor operation is about 2×10^{20} m^{-3} in T-1 Reactor. Considering starting-up conditions of plasma reactions, the vacuum vessel should be pumped down to 10^{-7} torr (about 3×10^{15} m^{-3} at 300 K) prior to reactor operation.

In order to obtain this high vacuum level in T-1 Reactor careful considerations are required in design, material selection, fabrication and maintenance of the reactor. More specifically we must pay attention to the following:

1) Material should satisfy strict specifications on the fabrication procedures, such as furnece process, degassing process, forging and rolling operations.
2) Welding methods should be examined carefully in order not to make welded parts high out-gassing sources.
3) Surface treatment of inner structures should be done with elaborate procedures.
4) Reliable sealing should be provided to avoid vacuum leak in vessel joints, various types of port joints, shut-off valves, welded lines. etc..
5) The inside of the vacuum vessel should be kept as clean as possible

throughout construction (including fabrication, installation, inspection, transportation, etc.), operation, and maintenance.

b. Vacuum Pumping Requirement

Pumping capacity, or pumping speed, required for the vessel evacuation is evaluated as follows:[32]

$$Q = P \cdot S_e \qquad (4.1.1)$$

where

Q = gas flow (torr·liters/sec)

P = pressure (torr)

S_e = effective pumping speed (liters/sec)

$$\frac{1}{S_e} = \frac{1}{S_p} + \frac{1}{C} \qquad (4.1.2)$$

where

S_p = required pumping speed (liters/sec)

C = conductance between the evacuated space and a pump suction

and

$$Q = Q_1 + Q_2 \qquad (4.1.3)$$

where

Q_1 = total out-gassing rate (torr·liters/sec)

Q_2 = total leak rate (torr·liters/sec)

Now, in T-1 Reactor we can come up with

$$P = 1 \times 10^{-7} \text{ torr}$$

Since the total leak rate is negligibly small relative to the total out-gassing rate, we can roughly estimate

$$
\begin{aligned}
Q &\simeq Q_1 \\
&\simeq A_g \cdot q_g \\
&= 3 \times 10^{8}\ \mathrm{cm}^2 \cdot 1 \times 10^{-11}\ \mathrm{torr \cdot liter/cm^2\ sec} \\
&= 3 \times 10^{-3}\ \mathrm{torr\ liter/sec}
\end{aligned}
$$

In the above calculation, the total surface area A_g is substituted approximately by six times the inside surface area of the vessel, which is expected to be a little greater than the actual area which consists of the surfaces created by particle collectors, blanket modules, the vacuum vessel, bellows joints, etc., and the out-gassing rate q_g is represented by that for stainless steel which is fully surface-treated as shown in Table 4.1.1.

Table 4.1.1 Surface treatment and out-gassing rate of stainless steel

Surface treatment	Out-gassing rate (torr·liter/sec·cm^2)
(As received)	10^{-8}
Mechanical abrasion	10^{-10}
Pickling Glass-bed shot blasting Aceton rince Freon rince	$10^{-11} - 10^{-12}$
(Baking)	$(10^{-12} - 10^{-13})$

Then

$$S_e = \frac{Q}{P} = 3\times10^{-3} / 1\times10^{-7} = 30000 \text{ liters/sec}$$

From Equation (4.1.2) we get

$$S_p = (1/S_e - 1/C)^{-1} = \left[1/3000 - 1/(1.5\times30000)\right]^{-1}$$
$$= 90000 \text{ liters/sec}$$

In the above calculation, the conductance is temporarily assumed to be 1.5 times S_e, which gives a greater value of S_p than an actual one, because the conductance, as described later, should be much greater due to other requirements.

Based on the above pumping speed, the required time of pump-down is estimated as follows:

In general, pressure-time relationship is given by

$$P = P_o \cdot e^{-\frac{S_e}{V} t} \qquad (4.1.4)$$

where

t = time (sec)

P_o = initial pressure (torr) $\simeq$ 760 torr

V = volume of the system (liters)

In T-1 Reactor

$$V \simeq (2\pi \cdot 2480) \cdot (\pi \cdot 400^2) \text{ cm}^3 \simeq 8\times10^6 \text{ liters}$$

Then

$$S_e / V = 30000/8\times10^6 \simeq 1/270 \text{ sec}^{-1}$$

Thus the pressure is to reach the required level within 2 hours.

4.2 Exhaust Conditions of D-T Gas and Helium Gas

The main function of the pumping system is to remove the unburned fuel and impurity particles through magnetic divertors, and a secondary function is to evacuate the chamber down to the required vacuum level described above. Therefore the pumping system should be designed considering exhaust conditions, as well as vacuum conditions. The exhaust conditions are dominant factors to determine the system, except that the vacuum conditions require a rough pumping function to obtain a low vacuum prior to a final vacuum.

Table 4.2.1 provides the design requirements of the exhaust system in T-1 Reactor.

Table 4.2.1 Design conditions of the exhaust system

	D-T gas	Helium gas	
Gas flow, Q (torr·liters/sec)	14,000 4,200	140 42	at 1000 K at 300 K
Gas pressure, P (torr)	2×10^{-3} 0.63×10^{-3}	$\ll 2 \times 10^{-3}$ $\ll 0.63 \times 10^{-3}$	at 1000 K at 300 K
Effective pumping speed, S_e (liters/sec)	7×10^{6}	———	at 1000 K & 300 K

The values of gas flow and gas pressure given in Table 4.2.1 were calculated as follows:

Helium gas flow:

$$Q_{He} = \frac{4230\ \text{MW}}{(20\ \text{MeV})\ (1.602\times 10^{-19}\ \text{J/eV})\ (6.02\times 10^{23}\ \text{mol}^{-1})}$$

$$= 0.00225\ \text{mol/sec}$$

$$= \begin{cases} 140 & \text{torr·liters/sec at 1000 K} \\ 42 & \text{torr·liters/sec at 300 K} \end{cases}$$

D-T gas flow:

$$Q_{D-T} = (2\ Q_{He})\left[(100/2)(1 - 2/100)\right]$$

$$\simeq 100\ Q_{He}$$

where 2 % fuel consumption is assumed, since D-T fuel consumption rate F_{D-T} is evaluated to be

$$F_{D-T} \simeq 2\cdot\tfrac{1}{4}\, n^2\langle\sigma v\rangle\, 3\tau_E / n = 3/2\ n\langle\sigma v\rangle\tau_E$$

$$\simeq 3/2\ (1.33\times 10^{20}\ \text{m}^{-3})\ (0.459\times 10^{-22}\ \text{m}^3/\text{sec})\ (2.24\ \text{sec})$$

$$= 0.0205 \quad \text{or} \quad 2\ \%$$

D-T gas pressure:

$$P_{D-T} = (10\ \%\ \text{of plasma pressure at T K is assumed})$$

$$= \frac{(2\times 10^{20}\ \text{m}^{-3})\ (8.317\ \text{J/mol K})\ (\text{T K})}{6.02\times 10^{23}\ \text{mol}^{-1}} \times 0.1$$

$$= 2.8\times 10^{-4}\ \text{T (Pa)}$$

$$= \begin{cases} 0.28\ \text{Pa} & \text{or } 2\times 10^{-3}\ \text{torr at 1000 K} \\ 0.084\ \text{Pa} & \text{or } 0.63\times 10^{-3}\ \text{torr at 300 K} \end{cases}$$

The conductance of a duct can be calculated as follows: [33]

1) Transition region ($0.02 < P \cdot D < 0.55$ torr·cm)

For a cylindrical duct the conductance C is given by

$$\frac{1}{C} = \frac{1}{D^3} \frac{L}{180D \cdot P + 12.17} \quad (\text{liters/sec})^{-1} \qquad (4.2.1)$$

where

D = diameter (cm)

P = average pressure (torr)

L = duct length (cm)

2) Molecular flow ($P \cdot D < 0.02$ torr·cm)

For a relatively short duct ($L < 12.5\ D$)

$$\frac{1}{C} = \left(\frac{3}{16} \frac{L \cdot U}{F} + 1\right) \sqrt{\frac{2\pi M}{R\,T}} \frac{10^3}{F} \quad (\text{liters/sec})^{-1} \qquad (4.2.2)$$

where

D = diameter (cm)

L = duct length (cm)

U = periphery of the duct (cm)

F = cross-sectional area (cm^2)

M = molecular weight (gram)

R = gas constant = $8.317\ 10^7$ (erg/mole)

T = gas temperature (K)

When forty pumps, that is, two out of three pumps installed on each reactor module are alway under operation, effective pumping speed of each pump should be

$$S_e > 7 \times 10^6 / 40 = 1.75 \times 10^5 \text{ liters/sec}$$

The required pumping speed S_{D-T} is given by

$$S_{D-T} = (1/S_e - 1/C)^{-1}$$

When $C = 1.5\, S_e$ is chosen,

$$S_{D-T} = 3\, S_e = 5.25 \times 10^5 \text{ liters/sec} \quad \text{(per pump)}$$

$$C = 1.5\, S_e = 2.63 \times 10^5 \text{ liters/sec} \quad \text{(per pump)}$$

Since the exhaust gas pressure P is estimated to be $0.63 \times 10^{-3} - 2 \times 10^{-3}$ torr and the duct diameter (or equivalent size) D might be around 1 m, the gas flow belongs to the transition pressure range to which Equation (4.2.1) can be applied. Figure 4.2.1 shows relationship between a conductance and a duct size given by Equation 4.2.1. For $C = 2.63 \times 10^5$ liters/sec we obtain the required minimum duct-diameter as a function of duct length shown in Table 4.2.2.

Pumping speed for helium is lower than that for D-T gas. When at least 10 % of the pumping speed for D-T gas is expected for helium, helium gas pressure at the divertor region P_{He} will be

$$P_{He} \simeq \frac{140 \text{ torr liters/sec}}{0.1 \cdot 7 \times 10^6 \text{ liters/sec}}$$

$$= 2 \times 10^{-4} \text{ torr}$$

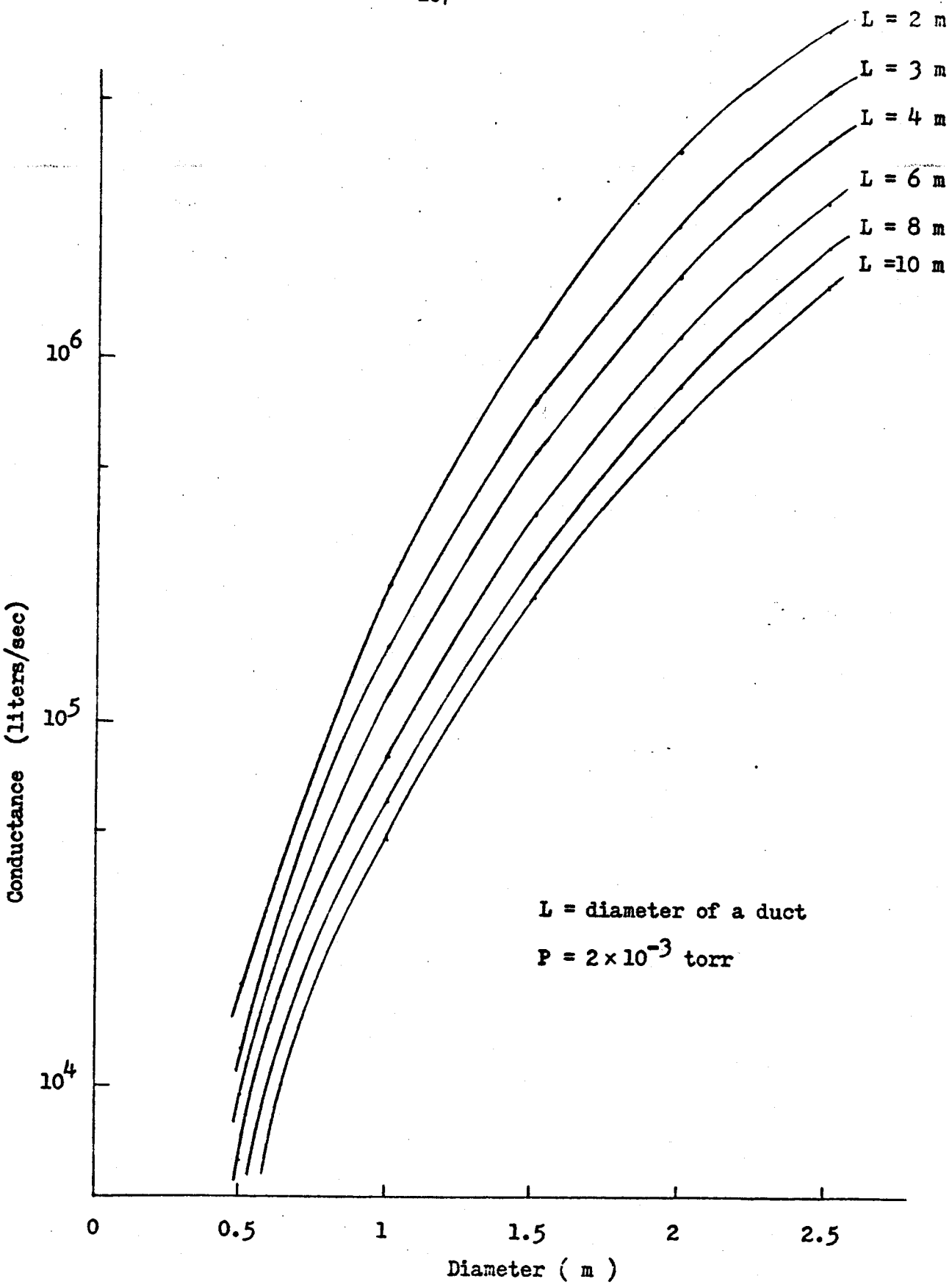

Fig. 4.2.1 Conductance for exhaust gas
($0.02 < P \cdot D < 0.55$ torr·cm)

Table 4.2.2 Required minimum duct-size as a function of duct length

Duct length (m)	Required duct diameter (m)
2	1.1
4	1.2
6	1.4
8	1.5
10	1.6

4.3 Vacuum/Exhaust System

a. Pumping System

The vacuum/exhaust system has two kinds of operation modes: rough pumping and high vacuum/exhaust pumping. The former is initial pumping-down from atmospheric pressure to about 10^{-3} torr, which is done by Roots-type blowers backed by mechanical pumps.

Main components for high vacuum/exhaust pumping will be either diffusion pumps or cryopumps, which compose the system together with Roots-type blowers, mechanical pumps, liquid nitrogen traps, valves, conduits, etc..

(1) Diffusion Pumping System [34]

Figure 4.3.1 shows a diffusion pumping system in which large-scale mercury vapor diffusion pumps are adopted. Since a mercury vapor diffusion pump with about 1.0 m diameter has the pumping speed of up to 50,000 liters/sec, at least seven or eight diffusion pumps will be needed for each module of the torus. We may conclude that it is difficult to apply this system to T-1 Reactor because of the following reasons:

A) Available space for large size ports around the vessel is considerably limited; the number of large-size evacuation ports should be no more than three under various restrictions.

B) A diffusion pump is hardly accompanied with a large conductance, since a liquid nitrogen cooled trap should be installed at its upstream.

(2) Cryopumping System [35]

Cryopumps have a great pumping speed, using a given space efficiently, in general. Figure 4.3.2 shows the proposed cryopunping system. Each module has three cryopumps, one of which is recycled while the two other

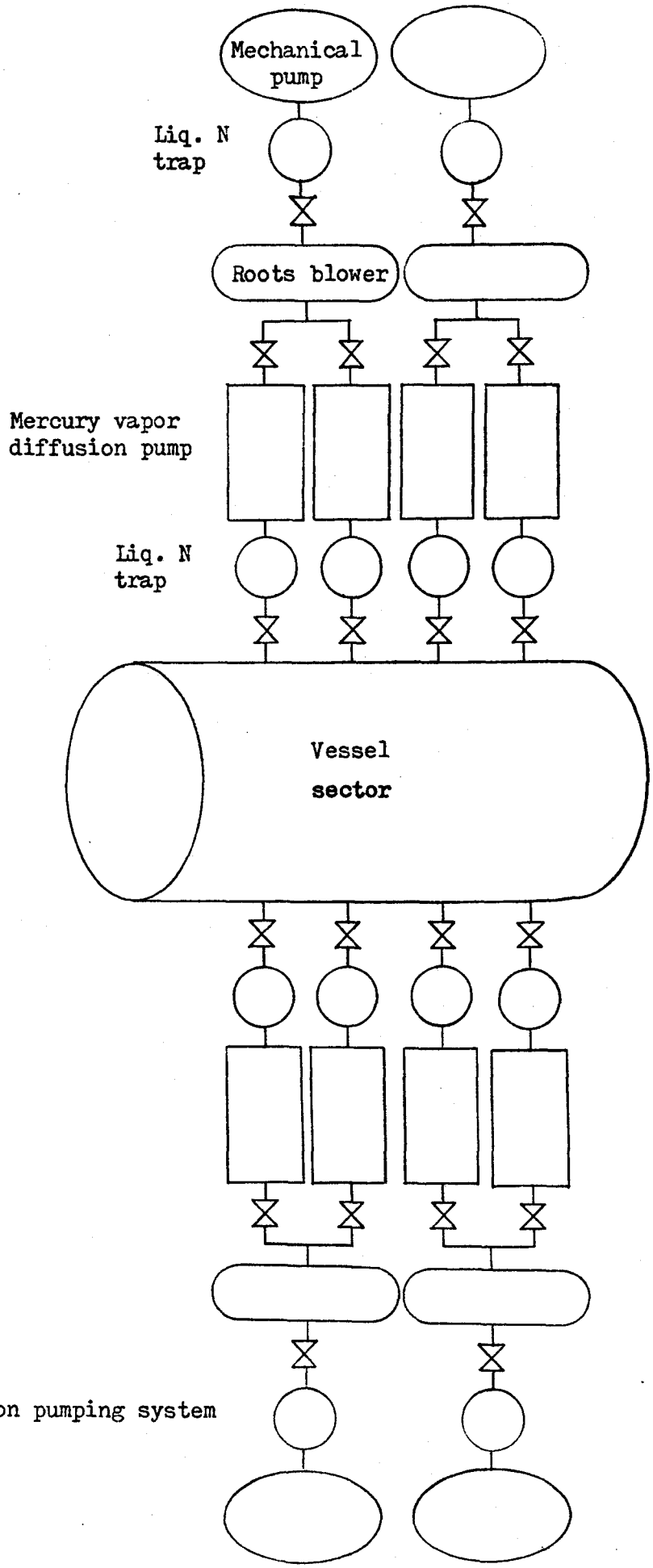

Fig. 4.3.1

Diffusion pumping system

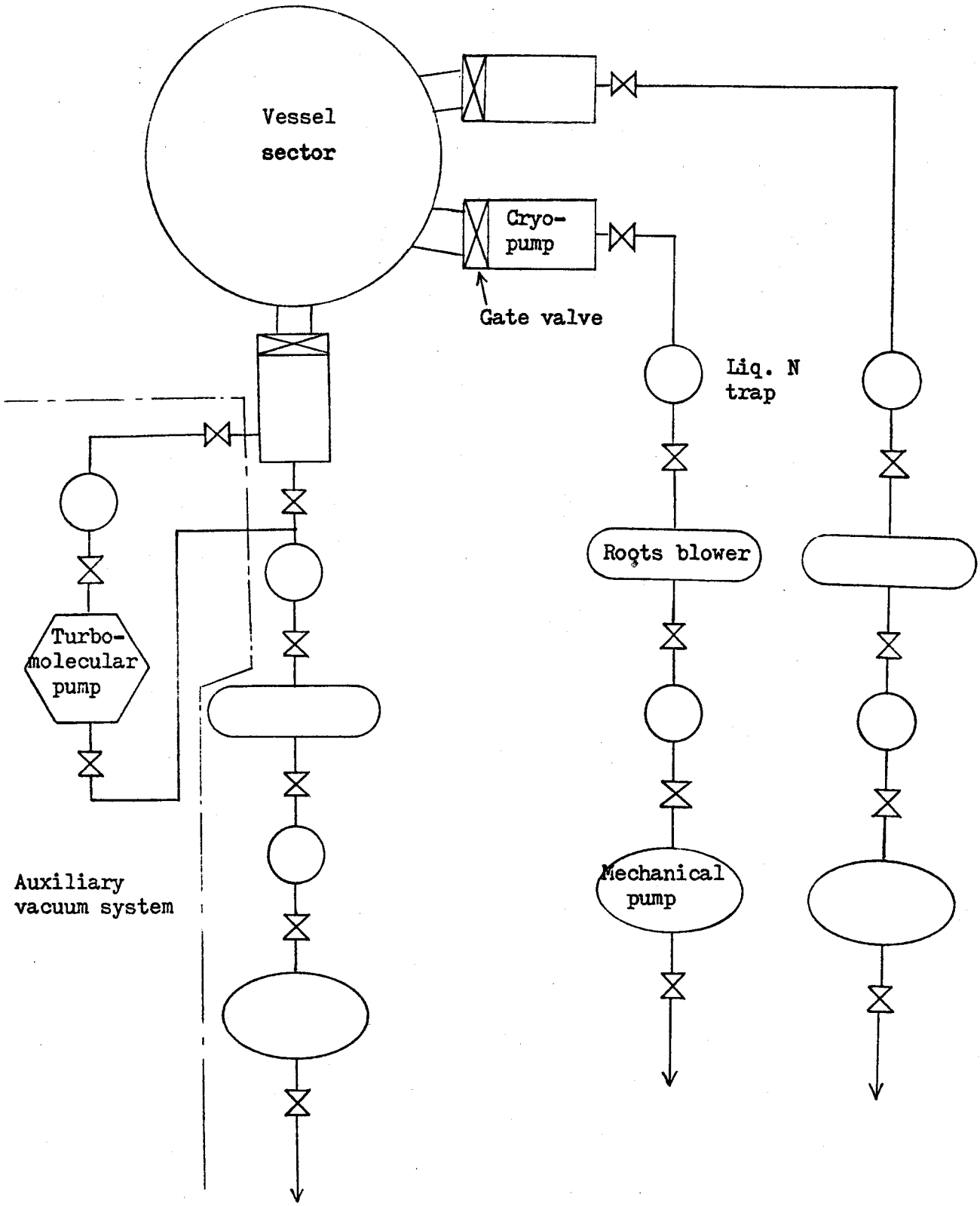

Figure 4.3.2 Cryopumping system

pumps are on line.

For hydrogen isotopes of deuterium and tritium, the expected pumping speed is about 9 liters/sec·cm^2 and is independent of surface coverrage up to at least 1.5×10^{21} molecules/cm^2,[36] so that the required cryo-condensation surface area (the projected area) A_p is given by

$$A_p = (5.25 \times 10^5 \text{ liters/sec}) / (9 \text{ liters/sec} \cdot \text{cm}^2)$$
$$= 58{,}400 \text{ cm}^2 = 5.9 \text{ m}^2$$

and the maximum loading time in one recycle operation $t_{p,max}$ is estimated as

$$t_{p,max} = \frac{(1.5 \times 10^{21} \text{ molecules/cm}^2)\ (58{,}400 \text{ cm}^2)}{(6.02 \times 10^{23} \text{ molecules/mole})\ (0.00225 \times 100 \times 1/40 \text{ mole} \cdot \text{sec}^{-1})}$$

$$= 26{,}000 \text{ sec} = 7.2 \text{ hours}$$

Thus so far as the cryopumping of D-T gas is concerned, the design of the pumping system will be done chiefly on the basis of present technology.

However, we find a serious necessity of further development on helium gas pumping. 4.2 K cryo-condensation pumps for D-T gas described above do not adsorb helium gas , and cryo-sorption pumps should be used for helium. According to the resent paper published by P. W. Fisher and J. S. Watson[37] (ORNL), experimental results have shown that the present cryo-sorption pumps may not be able to accommodate helium mixed with hydrogen isotopes, because condensed deuterium and tritium will block the adsorbent surface and prevent the pumping. In addition, the decline in helium pumping speed with continuous loading turned out to be much more significant than expected from earlier investigations. Their experimental results indicated that the helium pumping speed of 3.3 liters/sec·cm^2, which makes a good agreement with previously reported data, declines to only 30 % of its initial value after

1 % (0.156 torr·liter/cm^2) of the adsorption capacity.

Taking into account this significant decline of pumping speed in cryosorption sieve for helium, with all some expected scaling effect, it is too optimistic to assume that the pumping speed for helium is 75 % of that for hydrogen when cryo-sorption pumps adsorb both D-T gas and helium gas as shown in the UWMAK-III design.[23]

P.W. Fisher and J.S. Watson proposed that the problem of helium pumping should be alleviated either by developing new cryosorption pumps based on different adsorbents or by developing compound pumps employing separate panels for pumping hydrogen isotopes and helium.[38-40] Turbomolecular pumps seem to be another choice; however, their applicability as main pumps will be limited to relatively small devices or reactors because of the small ratio of available pumping speed to the amount of occupied space, the need to be shielded from high magnetic fields, complicated peripheral systems, etc.. Thus 4.2 K cryosorption pumps are most probable choice for helium pumping in the system; extensive research and development of these pumps is desired. In addition, in T-1 Reactor some pumping effect of the magnetic divertor is expected.

b. Particles Collectors

Unburned D-T particles, generated helium particles, and other impurity particles are exhausted through divertor regions formed by characteristic magnetic flux configurations of T-1 Reactor. Most of those particles lose their kinetic energy by impinging on the particle collectors. The cross-sectional configurations of the particle collectors and the exhaust ports are shown in Figure 4.3.3. Main design parameters of the particle collectors are given in Table 4.3.1.

Table 4.3.1 Main design parameters of particle collectors

Total surface area	2,800 m^2
Total heat deposion	980 MW
Average heat load	0.36 MW/m^2
Cooling method	Same as blanket cooling
Replacement interval	Same as blanket replacement interval

The particle collectors are modularized and each module is a part of the Type-B blanket module described in Section 3.2.

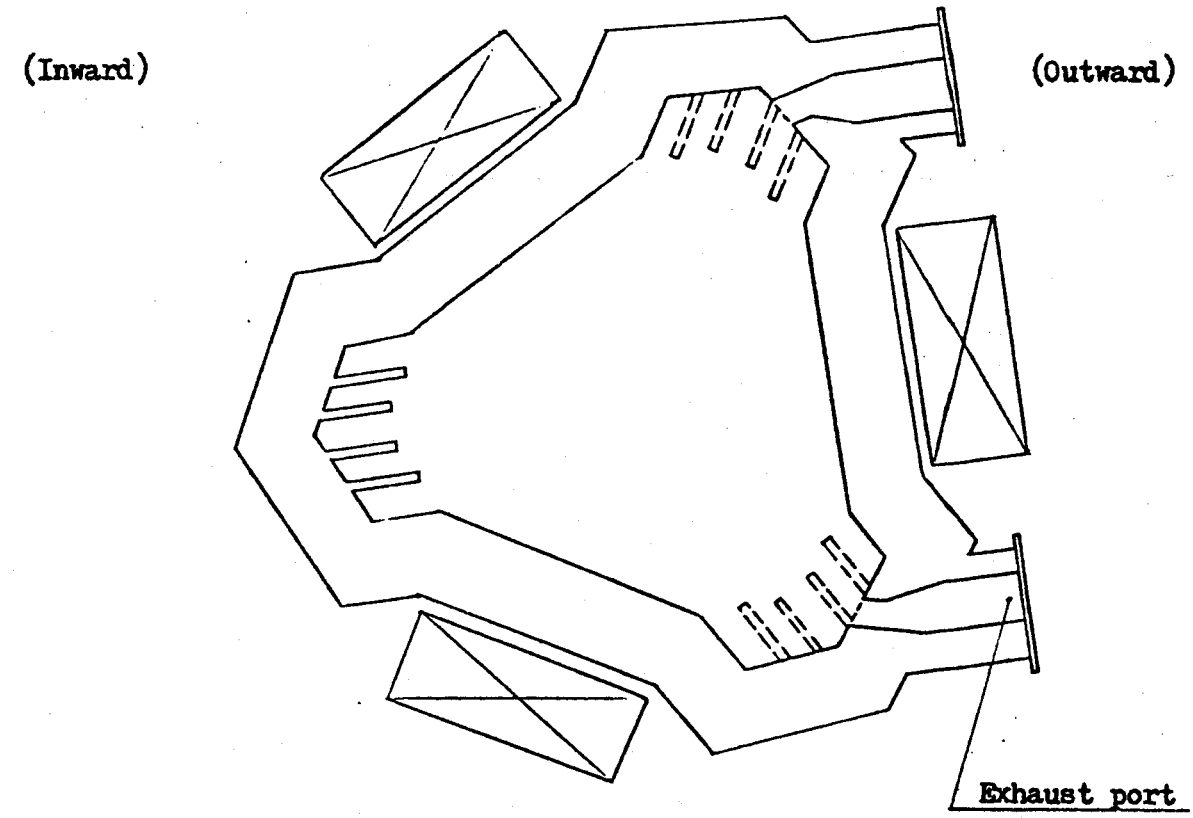

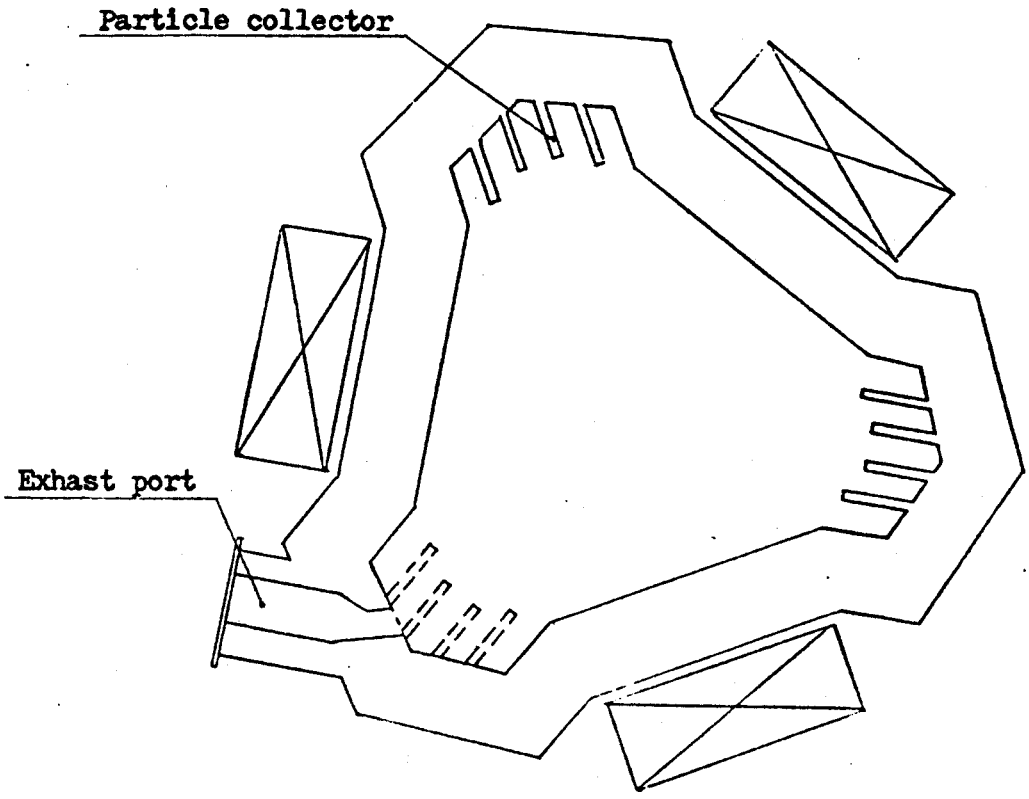

Figure 4.3.3 Configurations of particle collectors and exhaust ports

5. Reactor Structures

5.1 Vessel Structures

a. Toroidal Vessel

The vessel structures of T-1 Reactor have two functions: one is to form a boundary to keep vacuum atmosphere and also to contain radioactive fuel particles and other reaction products; the other is to hold blanket, reflector/shield, and other internal structures. Thus structural integrity and reliable sealing, as well as ease of maintenance, will be important factors in designing the vessel structures. Figure 5.1.1 shows a partial cross-sectional view of the vessel. Table 5.1.1 provides main design parameters of the vessel structures.

Table 5.1.1 Design parameters of the vessel structures

Number of vessel sectors	20
Vessel size	
Radial length (radius)	5.4 m (max.)
Longitudinal length	7.8 m (center line)
Design temperature	400 °C (assumed)
Design loads	
External pressure	0.104 MPa (1.02 atmosphere)
Own weight (Internals included)	700 tons
Radiation dose	———
Life time	30 years
Material	316 SS
Wall thickness	0.04 m

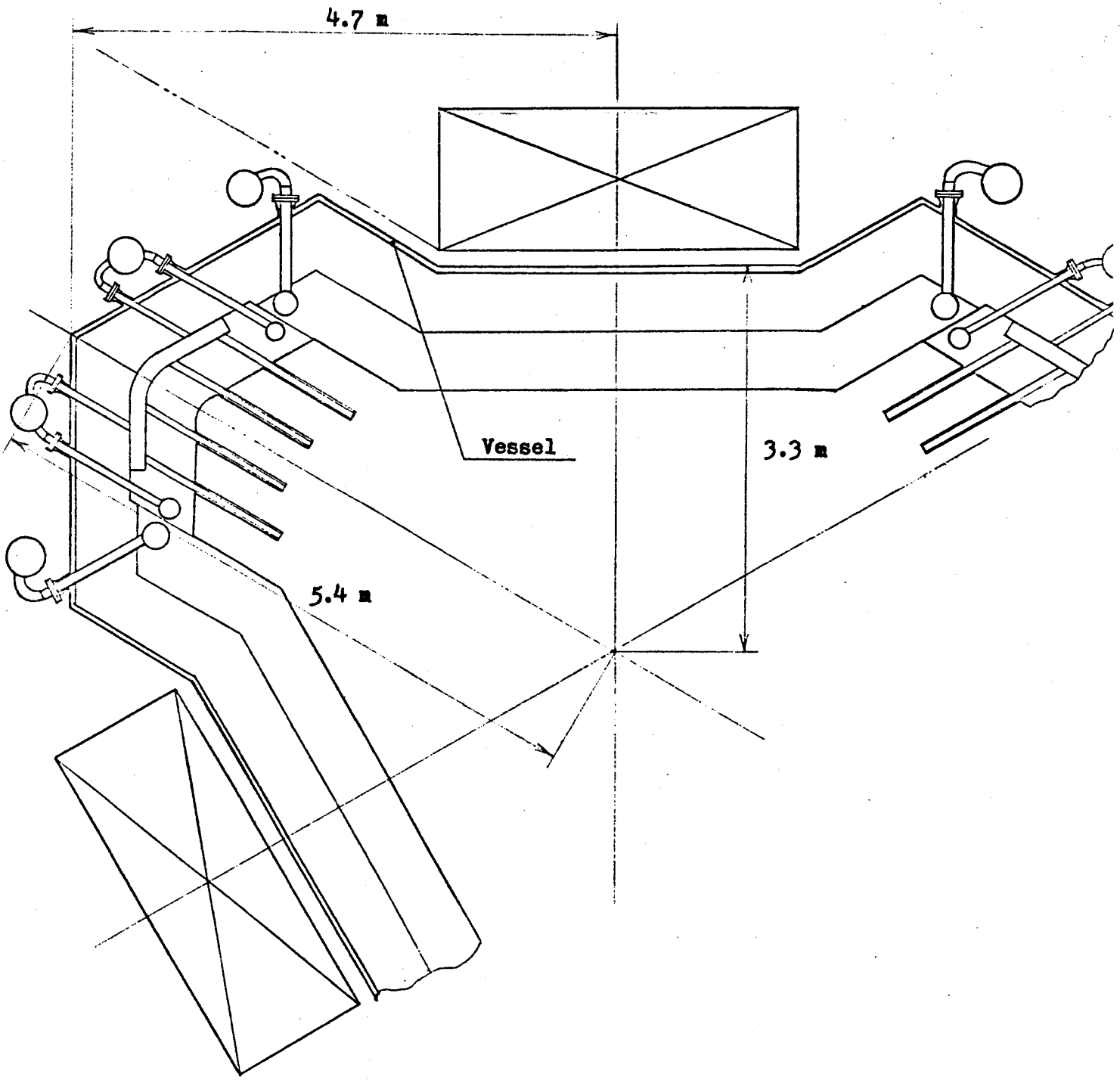

Figure 5.1.1 Cross-sectional view of vessel

The wall thickness is determined based on the following calculations:

1) Consideration of external pressure

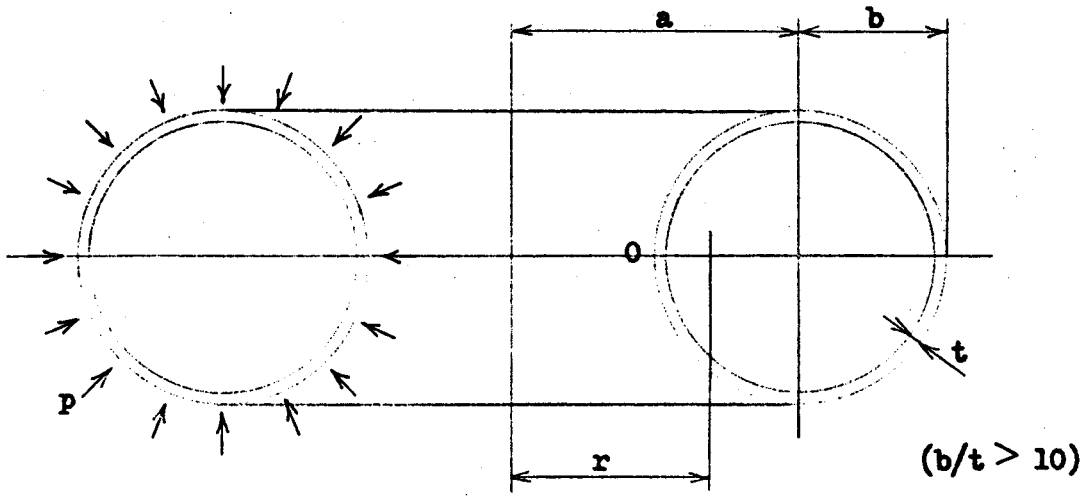

Figure 5.1.2 Toroidal shell subject to external pressure

In a simple toroidal shell shown in Figure 5.1.2, longitudinal stress σ_1 and hoop stress σ_2 caused by external pressure p are given by [41]

$$\sigma_1 = \frac{p\,b}{2\,t}\,\frac{r+a}{r} \qquad (5.1.1)$$

$$\sigma_2 = \frac{p\,b}{2\,t} \qquad (5.1.2)$$

where

$p = 0.104$ MPa

$a = 24.8$ m

$b \simeq 4$ m

According to the maximum shear stress theory

$$S = \sigma_1 - \sigma_2 \leq S_o \qquad (5.1.3)$$

where

$S \equiv$ stress intensity

$S_o \equiv$ maximum allowable stress intensity $\simeq$ 100 MPa [42]

From Equation (5.1.1) and Equation (5.1.2)

$$S = \frac{p\,b}{2\,t} \cdot \frac{r + a}{r} - \frac{p\,b}{2\,t} = \frac{p\,b}{2\,t} \cdot \frac{a}{r} \qquad (5.1.4)$$

Thus maximum stress intensity S_{max} arises at point 0 in Figure 5.1.2:

$$S_{max} = \frac{p\,b}{2\,t} \frac{a}{a - b} \qquad (5.1.5)$$

Using Equation (5.1.3) and Equation (5.1.5) we obtain

$$t \geq \frac{p\,b}{2} \frac{a}{a - b} \frac{1}{S_o}$$

$$= \frac{0.104 \text{ MPa} \times 4 \text{ m}}{2} \frac{24.8 \text{ m}}{(24.8 - 4) \text{ m}} \frac{1}{100 \text{ MPa}}$$

$$= 2.48 \times 10^{-3} \text{ m}$$

Hence the required wall thickness determined by the above calculations is 0.0025 m (or 2.5 mm).

2) Consideration of own weight

In Figure 5.1.3 the maximum bending moment M_{max} which is generated at point C is expressed by [41]

$$M_{max} = \frac{3\,w\,r_o^2}{2} \qquad (5.1.6)$$

where

$w \equiv$ own weight per unit length (weight of internals included)

$$\simeq \frac{700 \text{ tons}}{7.8 \text{ m}} = 8.8 \times 10^5 \text{ N/m}$$

$$r_o = 4 \text{ m}$$

Thus

$$M_{max} = \frac{3}{2} \cdot 8.8 \times 10^5 \text{ N/m} \cdot 4^2 \text{ m}^2 = 2.1 \times 10^7 \text{ N} \cdot \text{m}$$

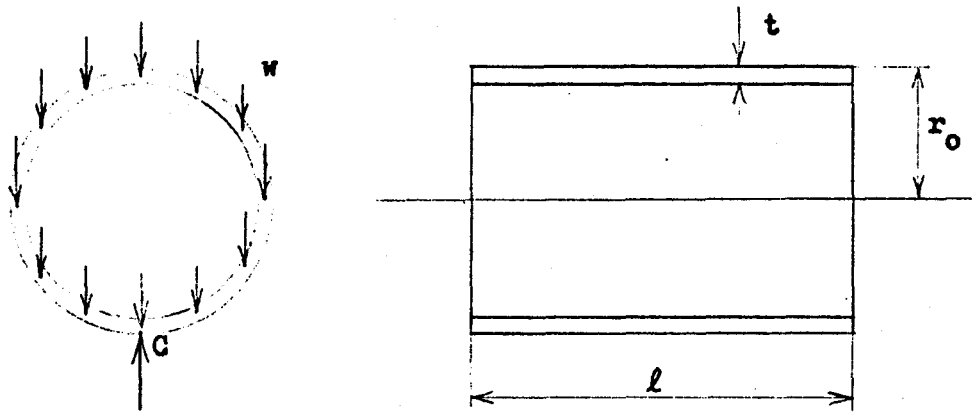

Figure 5.1.3 Vessel shell loaded by own weight

The bending stress corresponding to the maximum bending moment M_{max} is

$$\sigma_{max} = \frac{M_{max}}{Z} \qquad (5.1.7)$$

where

Z = section modulus (for unit length)

$$\simeq (1/12) \left[8 r_o^3 - 8 (r_o - t)^3 \right] / r_o \simeq 2 r_o t = 8 t \quad (m^3)$$

Then

$$\sigma_{max} = \frac{2.1 \times 10^7 \text{ N} \cdot \text{m}}{8 t} = 2.6 \times 10^6 \, t^{-1} \text{ N/m}^2 \text{ or } 2.6 \, t^{-1} \text{ MPa}$$

Since S is equal to σ_{max} in this case

$$\sigma_{max} \leq S_o$$

Then we obtain

$$t \geq \frac{2.6}{100} = 0.026 \text{ m} \quad \text{or} \quad 26 \text{ mm}$$

Consequently 0.026 m is the minimum wall thickness required for the vessel.

The above calculations are based on the approximate assumptions which are originally applied to thin shells of revolution which have no abrupt changes in slope or curveture. However, the results are expected to provide a rough estimation of the required wall thickness. The selected wall thickness ($t = 0.04$ m) may be reasonable, although precise stress analyses will be needed to determine the detailed shell structures including local reinforcements.

b. Vessel Joints

The toroidal vessel is composed of twenty vessel sectors, which are connected with bellows joints. There are two reasons to employ bellows joints forming a part of the pressure (or vacuum) boundary of the torus:

1) Some retractable portion of each vessel sector is needed to assemble and disassemble the toroidal structures.

2) The buffering region is needed between the vessel sectors to accommodate partial or local components of thermal expansion of the toroidal structures, although most of the displacement will be released by allowing radial movement of the vessel installed with 'radially-free' supports.

Figure 5.1.4 shows a cross-sectional view of the bellows joint. Welded bellows are emplyed because the large size and complex shape can not be achieved with formed bellows. A set of bellows is located between two flanges, each of which may be connected with a vessel sector by bolting.

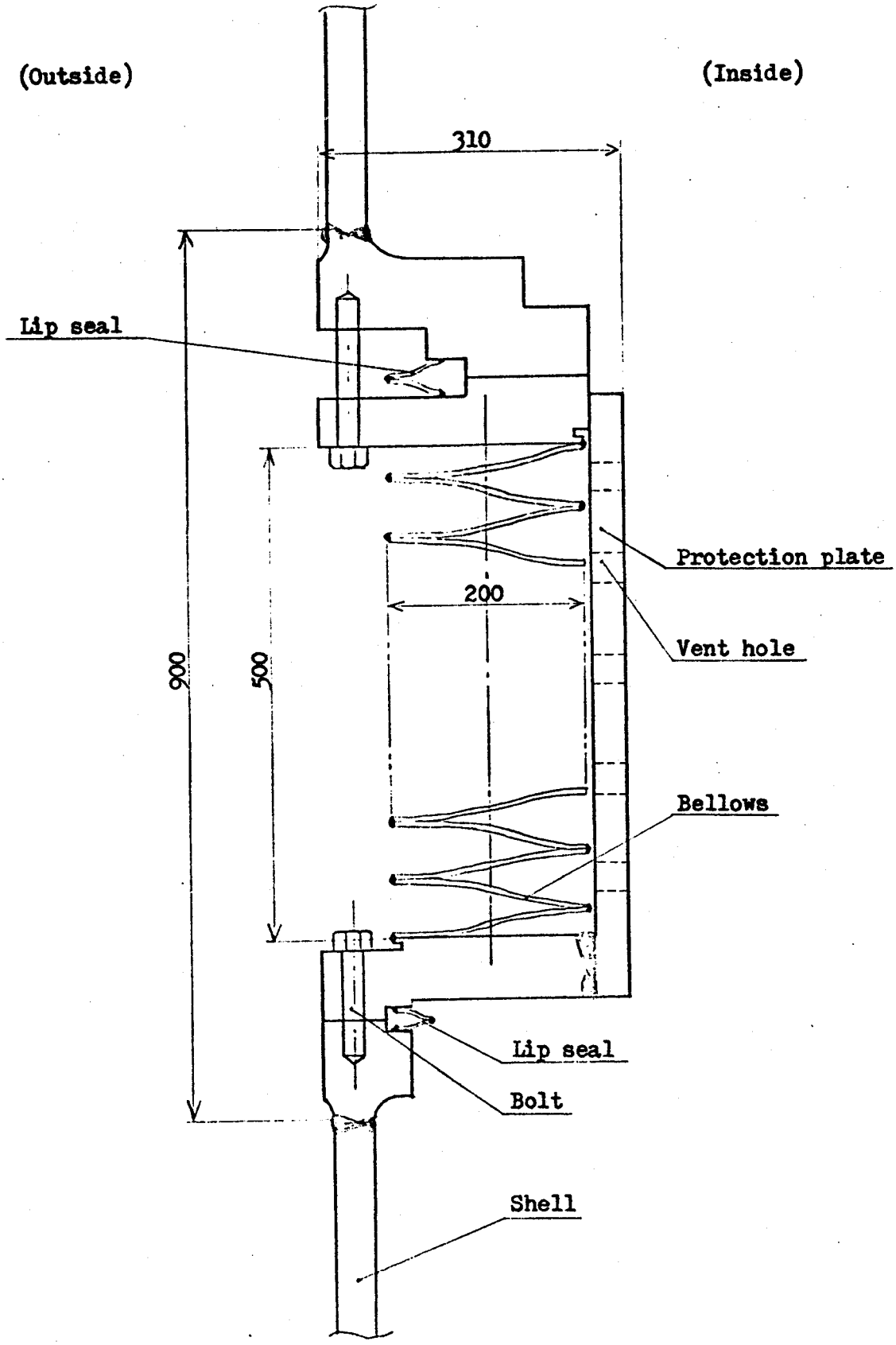

Figure 5.1.4 Cross-sectional view of bellows joint

The independent bellows component separable from vessel sectors makes it easy to perform vacuum leak tests of individual bellows and to replace them when necessary. Protection plates are installed inside the bellows to prevent their buckling due to external pressure. Interfaces between the matching flanges at both sides of the bellows are sealed by employing welded lip seals. In disassembly and re-assenbly of the vessel structures only one side of the interfaces will be disconnected and reconnected.

Structural integrity of the welded bellows and satisfactory remote operation of cutting, machining, and welding the lip seals are main technical subjects to solve in the future.

5.2 Magnet Supports

Magnet supports of the superconducting helical windings should be designed taking into account the following conditions:

1) Magnitude and direction of magnetic forces
2) Large temperature difference between both ends of the support
3) Thermal insulation and refrigeration
4) Ease of installment and maintenance

Each magnet segment is supported by three support elements which are installed between the helical windings and surrounding support rings. Load conditions (magnitude and direction) of the magnetic forces [43] are different for nine support elements which belong to each reactor module; however, they can be represented by

Maximum compressive load $\sim 10^7$ N for one support element

Maximum tensile load $\sim 2 \times 10^7$ N for one support element

Figure 5.2.1 shows a design concept of the magnet support elements. Multi-layered structures are employed to alleviate thermal stresses due to large temperature difference and temperature transient. Glass-reinforced epoxy is used as a main structural material because of its small thermal conductivity and excellent mechanical properties at low temperature. The proposed support elements will have satisfactory structural strength.

The support elements are cooled by 77 K nitrogen flowing in cooling channnls. In order to minimize required refrigeration power the position of the cooling channels is determined as follows:

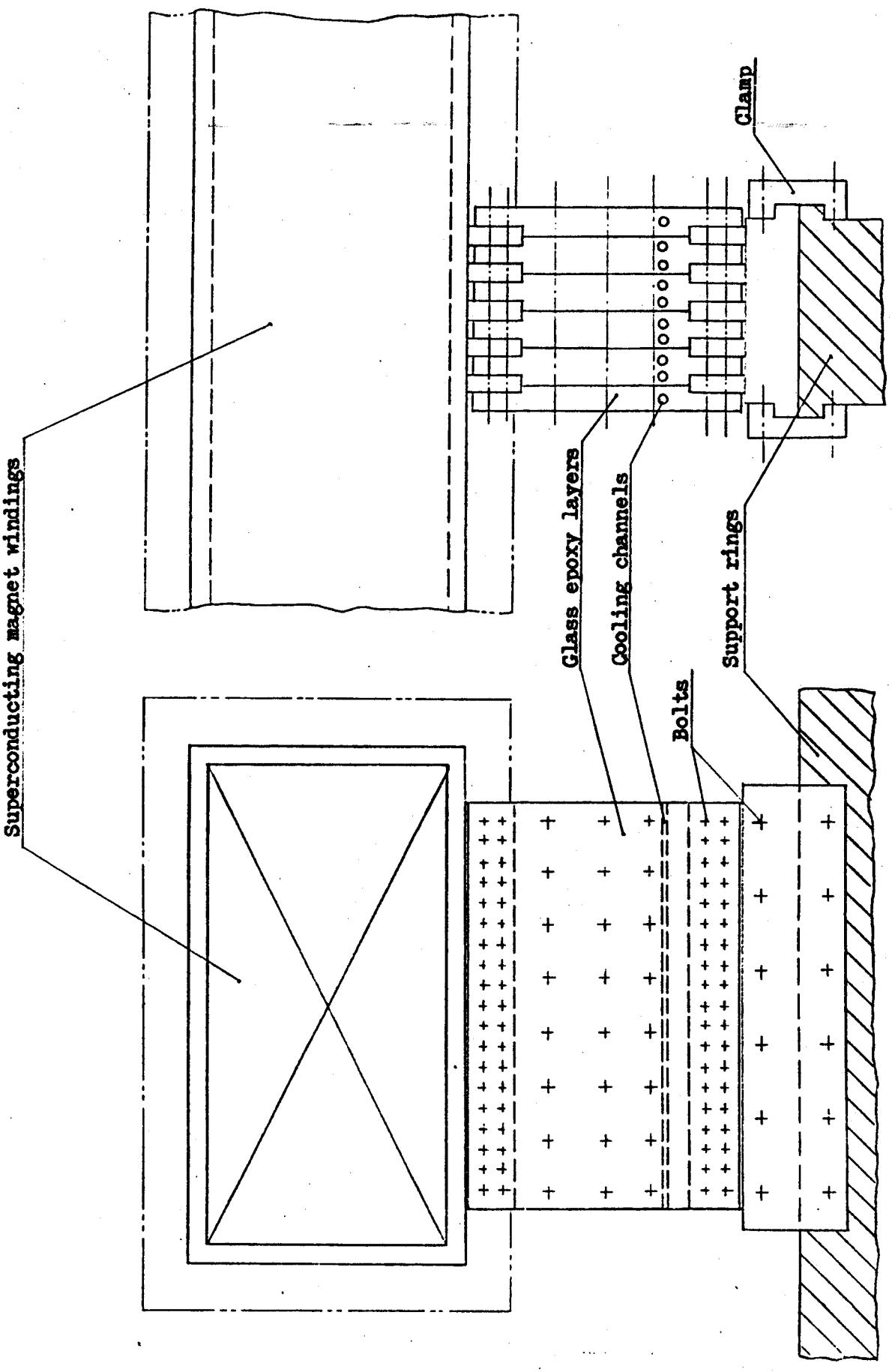

Figure 5.2.1 Support structures of superconducting magnet windings

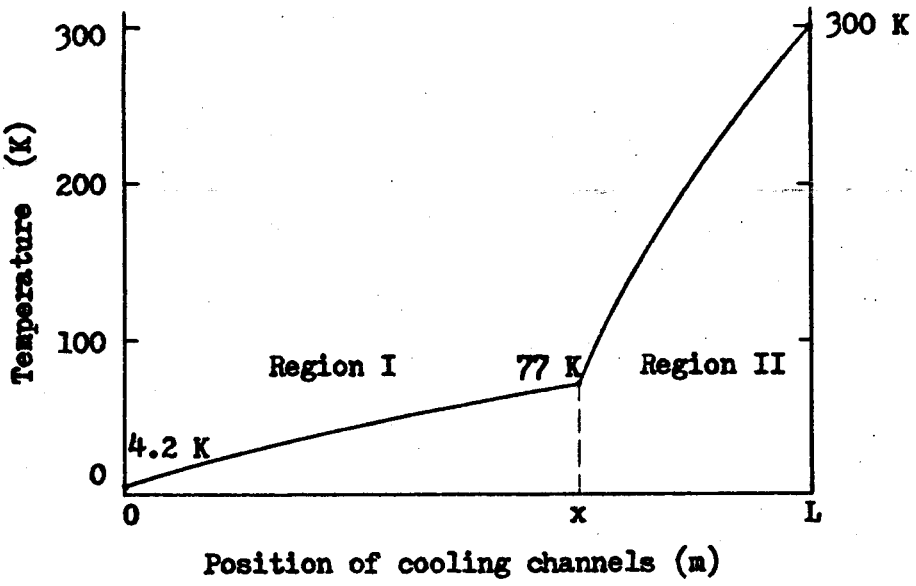

Figure 5.2.2 Temperature profile in magnet support elements

For Region I and Region II shown in Figure 5.2.2 we obtain the following relations based on Equation (2.3.3):

$$Q_{c,1} = A_c \frac{1}{x} \int_{4.2\ K}^{77\ K} k(T)\, dT \qquad (5.2.1a)$$

$$Q_{c,2} = A_c \frac{1}{L - x} \int_{77\ K}^{300\ K} k(T)\, dT \qquad (5.2.1b)$$

where

$Q_{c,1}$ = Conducting heat load in Region I

$Q_{c,2}$ = Conducting heat load in Region II

L = 1 m

Figure 2.3.4 (Parallel to reinforcement) gives

$$\int_{4.2\ K}^{77\ K} k(T)\, dT = 17.4 \ \text{W/m}$$

$$\int_{77\ K}^{300\ K} k(T)\, dT = 115 \quad W/m$$

The required refrigeration power W_r is given by

$$W_r = \frac{1}{C_{r,4.2K}} Q_{c,1} + \frac{1}{C_{r,77K}}(Q_{c,2} - Q_{c,1}) \qquad (5.2.2)$$

$$= 300\, A_c \frac{17.4}{x} + 6.5\, A_c \frac{115}{1 - x}$$

$$= A_c \left(\frac{5220}{x} + \frac{748}{1 - x}\right)$$

W_r becomes minimum when

$$\frac{dW_r}{dx} = 0 \qquad (5.2.3)$$

or

$$-\frac{5220}{x^2} + \frac{748}{(1 - x)^2} = 0$$

Thus we obtain the optimum position:

$$x = 0.73\ m$$

6. Reactor Layout and Maintenance

6.1 General

It is characteristic of fusion power reactors in general that large-scaled maintenance is periodically needed to replace first wall/blanket materials and, in addition, that special remotely-operated equipments and facilities ought to be introduced to do the scheduled maintenance and also unscheduled maintenance and repair because radioactive environment in the reactor room prevents personnel's direct approach to the reactor. Thus one of major concerns associated with reactor layout study is on how to improve maintenability of the reactor.

In T-1 Reactor the magnet windings spiraling around the torus should be disassembled in order to disconnect and remove vessel sectors for maintenance or repair work. Consequently sufficient space is required around the torus (inward and outward the torus) to get access to the magnet joints, vessel-sector joints, magnet & vessel supports, blanket cooling piping, magnet refrigerating piping, magnet leads, control & instrumentation cables, etc..

In the case of Tokamak power reactors [44-47] each reactor module may be removed in an outward direction through a large gap between adjacent TF (toroidal field) coils. However, in T-1 Reactor or generally in Torsatron reactors disassembly of the magnet windings is indispensable to allow the vessel sectors to move. Fortunately, in T-1 Reactor the required space inward the torus, as well as space outward the torus, is available for access and remote operations, since the aspect ratio of the torus is much larger than that of Tokamak reactors.

There are two different ways which may be proposed for replacement of first wall/blanket materials; that is,

1) An in-place first wall/blanket exchange [48,49]
2) A whole reactor module replacement

In this study of T-1 Reactor, the in-place exchange of first wall/blanket materials is not considered to be practical because of the following reasons:

a) Accessibility to the inside of the reactor through some ports is extremely limited
b) Complicated procedures to exchange first wall/blanket segments are not performed by in-place remote operations

Anyway, capability of reactor-module replacement accompanied with disassembly and re-assembly of the magnet windings, vessel sectors, and other structures is essential to T-1 Reactor in order to prepare for an unexpected failure of reactor components as well as scheduled maintenance.

Table 6.1.1 gives estimated weight of a reactor module. As this table implies, each reactor module is too much heavy, as well as too large, to handle and transport as a whole. Thus it ought to be disassembled into several parts such as upper beams of support structures, segments of the magnet windings, a vessel sector, etc., each of which can be moved out and in. The heaviest and also largest disassembled part is a vessel sector which is approximately 700 tons in weight (including blanket segments and other internal structures), 9 m in length, and 10 m in diameter.

Table 6.1.1 Estimated weight of reactor module

	Main parameters		Weight (tons)
Vessel sector (vessel only)	Surface area	250 m^2	
	Ave. thickness	0.05 m	120
	Material	316 SS	
Internal structures (Blanket, reflector/ shield, etc.)	Thickness	1 m	550
	Ave. density	2.5 g/cm^3	
Segments of magnet windings (including jumper conductors)	Number of segments	3	510
	Cross section area (conductor & coil case)	0.9× 1.8 m^2	(170/segment)
	Length	11.5 m	
	Ave. density	6.2 g/cm^3	
Magnet support elements	Number of elements	27	140
	Unit weight	5 ton	
(Subtotal)			(1320)
Support structures	Number of rings	3	
	Height	18 m	
	Width	16 m	490
	Thickness	0.6 m	
	Ave. density	2.4 g/cm^3	
(Total)			1810

6.2 Disassembly of Magnet Windings

In disassembling a reactor module into several movable parts, one of major concerns lies in how to take the magnet segments apart which are spiraling closely around a vessel sector. Figure 6.2.1 gives a horizontal plane view of the helical magnet windings. Figure 6.2.2 a) through Figure 6.2.2 g) show vertical plane views of the magnet windings, a vessel sector, and support structures at each circumferential positions. The series of figures also show possible moving directions of two magnet segments located in upper positions which should be taken apart. As the figures imply, some upper beams of the support structures should be removed prior to the removal of the magnet segments. The remaining magnet segment located in a lower position is not in the way of the vessel sector's moving upward, but will also have to be moved downward a little to provide a necessary room between the vessel sector and the magnet segment for disconnection of the vessel joints.

Re-assembly or installment of the vessel sector and the magnet segments can be performed by moving them in the reverse order and reverse directions.

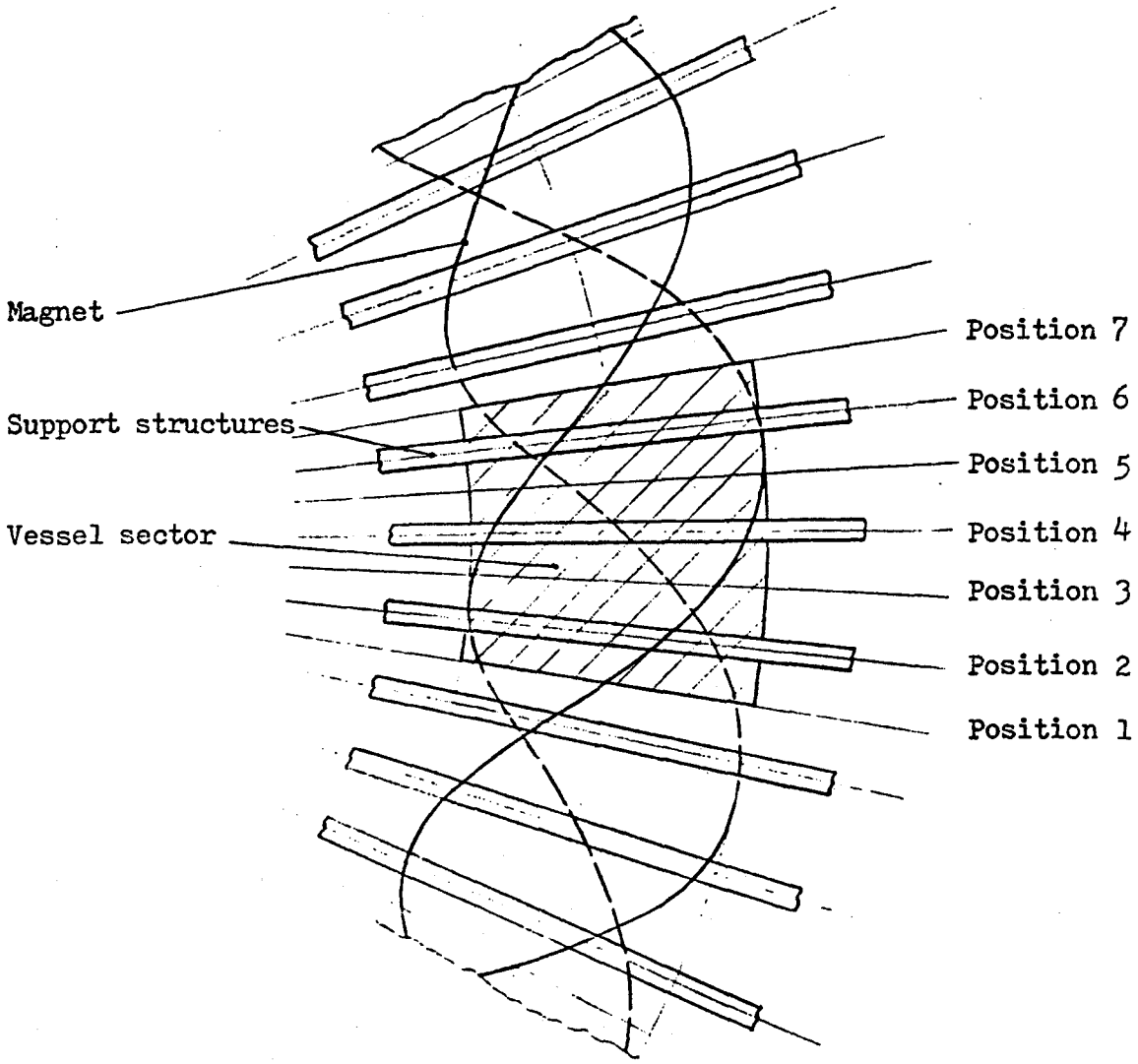

Figure 6.2.1 Horizontal plane view of helical magnetic windings

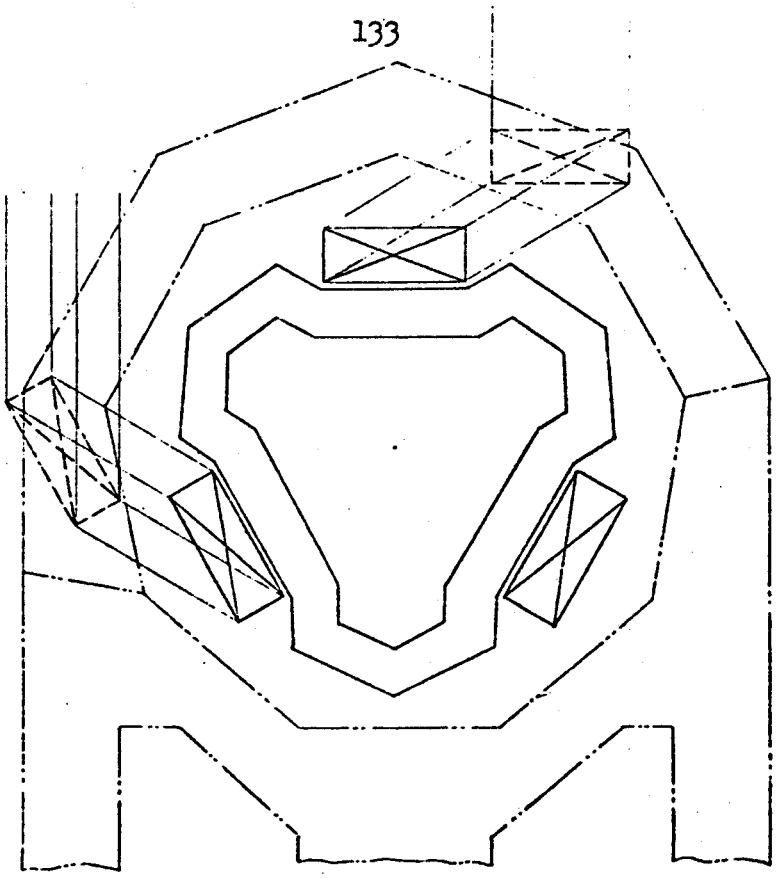

a) Position 1

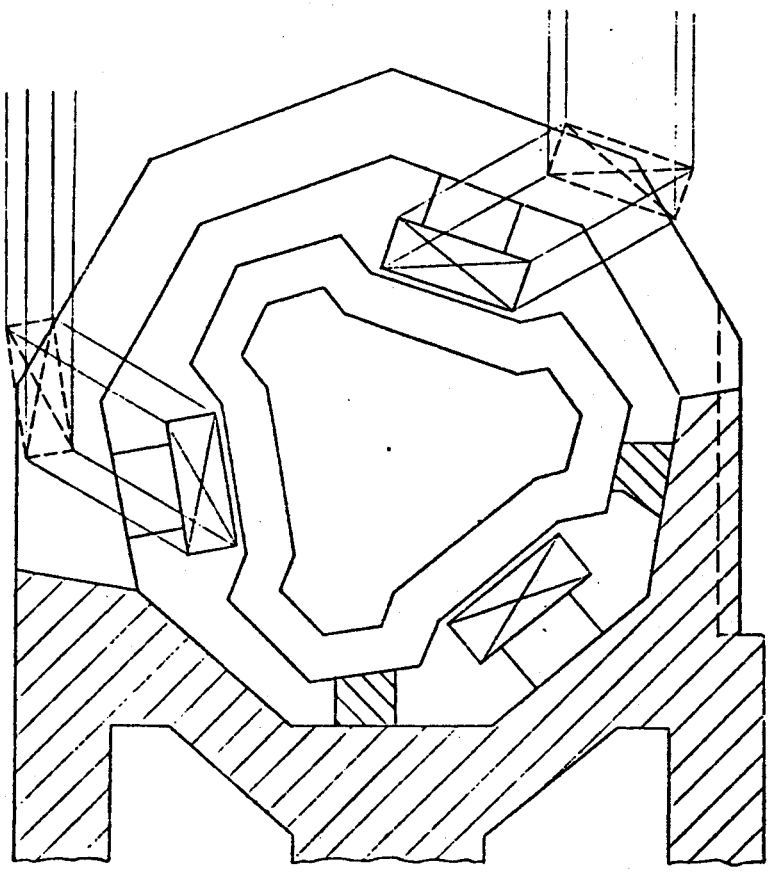

b) Position 2

Figure 6.2.2 a) & b) Vertical plane view of magnet windings

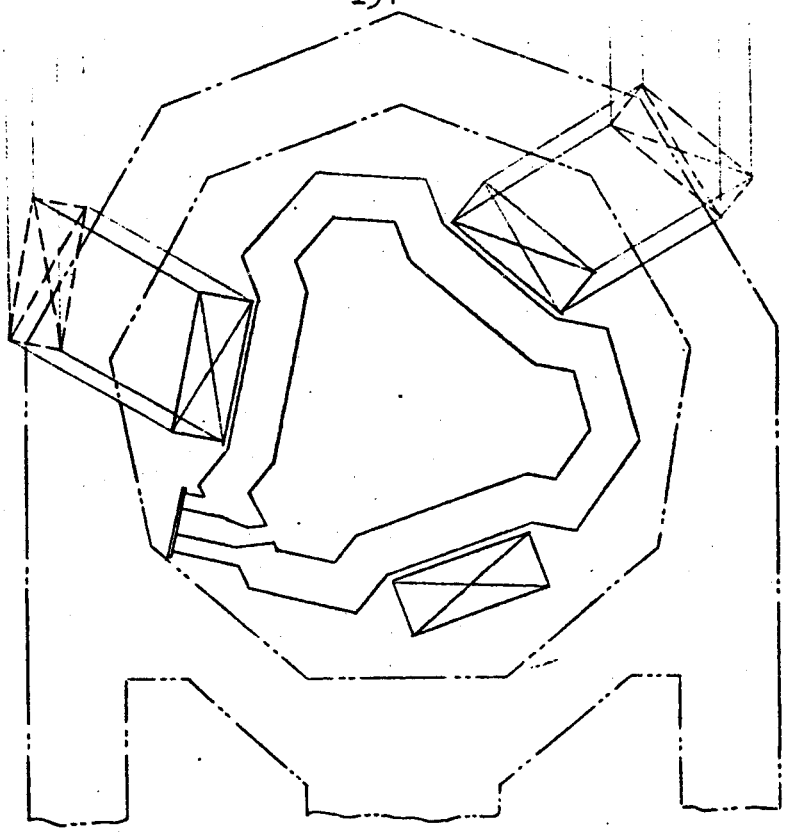

c) Position 3

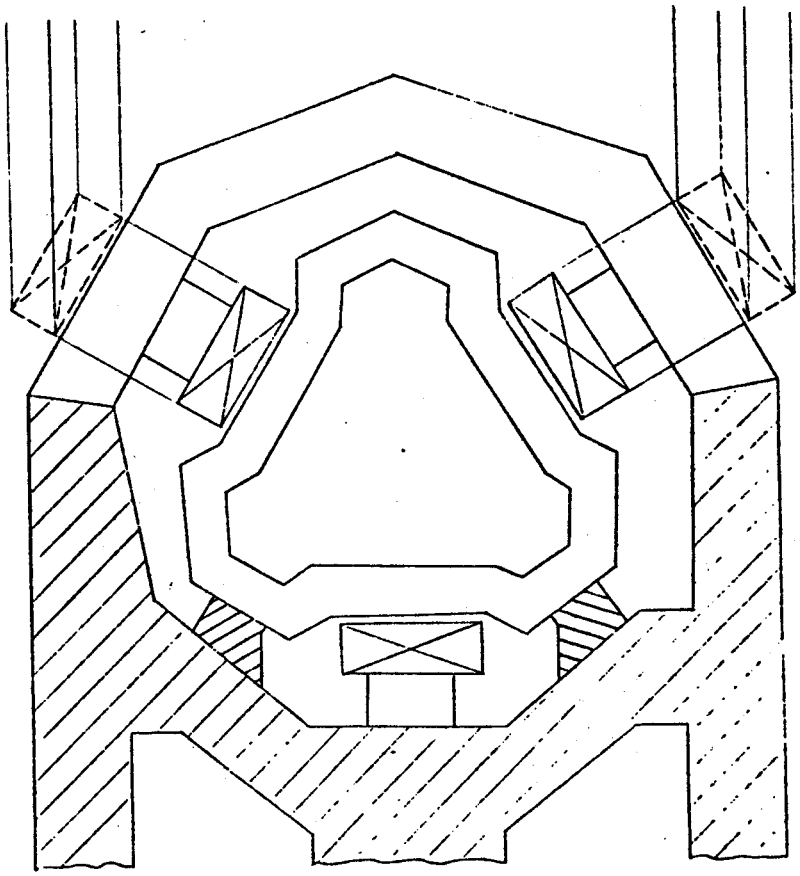

d) Position 4

Figure 6.2.2 c) & d) Vertical plane view of magnet windings

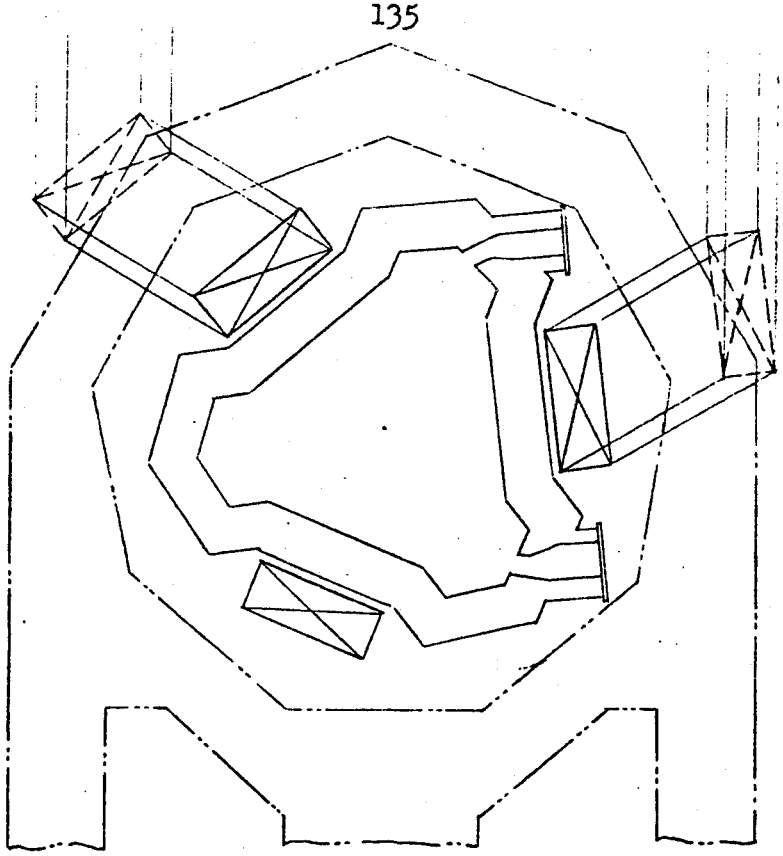

e) Position 5

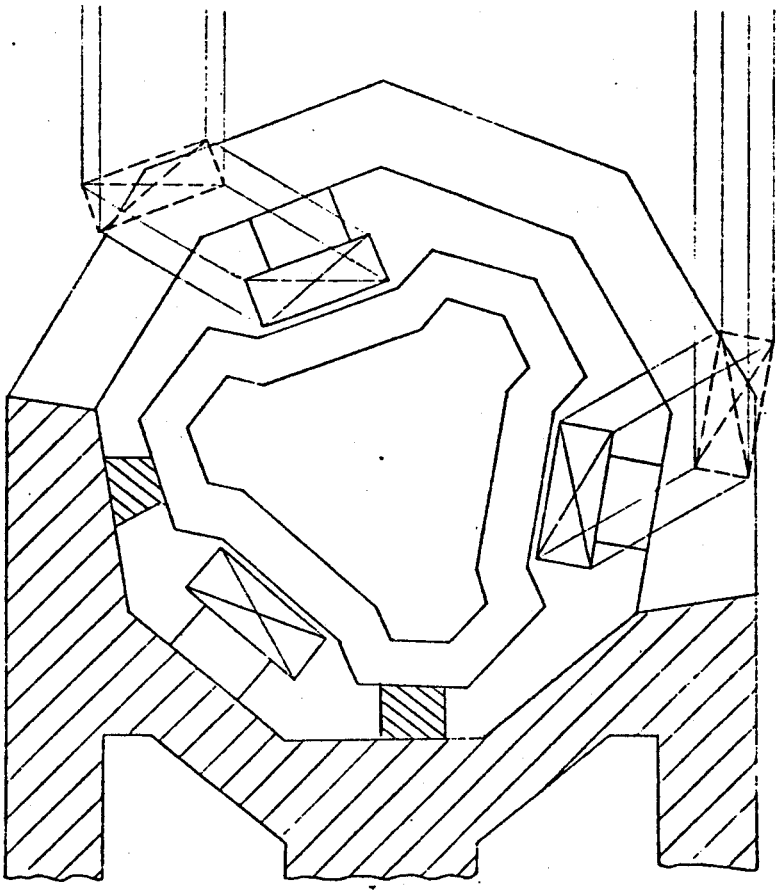

f) Position 6

Figure 6.2.2 e) & f) Vertical plane view of magnet windings

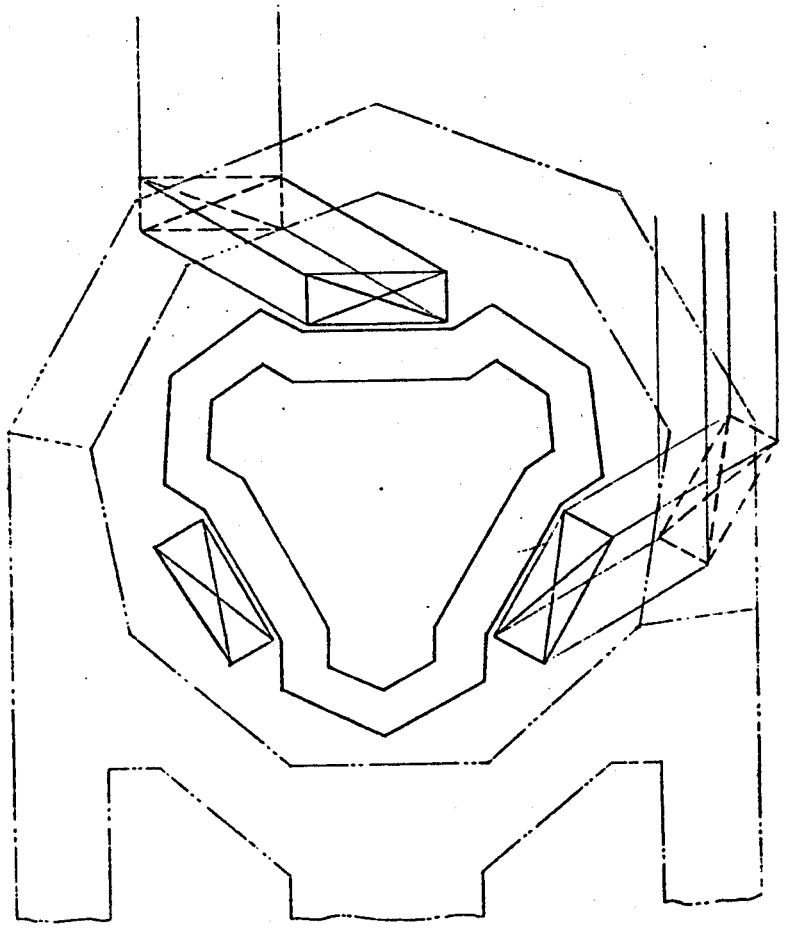

g) Position 7

Figure 6.2.2 g) Vertical plane view of magnet windings

6.3 Reactor Layout

The reactor layout of T-1 Reactor ought to be designed on the basis of the following conditions and considerations: [50]

1) The magnet windings and vessel sectors should be disassembled and re-assembled for scheduled maintenance and unscheduled maintenance and repair work.

2) Remote-handling tools and facilities should be introduced.

3) Disconnected vessel sectors for maintenance or repair should be moved out to the associated maintenance facilities and, instead, new or reprocessed vessel sectors should be moved in and installed.

4) Neutral beam injectors (NBIs), vacuum/exhaust pumps, and other large components surrounding the reactor module should be disconnected and removed prior to disassembly of the reactor modules.

5) It is desired that VF (vertical field) coils do not have to be disassembled in each scheduled maintenance of the reactor and also that they are provided with good accessibility for their own manintenance.

6) Feasibility of facility construction and reactor installment should be examined.

7) The size of the facilities (especially, the reactor building and associated maintenance facility) and the required amount of construction materials (steels, concrete, etc.) should be as small as possible in order to reduce construction cost and time.

8) Considerations of accessibility and maintainability of the reactor should include those for blanket cooling piping, magnet refrigerating piping, vacuum/exhaust pumping ducts, magnet leads, control & instrumen-

tation cables, tritium recovery lines, etc..

9) The reactor building and associated facilities should satisfy general requirements for radioactive protection and other safety considerations.

Detailed design work on all the items described above is beyond the scope of this study; however, some overall design studies are carried out mainly considering the above items 1) through 7).

Figure 6.3.1 shows vertical and horizontal plane views of the composition of T-1 Reactor. Major components of the reactor are the reactor sectors, magnet windings, support structures, NBIs, vacuum/exhaust pumps, and, in addition, VF coils which do not appear in this figure. Three vacuum/exhaust pumps are installed in each vessel sector. Figure 6.3.2 a) and Figure 6.3.2 b) show the configuration of vacuum/exhaust ports and NBI ports. Since neutral beam lines are required to have a certain angle (e.g. 45° or less) with a cercumferential line of the torus, the NBIs ought to be installed obliquely in a limited space between the support structures outwards the torus.

Figure 6.3.3 and Figure 6.3.4 respectively show a vertical plane view and a horizontal plane view of T-1 Reactor layout. The reactor is placed in the reactor building of a sort of annular shape which is 48 m in total height, 41 m in outer radius, and 12 m in inner radius. Disassembling and re-assembling operations of the reactor structures are performed through six radiation-shielded remote-operation boxes, each of which can move circumferentially and vertically along the reactor building wall; two of them cover inward regions of the torus and the other four cover outward regions. The reactor building is equipped with two large cranes which can be operated individually. Disassembled vessel sectors, segments of the magnet windings, upper beams of support structures, and other large

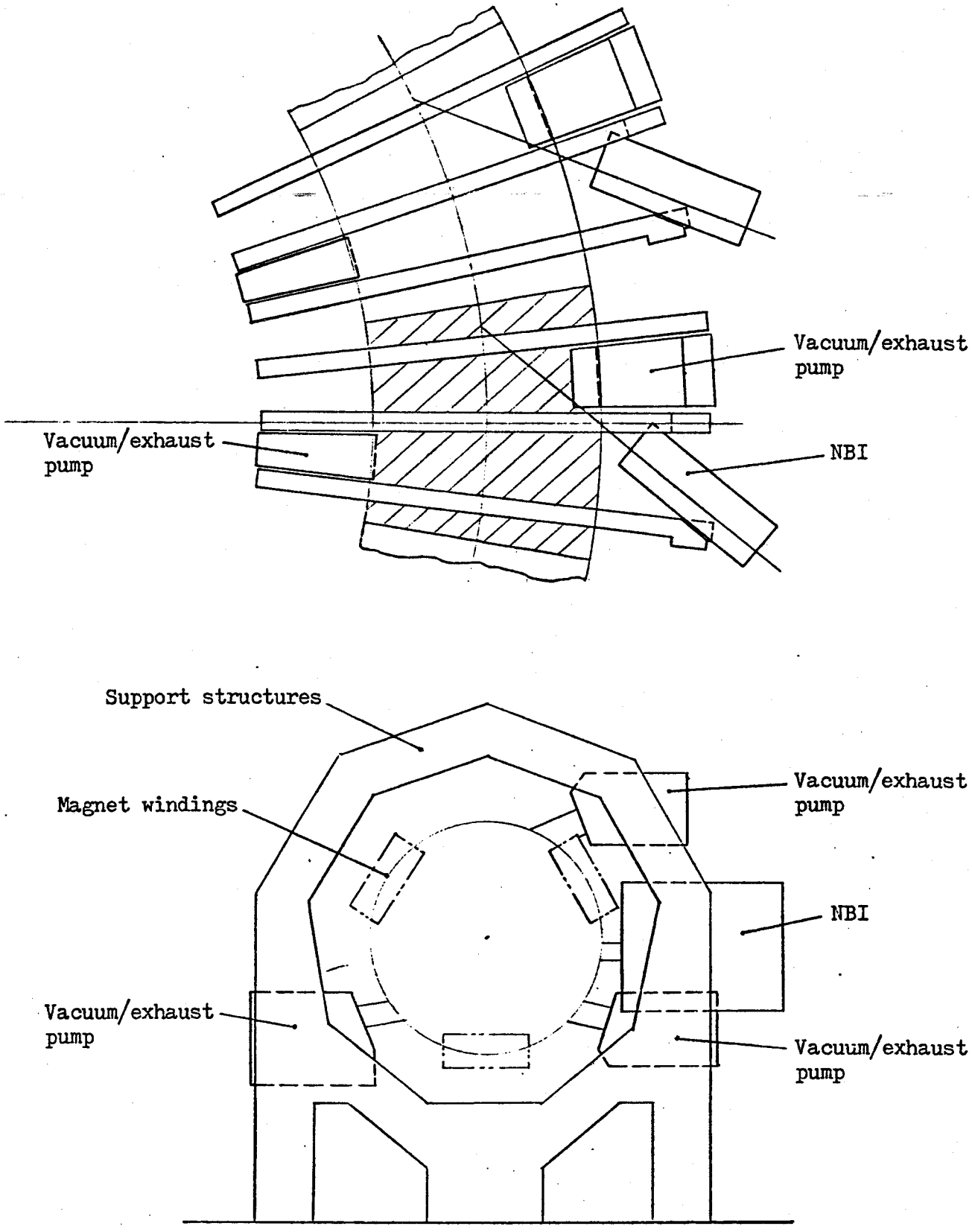

Figure 6.3.1 Composition of T-1 Reactor module

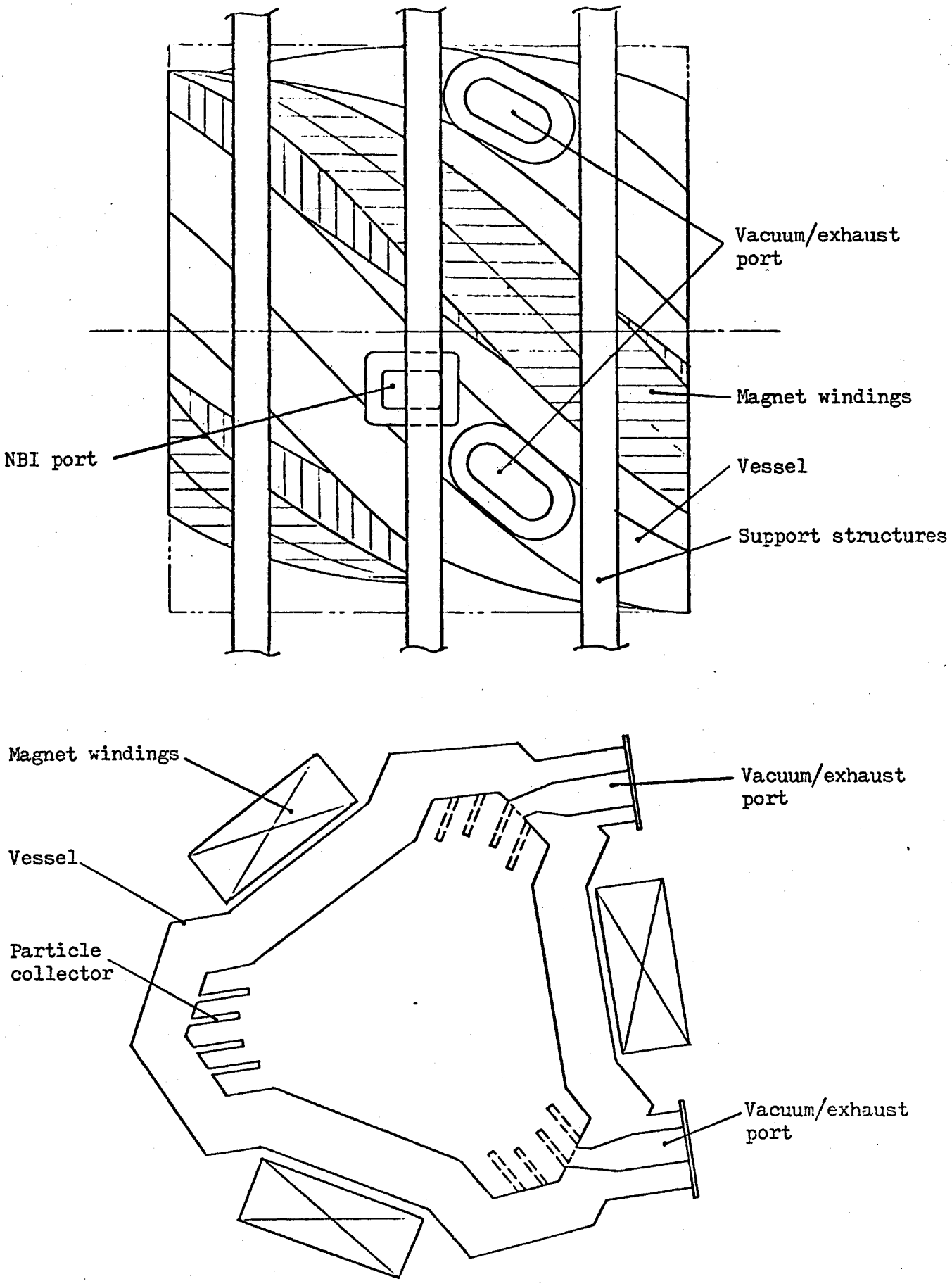

Figure 6.3.2 a) Configuration of vacuum/exhaust ports and NBI ports

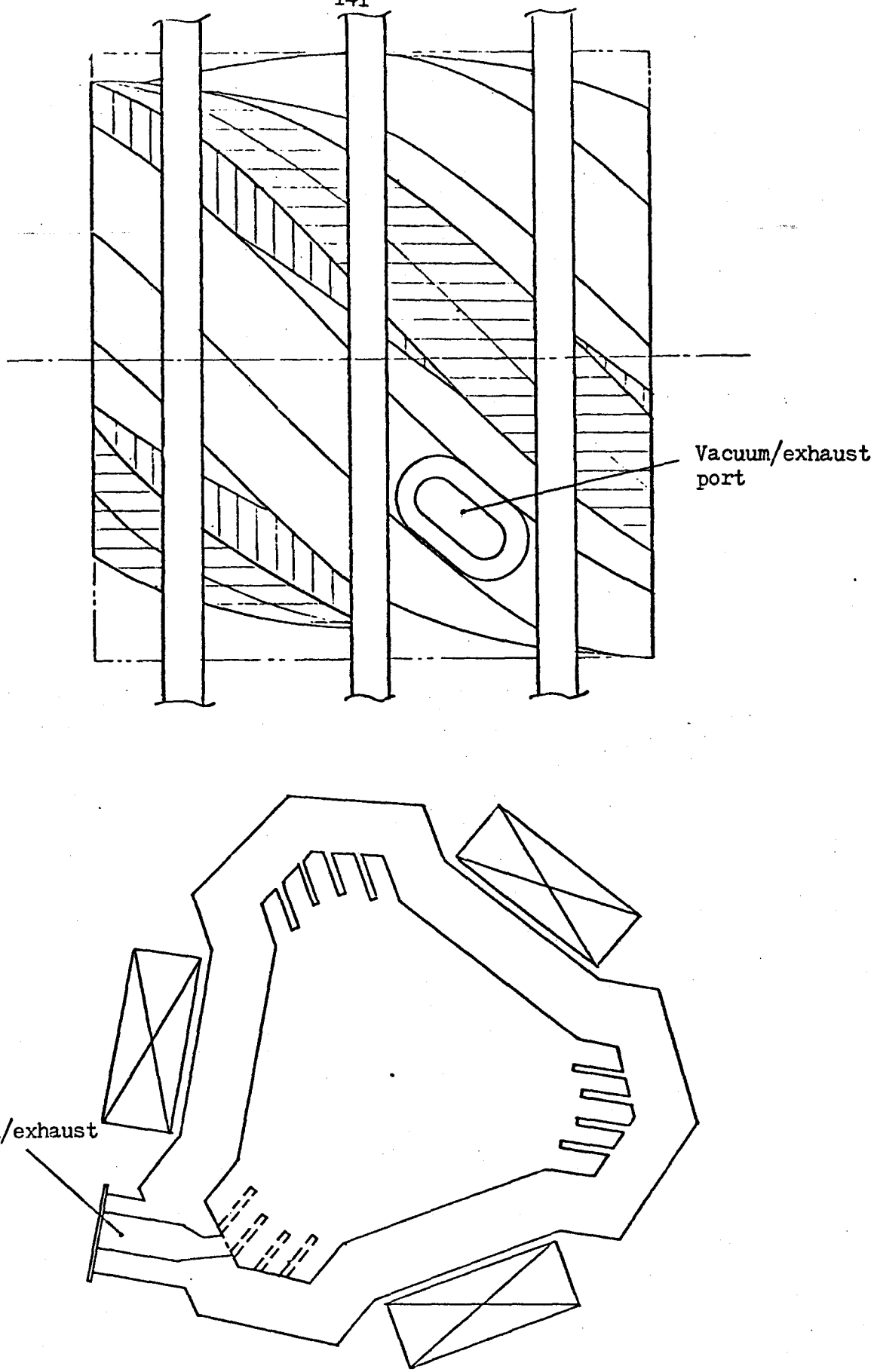

Figure 6.3.2 b) Configuration of vacuum/exhaust ports

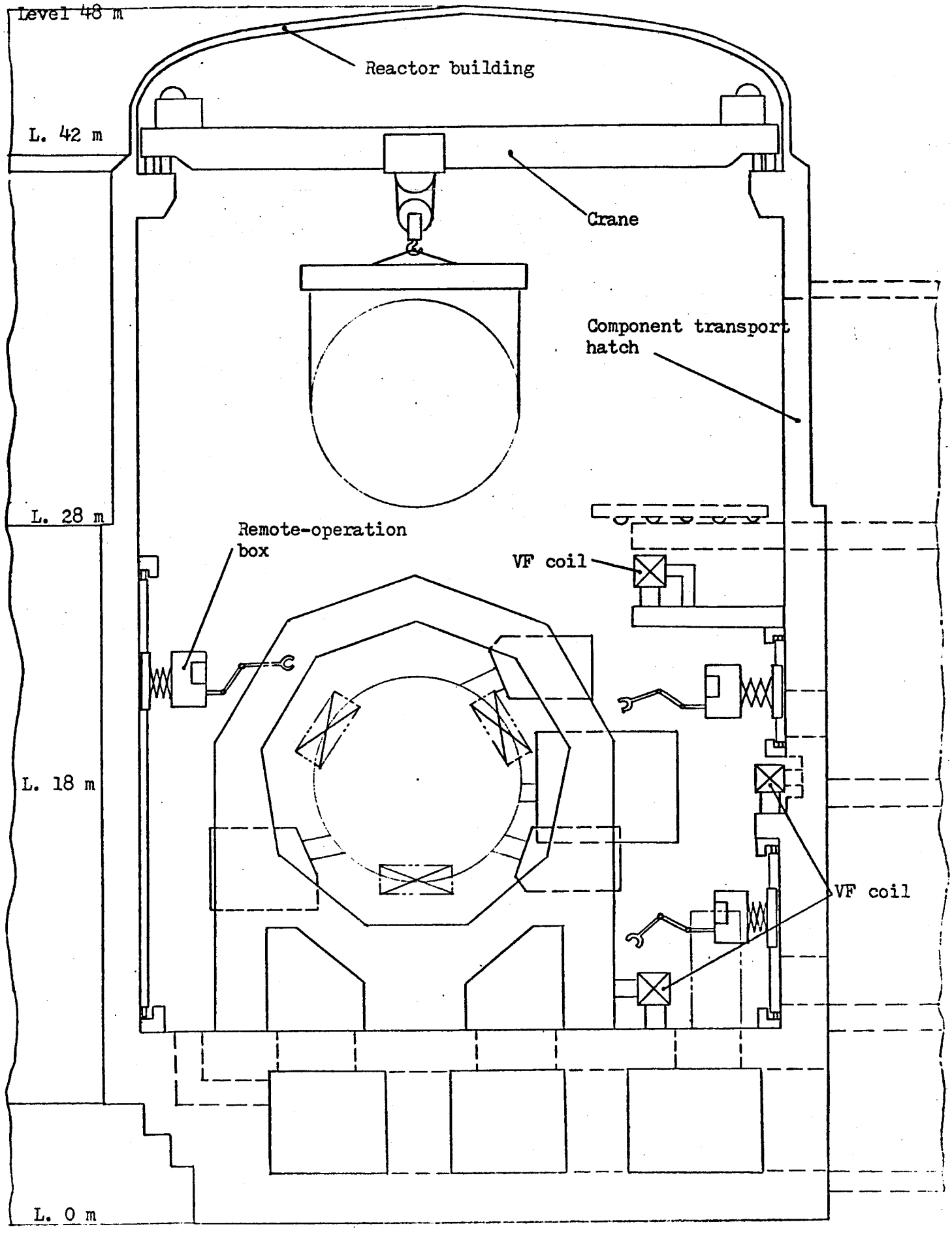

Figure 6.3.3 Vertical plane view of T-1 Reactor layout

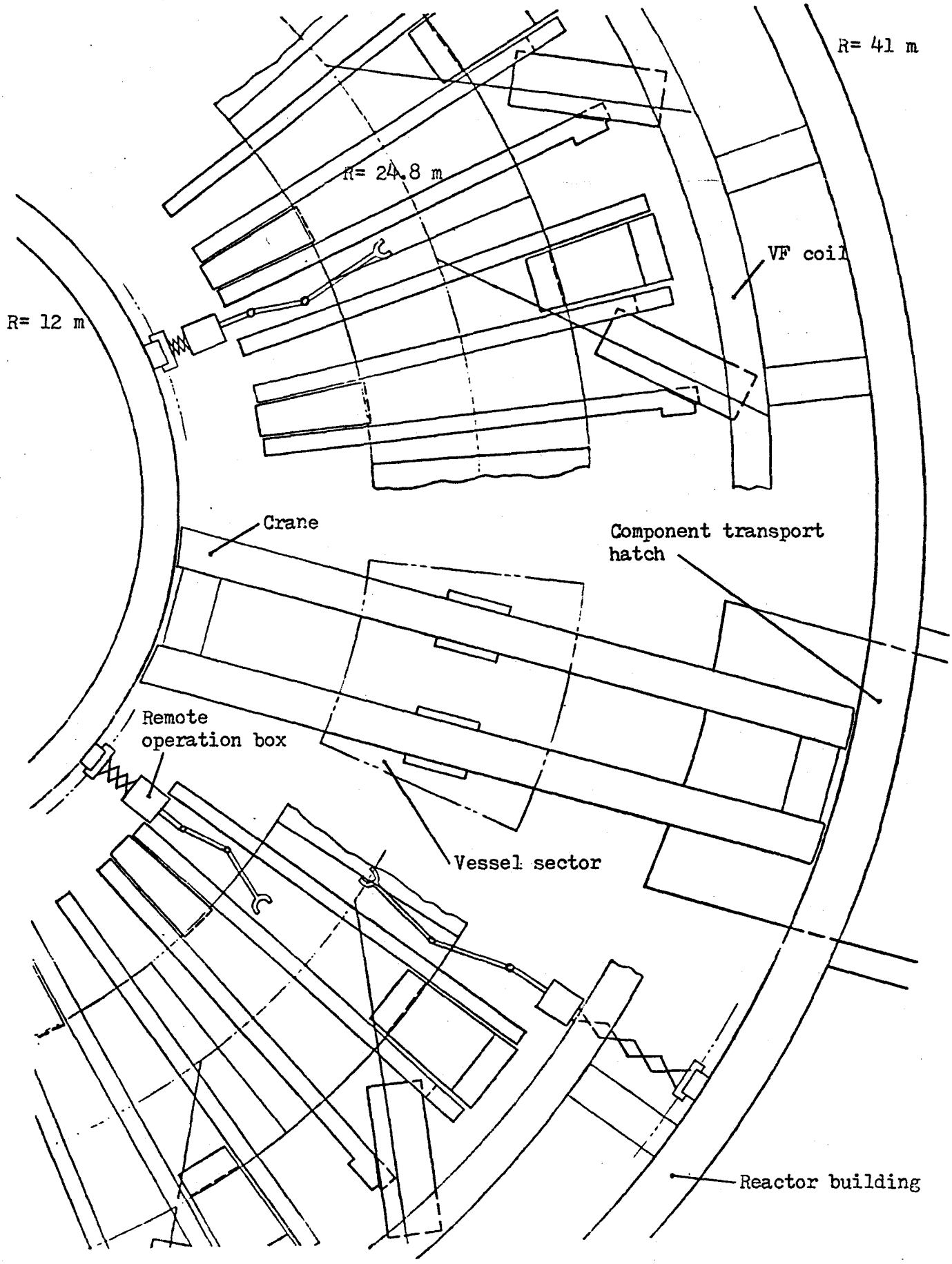

Figure 6.3.4 Horizontal plane view of T-1 Reactor layout

components will be lifted up and carried by the cranes to move out of the reactor room through two component-transportation hatches located at the upper outside-wall of the reactor building, and vice versa.

In the layout shown in Figure 6.3.3 and Figure 6.3.4 the VF coil located in an upper position is in the way of NBIs' moving up. Thus NBIs should be moved first onto the floor near the outside wall of the reactor room, and then, if necessary, be lifted up along the wall to move out. Auxiliary cranes or hoists installed beneath the upper VF coil may assist the NBIs' movement onto the floor.

Figure 6.3.5 shows the concept of plant arrangement in T-1 Reactor. The reactor are provided with the maintenance facility where removed modules (vessel sectors and internals) are processed to exchange first wall/blanket structures, new or processed spare modules and disassembled reactor components are stored, and large components such as vessel sectors, superconducting magnet segments are assembled or repaired. The removed modules are processed while the reactor is operating, and stand by for the next first wall/blanket replacement maintenance. The concept of this on-site maintenance facility is due to difficulty of the transportation of large and radioactive modules and other components. Tne reduced down-time and ease of maintenance operation will make up for the cost increase associated with the construction of this facility.

As described later in this section, maintenance or repair work accompanied with disassembly and re-assembly of the reactor modules requires a series of complicated remote operations. The conceptual reactor-layout proposed in this study is not enough to examine in detail the accessibility and the capability of remote operation required for each of the procedures.

It is desired that at a next stage of detailed design all the reactor-layout conditions and considerations including 7) and 8) mentioned earlier will be examined precisely.

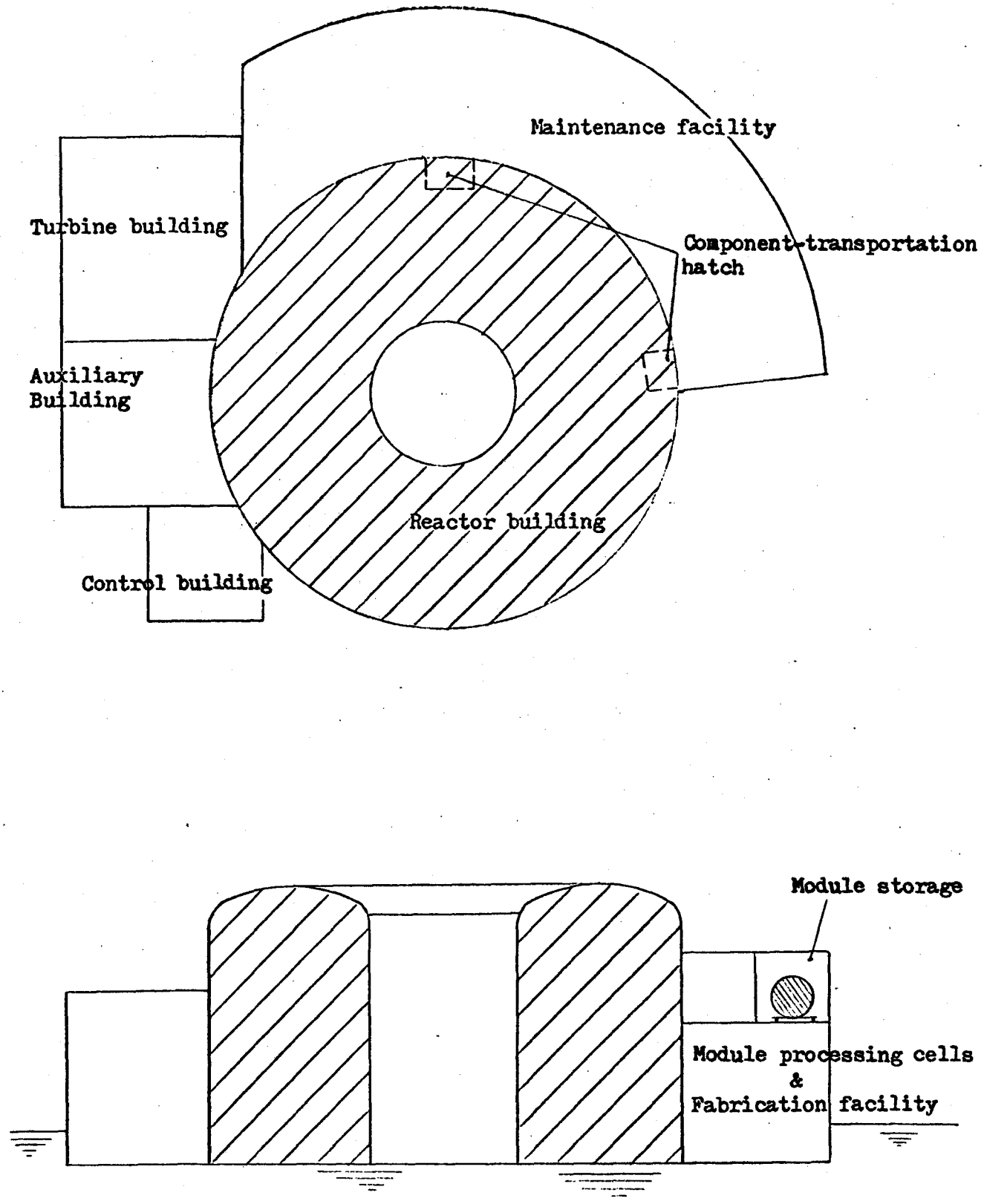

Figure 6.3.5 Concept of plant arrangement

6.4 Maintenance Procedures

Among various kinds of maintenance and repair work which should be expected in the reactor design, periodic replacement of first wall/blanket materials will be most important, since it should be frequently (e.g. every 1 - 4 years) performed and is accompanied with large-scaled complicated operations such as disassembly and re-assembly of the reactor modules. (As described earlier, in-place replacement of first wall/blanket materials is not considered to be practical in T-1 Reactor.)

In T-1 Reactor periodic first wall/blanket replacement may be performed based on, for example, the plans and conditions shown in Table 6.4.1.

Table 6.4.1 Plans and conditions of periodic first wall/blanket replacement

Replacement interval	2 years
Replacement method	Reactor module replacement
Number of replaced reactor modules	10 modules
Operation hours	3 shifts (24 hours a day)
Handling of VF coils	In-place (no disassembly)
Number of remote-operation boxes	6
Number of reactor-room cranes	2 plus auxiliary hoists
Load capacity of cranes	800 tons each

Main procedures of the reactor module replacement are listed as follows:

(Disassembly of the reactor module)

1) Shut down the reactor
2) Cool down the blanket cooling system and tritium recovery system
3) Warm up the superconducting magnet windings
4) Disconnect and remove NBIs
5) Disconnect and remove vacuum/exhaust pumps
6) Disconnect blanket cooling piping
7) Disconnect magnet refrigerating piping
8) Disconnect magnet joints
9) Set supporting jigs of magnet segments
10) Disassemble magnet support elements
11) Disassemble and remove upper beams of support structures
12) Move out magnet segments
13) Remove supporting jigs of magnet segments
14) Disconnect vessel-sector joints
15) Disconnect vessel support elements and remove vessel sectors

(Re-assembly of the reactor module)

16) Move in new vessel sectors and install vessel support elements
17) Connect vessel-sector joints
18) Perform vacuum leak tests of the vessel
19) Set supporting jigs of magnet segments
20) Replace magnet segments
21) Install upper beams of support structures
22) Connect magnet support elements

23) Remove supporting jigs of magnet segments

24) Connect magnet joints

25) Perform electrical tests of the magnet windings

26) Connect magnet refrigerating piping

27) Connect blanket cooling piping and tritium recovery piping

28) Perform pressure tests of the blanket cooling system

29) Connect vacuum/exhaust pumps

30) Connect NBIs

31) Perform integral vacuum leak tests of the system including vacuum/exhaust pumps and NBIs

32) Cool down the superconducting magnet windings

33) Pre-heat the blanket cooling system and tritium recovery system

34) Pre-operational adjustments and tests of control & instrumentation systems

Expected or planned time schedule for the above series of procedures is shown in Table 6.4.2. As the table indicates, the required reactor shut-down period for the scheduled replacement of first wall/blanket materials is estimated to be about 80 days. Also the expected shut-down time for unscheduled maintenance or repair accompanied with disassembly of one or two reactor modules is about 60 days.

Most complicated or time-consuming processes in the above maintenance procedures are the following:

a) Warming-up and cooling-down of the superconducting magnet windings

b) Disconnection and re-connection of blanket cooling piping and tritium recovery system

c) Disconnection and re-connection of magnet refrigerating piping

Table 6.4.2 Time-table of first wall/blanket replacement procedures

(continued)

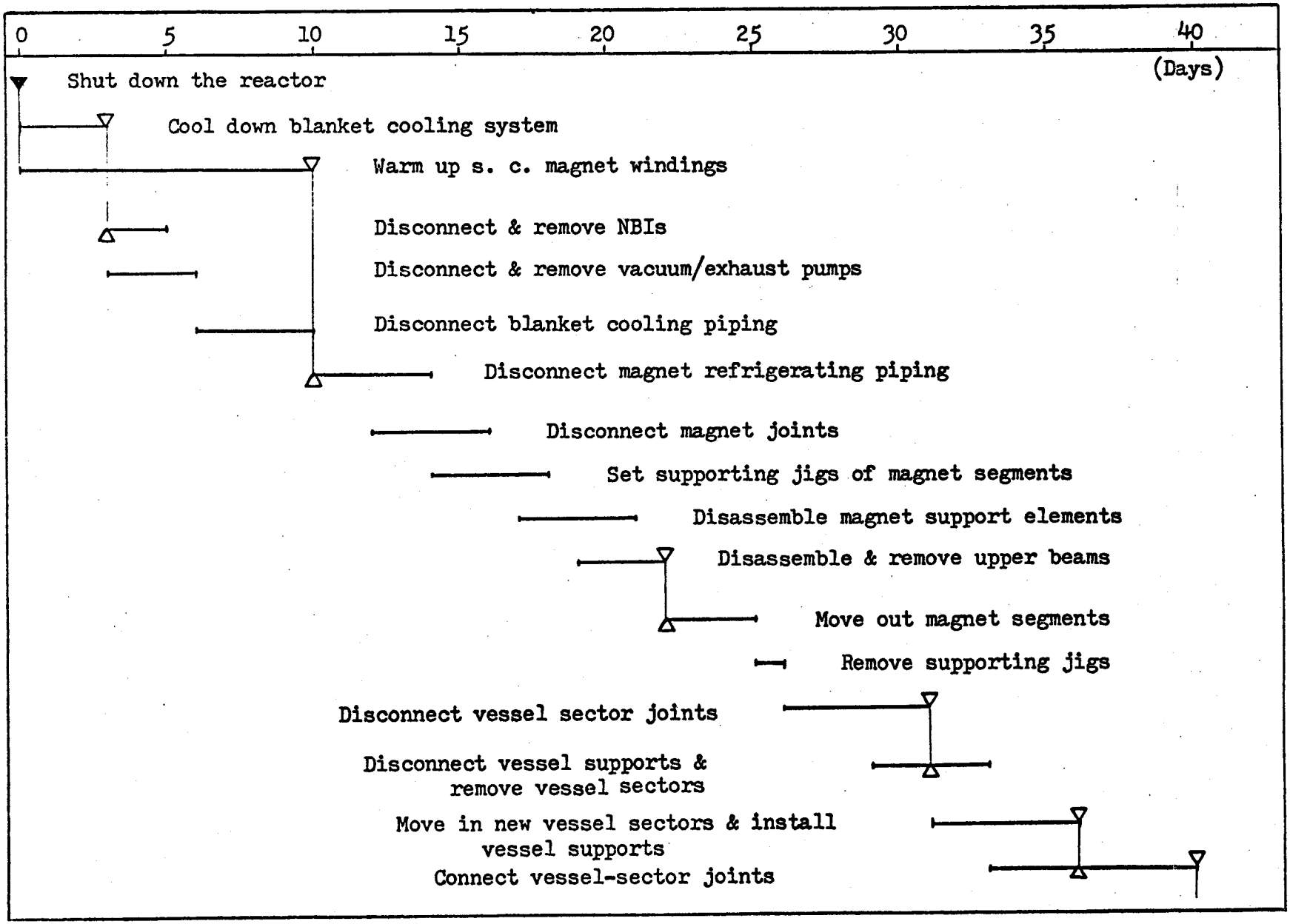

Table 6.4.2 (continued)

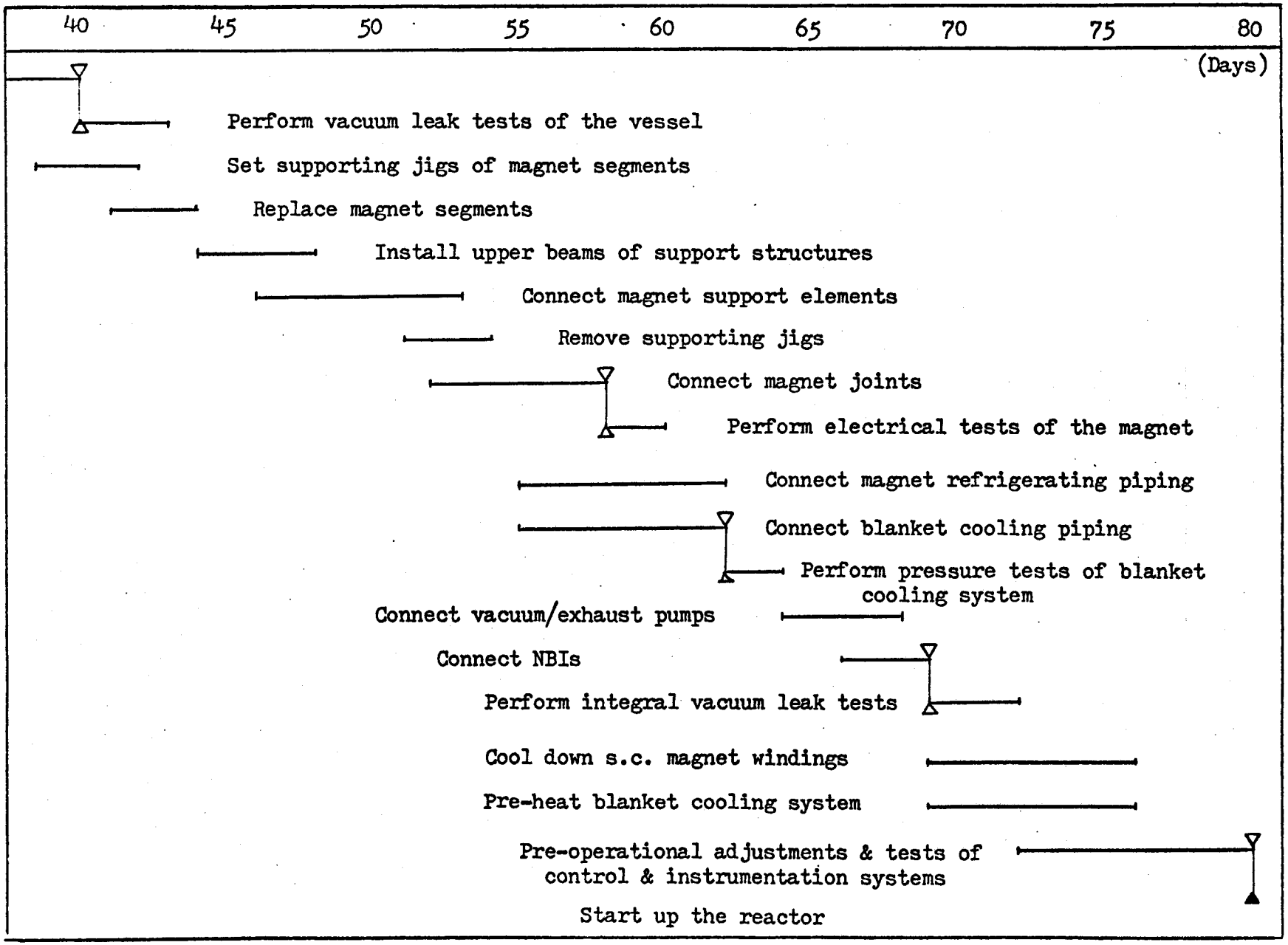

d) Disconnection and re-connection of magnet joints

e) Re-assembly of magnet support elements

f) Disconnection and re-connection (including vacuum sealing) of vessel sector joints

Required time for warming-up or cooling-down the magnet windings will not be reduced significantly, since they depend upon thermal-stress limitations, available refrigeration power (for cooling-down), large heat capacity, etc.. Disconnection and re-connection of large blanket cooling piping which is about 0.5 m in diameter will require advanced technique of remote operations such as cutting, machining, and welding the piping satisfactorily. Concerning disconnection and re-connection of the magnet refrigerating piping, handling of thermal-insulating structures gives rise to another technical subject. In disconnection and re-connection of magnet joints, unbolting & bolting will be time-consuming procedures. Re-assembly of magnet support elements will need delicate operations to adjust their supporting conditions. Regarding disconnection and re-connection of vessel sectors, handling of vacuum seals between vessel sectors will need special tools and elaborate operations.

Since reactor availability has a great effect on the cost and usefulness of the reactor, it is desired that the reactor shut-down time required for maintenance and repair be reduced as much as possible by all kinds of efforts in the fields of reactor structural design, reactor layout, and maintenance operations.

7. Main Results

Main results obtained in this design study, as well as future technical subjects found through this work, are summarized in the following:

1) Forced circulation of supercritical helium and forced circulation of two-phase helium are two probable options of cooling methods for the superconducting magnet windings.

2) Special considerations are needed to achieve vacuum conditions required for superinsulations of the magnet windings under a restricted space.

3) Required power to refrigerate the superconducting magnet windings under reactor operation is estimated to be 14.2 MW_e.

4) Sliding movement of the magnet windings caused by thermal contraction can be accommodated in the magnet joints.

5) During reactor operation the contact pressure of the magnet joints is large enough due to induced magnetic forces; however, the contact resistance at lower contact pressure (e.g. 4 MPa) should be reduced by further optimization of contact surfaces in order to facilitate start-up operation.

6) The refrigeration system of the magnet windings should provide 20 K coolant output in addition to 80 K and 4.2 K outputs so as to reduce the cooling-down time below 80 K to an acceptable level.

7) In cooling-down of the magnet windings heat leak through the magnet supports and spacers becomes innegligible especially below 20 K.

8) Cooling-down time of the magnet windings is restricted by available refrigeration power. When 20 MW_e off-site power is available, it will take at least about 6 days to cool down the whole magnet windings.

9) Forced circulation of liquid lithium is not applicable to blanket

cooling of T-1 Reactor, since MHD pressure drop is unacceptably large.

10) Required pumping power corresponding to helium gas pressure drop in blanket channels is about 80 MW_e.

11) Each reactor module is equipped with three cryopumps (two for operation and one for recycle); the required pumping speed of each pump is about 5.3×10^5 liters/sec.

12) Particle collectors are installed in divertor regions. They are built-in parts of Type-B blanket segments. (The blenket is composed of Type-A and Type-B blanket segments.)

13) Vessel sectors are connected with bellows joints, which will accommodate thermal expansion of the toroidal vessel and also facilitate its assembly and disassembly.

14) Each magnet segment of the helical windings (the helical windings are composed of 60 segments) is supported by three support elements. Multi-layered glass-reinforced epoxy plates are employed as structural members of the support elements.

15) The toroidal structures of T-1 Reactor are composed of twenty modules. Main components of each module are the vessel sector & internal structures, three magnet segments, one neutral beam injector, three vacuum/exhaust pumps, three support rings, etc.. To perform scheduled and unscheduled maintenance and repairs with remotely operated equipments, accessibility is an important factor in designing the reactor layout. In T-1 Reactor remote operation is performed from inward, as well as from outward, the toroidal structures.

16) Blanket replacement is done by disassemling the reactor module into several parts and exchanging the vessel sector. The plant has a maintenance facility where removed modules are processed and stored on site. (Assembly of large components is also performed in this facility.)

17) Advanced techniques and special tools should be developed especially to perform remote operations of cutting, machining, and welding pipings and vacuum seals, etc..

REFERENCES

1. "The Torsatron Reactor", MIT report (1978)

2. G. Pasotti and M. Spadoni (CNEN), "Superconducting Magnet for Fusion Reactors: The Program of a Reliable and Effective Cooling System", Proc. of 7th Sympo. of Eng. Prob. of Fusion Research (1977)

3. J. Murphy et al. (WH), "Designing Superconducting Toroidal Field Windings for a Fusion-driven Actinide Burner", IEEE Vol. MAG-13, No. 1 (1977)

4. S. Van Sciver (Univ. of Wisconsin), "Cryostabilization of Large Superconducting Magnets using Pool Boiled Helium II", Proc. of 7th Sympo. of Eng. Prob. of Fusion Research (1977)

5. S. Sato and H. Ogata, "Review of Heat Transfer to Helium - Part 2", Cryogenic Engineering Vol. 13, No. 1, in Japanese (1978)

6. G. Pasotti et al. (CNEN), "A Preliminary Study of the Superconducting Toroidal Magnet for FINSOR I Reactor", IEEE Vol. MAG-13, No. 1 (1977)

7. R. Ayman et al. (CEA), "Conceptual Design of a Superconducting Tokamak: "Torus II SUPRA", IEEE Vol. MAG-15, No. 1 (1979)

8. M. Morpurgo (CERN), "A Large Superconducting Dipole Cooled by Forced Circulation of Two Phase Helium", Cryogenics Vol. 19, No. 7 (1979)

9. R. H. Perry et al. edit., "Chemical Engineer's Handbook", 5th ed., McGraw-Hill (1973)

10. M.B. Kasen (NBS), "Mechanical and Thermal Properties of Filamentary-reinforced Structural Composites at Cryogenic Temperatures", Cryogenics Vol. 15, No. 6 (1975)

11. N. Inai, "Experimental Investigation of Multilayer Insulation with Room Temperature Outside and Liquid Helium Temperature Inside", J. of Thermal Insulation Vol. 1 (1977)

12. R.F. Barron, "Princeples of Evacuated Cryogenic Insulations", AIChE Sympo. Series No. 125, Vol. 68 (1972)

13. G. Haselden, "Cryogenic Fundamentals", Academic Press, P. 12 (1971)

14. V.E. Keilin et al., "Temperature Distribution along Superconducting Power Transmission Lines", Cryogenics Vol. 15, No. 6 (1975)

15. W.M. Rohsenow and J.P. Hartnett, "Handbook of Heat Transfer", McGraw-Hill, Section 14 (1973)

16. M.M. El-Wakil, "Nuclear Heat Transport", ANS, Chapter 12 (1971)

17. J.R. Powel et al. (BNL & Grumman Aero. Co.), "DEALS: A Demountable Superconducting Magnet System for Fusion Reactors", Cryogenics Vol. 20 No. 2 (1980)

18. D.C. Larbalestier and D. Evans, "High Strength Austenitic Stainless Steels for Cryogenic Use", 6th Int. Cryo. Eng. Conf. (1977)

19. "A Compendium of the Properties of Materials at Low Temperature (Phase - I)", PB171619 (1968)

20. M.A. Hoffman et al. (LLL), "Review of Heat Transfer Problems associated with Magnetically Confined Fusion Reactor Concepts", AIChE Sympo. Series No. 168, Vol. 73 (1977)

21. J.A. Fillo and J.R. Powell (BNL), "Heat Transfer Problems in Gas Cooled Solid Blankets", AIChE Sympo. Series No. 168, Bol. 73 (1977)

22. A.P. Fras, "Conceptual Design of the Blanket and Shield Region and Related Systems for a Full Scale Toroidal Fusion Reactor", ORNL-TM-3096 (1973)

23. B. Badger et al., "UWMAK III", UWFDM-150 (1976)

24. R.W. Moir et al., "Preliminary Design Study of the Tandem Mirror Reactor (TMR)", UCRL-52302 (1977)

25. N.B. Vargaftik, "Tables on the Thermophysical Properties of Liquids and Gases", 2nd Ed, Hemisphere Pub. Co. (1975)

26. J.H. Rust, "Nuclear Power Plant Engineering", Haralson Pub. Co. (1979)

27. A.V. Nero, "A Guide Book to Nuclear Reactors", Univ. of California Press. (1979)

28. "Development Status and Operational Features of the High Temperature Gas-Cooled Reactor", EPRI-NP-142 (1976)

29. "An Evaluation of High Temperature Gas-Cooled Reactors", WASH-1085 (1969)

30. R.N. Lyon et al. edit., "Liquid-Metal Handbook ", 2nd Ed., U.S. Navy (1952)

31. W.E. Stewart and D.K. Sze (Univ. of Wisconsin), "Transport Problems in Lithium Cooling of Tokamak Reactors", AIChE Sympo. Series No. 168, Vol. 73 (1977)

32. C.M. Van Atta, "Vacuum Science and Engineering", McGraw-Hill (1965)

33. H.A. Steinherz, "Handbook of High Vacuum Engineering", Reinhold Pub. (1963)

34. G.F. Weston, "Pumps for Ultra-High Vacuum", Vacuum Vol. 28, No. 5 (1978)

35. J.P. Habson, "Cryopumping", J. Vac. Sci. Technol. Vol. 10, No. 1 (1973)

36. H.J. Halama et al. (BNL), "Large-Capacity Cryogenic Pumping of D_2 and H_2 for Fusion", J. Vac. Sci. Technol. Vol. 14, No. 5 (1977)

37. P.W. Fisher and J.S. Watson (ORNL),"Helium Pumping at 4.2 K by Molecular Sieve 5A", J. Vac. Sci. Technol. Vol. 16, No. 1 (1979)

38. B.D. Abel (Gramman Aero. Co.), "TFTR Vacuum System", J. Vac. Sci. Technol. Vol. 15, No.2 (1978)

39. H.F. Dylla (PPPL), "Turbomolecular Pump Vacuum System for the Princeton Large Torus", J. Vac. Sci. Technol. Vol 15, No. 2 (1978)

40. W. Becker and J. Henning, "Problems with Turbomolecular Pumps in Magnet Shields", J. Vac. Sci. Technol. Vol. 15, No, 2 (1978)

41. R.J. Roark and W.C. Young, "Formulas for Stress and Strain", 5th ed., McGraw-Hill (1975)

42. "Cases of ASME Boiler and Pressure Vessel Code - Case 1592-4", ASME (1975)

43. John Aspinall, Computer Output (T-1 Reactor Solve Run 1032), unpublished (1979)

44. J.T.D. Mitchell (Culham Lab.), "Blanket Replacement in Toroidal Fusion Reactors", Proc. of 3rd Topical Meeting on Tech. of Controlled Nuc. Fusion (1978)

45. G.M. Fuller and H.S. Zahn (Mcdonnell Douglas), "A Comparison of Five Reactor Concepts on the Basis of Scheduled Maintenance Requirements", Proc. of 3rd Topical Meeting on Tech. of Controlled Nuc. Fusion (1978)

46. I.N. Sviatoslavsky (Univ. of Wisconsin), "Engineering Design Considerations for Facilitating Maintainability of Fusion Reactors", Proc. of 3rd Topical Meeting on Tech. of Controlled Nuc. Fusion (1978)

47. J.A.S. Guthrie and J.T.D. Mitchell (Culham Lab.), "Remote Operated Shield Door and Transporter for the Culham Conceptual Tokamak Reactor Mark II", ANS Winter Meeting (1979)

48. E. Jimenez (Grumman Aero. Co.), "In-vessel Manipulator for the Tokamak Fusion Test Reactor", Proc. of 26th Conf. on Remote Systems Tech. (1978)

49. H.L. Allen (PPPL) and B.J. Fedor, "Operations and Maintenance Plans of for the TFTR", Proc. of 3rd Topical Meeting on Tech. of Controlled Nuc. Fusion (1978)

50. C.A.Shorts (Bechtel Nat.), "Tandem Mirror Reactor Maintainability Study", Proc. of 26th Conf. on Remote Systems Tech. (1978)